Electron-electron interaction and confinement
in the Integer Quantum Hall Effect

**Dissertation
zur Erlangung des Doktorgrades
des Fachbereichs Physik
der Universität Hamburg**

vorgelegt von

Alexander Struck

aus Lübeck

**Hamburg
2005**

Abstract

The purpose of this work is to investigate the role of electron-electron interaction and confinement in disordered two-dimensional systems with a strong perpendicular magnetic field.

In these systems, the integer quantum Hall effect is observed. The kinetic energy of the electrons is quantized into equidistant Landau levels, which are broadened into bands due to the presence of a disorder potential. If the Fermi energy is in the tail of Landau band i, the Hall conductance exhibits a plateau of magnitude $e^2/h \cdot i$, whereas the magnetoconductance vanishes. This phenomenon is well understood within a single-particle picture as a second order phase transition between localized electronic states at the band edges and extended states in the center, governed by a power law dependence of the localization length with respect to the energy distance to the band center with an universal static critical exponent.

One of the topics of this thesis is to scrutinize this power law behaviour in the presence of mutual electron interactions, which are treated in spin-unrestricted self-consistent Hartree-Fock approximation. We show for the lowest Landau level that the static critical exponent is unchanged in the presence of electron-electron interaction and for various types of disorder. Moreover, we estimate the effects of interaction and disorder type on the dynamical critical exponent, which governs the impact of quantum fluctuations induced by an external time-dependent electric field. We demonstrate by calculating the frequency-dependent conductivity in linear response theory that the dynamical critical exponent can be altered by interaction and disorder.

Furthermore, we discuss an experiment detecting signatures of charging in an integer quantum Hall system, which in general are attributed to Coulomb interaction in correlated systems. We derive a mean-field description for these charging patterns, that reproduces the experimental observations at least in the localized regions and is compatible with the single-particle picture of the localization-delocalization transition. In agreement with experimental observations we show that electron-electron interaction cannot be neglegted in a comprehensive theory of the integer quantum Hall effect.

In the third part, we calculate the two-terminal conductance in a disordered quantum wire in dependence of energy and wire width. It is found that the conductance plateaux discontinuously collaps to exactly zero between two plateau levels. Employing an exact diagonalization study, we find electron states in the vicinity of these transitions that are superpositions of edge states with opposite chirality, with a vanishing bulk contribution. We provide arguments that these nonchiral edge states govern the new chiral metal-insulator transition.

In the last chapter, we calculate the effective g-factor in dependence of magnetic field and confinement strength and discuss a smooth suppression of the g-factor enhancement governed by both direct and exchange interaction in dependence of the electron density.

Zusammenfassung

In dieser Arbeit untersuchen wir die Rolle von Elektron-Elektron-Wechselwirkung und räumlicher Beschränkung in ungeordneten, zweidimensionalen Systemen mit einem starken, senkrechten Magnetfeld.

In diesen Systemen tritt der integrale Quanten-Hall-Effekt auf. Die kinetische Energie der Elektronen ist in Landau-Niveaus mit konstantem Abstand quantisiert, die in Gegenwart eines Unordnungspotentials in Bänder aufgespalten werden. Liegt die Fermi-Energie am Rand des i-ten Bandes, zeigt sich ein Plateau der Größe $e^2/h \cdot i$ in der Hall-Leitfähigkeit, während die Magnetoleitfähigkeit verschwindet. Diese Phänomen kann gut im Rahmen eines Einteilchenbildes als Phasenübergang zweiter Ordnung zwischen lokalisierten Elektronenzuständen an den Bandkanten und ausgedehnten Zuständen in der Bandmitte verstanden werden, wobei der Übergang als Potenzgesetz für die Lokalisierungslänge in Abhängigkeit vom Energieabstand vom Bandzentrum formuliert ist, mit einem universellen, statischen kritischen Exponenten.

Eines der Themen der vorliegenden Arbeit ist die genaue Untersuchung des Potenzgesetzes in Gegenwart von Wechselwirkung zwischen den Elektronen, welche in spin-aufgelöster, selbstkonsistenter Hartree-Fock-Näherung behandelt wird. Wir zeigen für das unterste Landau-Band, dass der statische kritische Exponent unabhängig von Wechselwirkung und verschiedenen Arten von Unordnung ist. Weiterhin schätzen wir Effekte von Wechselwirkung und Unordnung auf den dynamischen kritischen Exponenten ab, der den Einfluss von durch äußere zeitabhängige elektrische Felder verursachten Quantenfluktuationen widerspiegelt. Dazu berechnen wir in linearer Antworttheorie die frequenzabhängige Leitfähigkeit und demonstrieren eine mögliche Veränderung des dynamischen Exponenten.

Darüberhinaus diskutieren wir ein Experiment, in dem Hinweise auf Ladungseffekte in integralen Quanten-Hall-Systemen gefunden wurden. Diese werden normalerweise mit Coulombwechselwirkungen in korrelierten System erklärt. Wir entwickeln eine *Mean-field*-Beschreibung für diese Beobachtungen, die diese wenigstens in den lokalisierten Bereichen wiedergeben und im Einklang mit dem Einteilchen-Bild des Lokalisierungs-Delokalisierungs-Übergangs stehen. In Übereinstimmung mit den experimentellen Daten zeigen wir, dass Elektron-Elektron-Wechselwirkung für eine vollständige Theorie des integralen Quanten-Hall-Effekts nicht vernachlässigt werden kann.

Im dritten Teil berechnen wir die Zweipunktleitfähigkeit eines ungeordneten Quantendrahtes in Abhängigkeit von Energie und Drahtbreite. Wir finden, dass die Leitwertstufen zwischen zwei Werten diskontinuierlich auf exakt Null abfallen. Mit exakter Diagonalisierung finden wir Zustände im Bereich dieser Übergänge, die Superpositionen von Randzuständen mit entgegengerichteter Chiralität sind, mit verschwindend kleiner

bulk-Beteiligung. Wir argumentieren, dass diese nichtchiralen Randzustände verantwortlich für den neuartigen chiralen Metall-Isolator- Übergang sind.

Im letzten Kapitel gehen berechnen wir den effektiven g-Faktor für einen parabolischen Quantendraht in Abhängigkeit von Magnetfeld und Stärke des Einschlusspotentials und diskutieren eine glatte Unterdrückung der g-Faktor-Vergrößerung, die von direktem Coulomb- und Austauschterm gleichermaßen gestützt wird und von der Elektronendichte abhängt.

Contents

1

Introduction

One of the most important topics of solid state research within half the last century has been the investigation of electron systems in semiconductor heterostructures and MOSFETS. The ability to fabricate structures which confine the motion of the carriers in zero, one or two dimensions brought the possibility to create new and unique electronic devices, but also opened a vast range of fundamental problems.

A remarkable observation was made by von Klitzing [1], when measuring the Hall coefficient on a two-dimensional Si-MOSFET at very low temperature and very large external magnetic field perpendicular to the plane of electron motion. The outcome of this experiment was spectacular: Whereas the classical Hall experiment gave a linear dependence of the Hall resistance on the external field and a constant, non-zero device magnetoresistance, von Klitzing's results yielded

- the formation of plateaux in the Hall resistance around certain magnetic fields with quantized values

$$R_{\mathrm{H}} = \frac{h}{e^2}\frac{1}{n}, \quad n = 1, 2, 3, \dots. \tag{1}$$

- vanishing magnetoresistance in the same range of magnetic fields in which the Hall plateaux formed.

This phenomenon is referred to as the Integer Quantum Hall effect, in contrast to the Fractional Quantum Hall effect, which was subsequently discovered by Störmer [2]. The positions of magnetoresistance peaks can be related to the Landau energies

$$E_n = (n + \frac{1}{2})\hbar\omega_c, \quad n = 0, 1, 2, \dots, \tag{2}$$

which constitute the discrete spectrum of a quantum particle with charge e and mass m in a magnetic field, undergoing cyclotron motion with frequency $\omega_c = eB/m$.

Hall measurements at even higher magnetic fields and samples with larger electron mobility ("cleaner" samples) show plateaux also at non-integer fractional fillings $\nu = p/q$, where $p, q = 1, 2, 3, \ldots$. Although similar in outcome, fractional quantum Hall measurements do not fit in the standard theories for the explanation of the integer effect. We will simply ignore them for the moment and discuss the integer effect in greater detail.

A useful reformulation of the effect is obtained by inverting the resistivity tensor into the conductivity tensor. Away from the Landau energies E_n, one gets

$$\sigma_{xx} = 0, \tag{3}$$

$$\sigma_{xy} = \nu \frac{e^2}{h} \tag{4}$$

and

$$\sigma_{xx} = \frac{e^2}{2h}, \tag{5}$$

$$\sigma_{xy} = \left(\nu + \frac{1}{2}\right) \frac{e^2}{h} \tag{6}$$

in the vicinity of E_n.

It has been found that the Hall plateaus are extremely stable against sample quality, geometry and other microscopic details, and can be reproduced with a precision of the order 10^{-10}. The plateau value

$$R_{\mathrm{K}} = h/e^2 = (25812.807572)\Omega \tag{7}$$

has therefore become the metrological resistance standard, and because it is comparatively easy and to enormous precision to determine, an actual discussion is to include it in the SI set of standard units, along with dropping the Ampere as a standard current unit.

Apart from this practical relevance, a fundamental question rises: Why do different samples with different surface conditions, damage at contact regions, bulk inhomogeneities and other defects produce even quantitatively the same results ?

Obviously, the proper explanation is connected with the rather peculiar motion of two-dimensional conduction band electrons in their quantum limit, i.e. vanishing temperature and strong magnetic field. In the following, we will give a brief overview over the intuitive pictures taken to understand the integer quantum Hall effect.

(a)   (b)
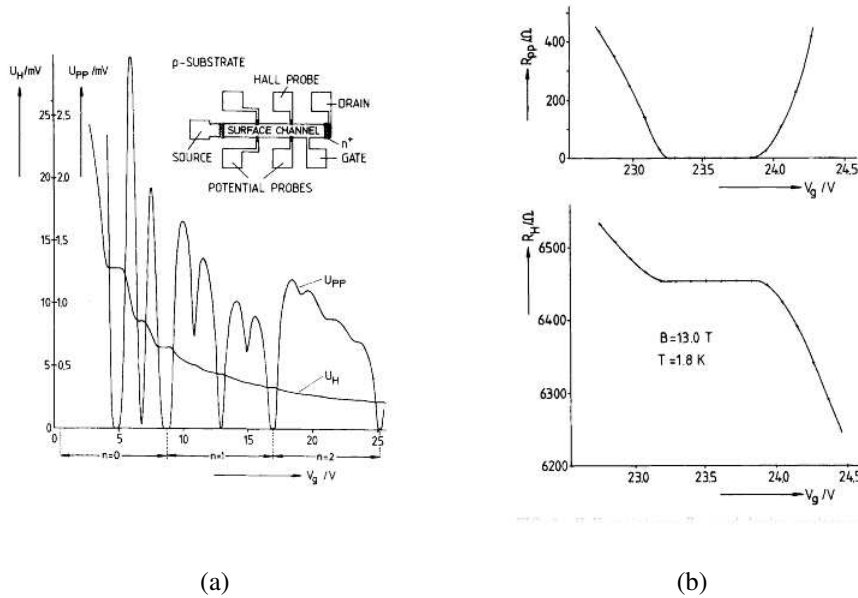
Figure 1: (a) Recordings of the Hall voltage U_H, and the voltage drop between the potential probes, U_pp, as a function of the gate voltage V_g at $T = 1.5$ K. The constant magnetic field (B) is 18 T and the source drain current, I, is 1 μA. The inset shows a top view of the device with a length of $L = 400$ μm, a width of $W = 50$ μm, and a distance between the potential probes of $L_\mathrm{pp} = 130$ μm. (b) Hall resistance R_H, and device resistance R_pp, between the potential probes as a function of the gate voltage V_g in a region of gate voltage corresponding to a fully occupied, lowest ($n = 0$) Landau level. The plateau in R_H has a value of 6453.3 ± 0.1 Ω. The geometry of the device was $L = 400$ μm, $W = 50$ μm, and $L_\mathrm{pp} = 130$ μm; $B = 13T$. Pictures and captions taken from von Klitzing *et. al.*, Phys. Rev. Lett. (1980) [1].

Disorder-induced localization

A two-dimensional electron system created in a semiconductor is influenced not only by the artificial electrostatic potential created in the semiconductor in order to freeze one component of the electron motion, or externally applied electric or magnetic fields, but also by the effects of crystal defects, impurities or interface roughnesses. These inhomogeneities (among others) are summarized in the assumption of "disorder" in the semiconductor. They are characterized by an immobile electrostatic potential with an arbitrary shape.

A naive view on the Hall plateaux suggests insulating electronic states everywhere except at selected positions in magnetic field or energy, which correspond to extended, "metallic" states. In an insulating state, an electron is stripped off the possibility to move

through the whole sample and thus contribute to charge transport between the contacts, since it is localized to a finite area.

It has been shown that electrons moving in such a random disorder potential, presumably also without mutual Coulomb interaction, are more or less localized [3–6]. In other words, the probability to find an electron in a localized states is finite only in a small area of the sample, independent of strength and microscopic detail of the disorder. This absence of a metallic phase in two-dimensional electron systems has been studied extensively in the context of the scaling theory of localization, which started with the seminal works of Anderson and cow-workers [3, 7] and has continued up to now (see [8] for a recent overview of the topic).

The lack of a truly extended and thus conducting 2D state is often described by the ”beta”- function $\beta(g)$, which relates the dimensionless conductance parameter g to the linear system size L via

$$\frac{d \ln g}{d \ln L} = \beta\left(g(L)\right).\tag{8}$$

The knowledge of β thus allows for computation of the overall conductance in the thermodynamic limit $L \rightarrow \infty$. Its explicit form depends on the underlying statistical ensemble, which can be *orthogonal* (time-reversal symmetry is given), *unitary* (time-reversal symmetry is broken e.g. by an external magnetic field) or *symplectic* (disorder is associated with spin-flip scattering or spin-orbit interaction). A perturbative calculation at $B = 0$ yields $\beta(g) \propto g^{-1}$ [9], which implies that the orthogonal ensemble is dominated by a localization length

$$\xi \propto e^{g_0},\tag{9}$$

with the mean-field conductance parameter g_0. For strong disorder, g_0 is small, and consequently the spatial extend of the wavefunction is small. This strong localization is exponentially lifted for weak disorder and g_0 large, but still is ξ finite. The transition between these two regimes is merely a crossover, with no (quantum) critical point separating strong and weak localization phases.

The application of an external magnetic field breaks the time-reversal symmetry and thus requires the usage of the unitary ensemble. The localization length now behaves as

$$\xi \propto e^{g_0^2},\tag{10}$$

which results in an even weaker, but yet finite localization as compared to the orthogonal case. Again, at least a crossover in terms of g_0 is expected which is unlikely to lead to the formation of well defined resistance plateaux. One must therefore conclude that the demanded existence of 2D extended states is non-perturbative, which in turn might imply that the quantum Hall plateau transition is in fact a quantum phase transition including quantum critical points in the magnetic field which separate phases of localized and extended states.

Although there is up to now no closed and comprehensive analytical theory for this phenomenon, numerical calculations [10, 11] have established phenomenologically a power law divergence

$$\xi(E) \propto |E - E_n|^{-\tilde{\nu}} \tag{11}$$

of the localization length at the critical energies. The most successful approach to investigate scaling behaviour of the localization length is the method of finite-size scaling. The localization length ξ_M is calculated in a finite strip of width M, solving the Schrödinger equation for the disordered Hamiltonian with magnetic field via transfer matrix or recursive Green's functions techniques, and extrapolates to the infinite system size localization length via the scaling hypothesis

$$\frac{\xi_M(E)}{M} = f\left(\frac{M}{\xi(E)}\right), \tag{12}$$

with a universal scaling function $f(x)$ with asymptotic limits $f(x \ll 1) \approx$ const. and $f(x \gg 1) \propto 1/x$. Many slightly different models of disorder with differing concentration and correlation length have been tested by this scaling approach [10–14]. They all found

$$\tilde{\nu} = 2.34 \tag{13}$$

for the lowest Landau level. On the contrary, the exponent for the next Landau level ranges between roughly $2 - 6$, depending on the range of the scatterers, if they exceed the smallest length scale $l_B = \sqrt{\hbar/(eB)}$, the magnetic length, or if disorder coupling between the Landau levels is taken into account. However, calculations in higher bands are less accurate.

The universality of the critical exponent at least in the lowest Landau level has further support from calculations within a quantum percolation network [15–17]. In the percolation scenario, the disorder varies slowly (on length scales $d \gg l_B$) and the center-of-mass coordinate ("guiding center") of the electron wavefunction drifts along equipotential lines. If treated classically [18], one can identify a single percolation threshold at the critical energy, where the percolating cluster covers the entire area. The corresponding classical critical exponent is obtained as $\tilde{\nu} = 4/3 \approx 1.33$.

Quantum mechanics can be introduced via tunneling processes in the percolation picture. A network is set up with its nodes representing saddle points of the disorder potential and its links being the equipotential contours. Transfer matrix calculations [16, 17] result in the expected exponent $\tilde{\nu} = 2.5 \pm 0.5$. The result has been further supported by classical arguments including quantum tunneling correction [19], with $\tilde{\nu} = 7/3 \approx 2.33$.

Apart from the phase transition of static properties like the localization length, most quantum phase transitions [5, 20] are driven also by dynamical effects resembling quantum fluctuations. This is quantified by a dynamical exponent z, which governs the

fluctuation of the critical state. The dynamical exponent is obtained by probing the transition at finite temperatures and/or by applying external AC electric fields with finite frequency. It turned out, that experiments performing temperature and frequency scaling [21–26] found either $z = 2$, associated with diffusive behaviour of non-interacting electrons in two dimensions, or $z = 1$ indicating anomalous diffusion, which is commonly attributed to electron-electron interaction. So far, a single experiment [27] indicated no scaling behaviour at all. Still, the issue of dynamical scaling and the mechanisms that can lead to a reduction of the dynamical critical exponents, remains one of the most important, yet unsolved problems in the theory for the integer plateau transition.

Electron-electron interaction is also important for the explanation of the emergence of fractional plateaux. It has been suggested for low fractional fillings, for instance $\nu = 1/5$, that in this regime occurs from a Wigner crystal [28] with highly correlated electrons which are frozen into a regular lattice, to an incompressible liquid state [29, 30]. Here, the Wigner crystal is identified as an insulating state, entirely determined by Coulomb correlation, with an activation gap much smaller than the gap for the integer transition (the cyclotron energy). The mechanisms of these fractional quantum Hall phase transitions are somewhat more involved than the disorder-driven localization and not subject of this thesis. However, a consistent theory unifying the effect of correlation and disorder induced localization has yet to be formulated.

We continue with another model for the integer transition, which takes into account the finite boundaries of a semiconductor sample.

Edges and the existence of extended states

Another approach to the integer quantum Hall effect was formulated by Laughlin [31] and further extended by Halperin [32]. A Corbino disk, a circular (semi)conducting sheet with a hole in the center, is placed in a magnetic field perpendicular to the plane of the disk. In this setup, the directions of the currents along the inner and outer edges are opposite to each other. As long as the Fermi levels are equal at both edges, they do not add any net current around the annulus. A mismatch of the Fermi levels by an amount $e\Delta$ leads to a net current contribution of

$$\delta I = ne^2\Delta/h \qquad (14)$$

resulting from the edge states around the ring, with n an integer number. This contribution is in agreement with the quantized Hall conductance.

This annular geometry can furthermore be used to give an intuitive argument for the existence of extended states in the sample. We have already seen that in infinite two-dimensional samples with, say, not too strong disorder and perpendicular magnetic field, there exist energy ranges with extended states, separated by ranges with localized states and gap regions with vanishing density of states.
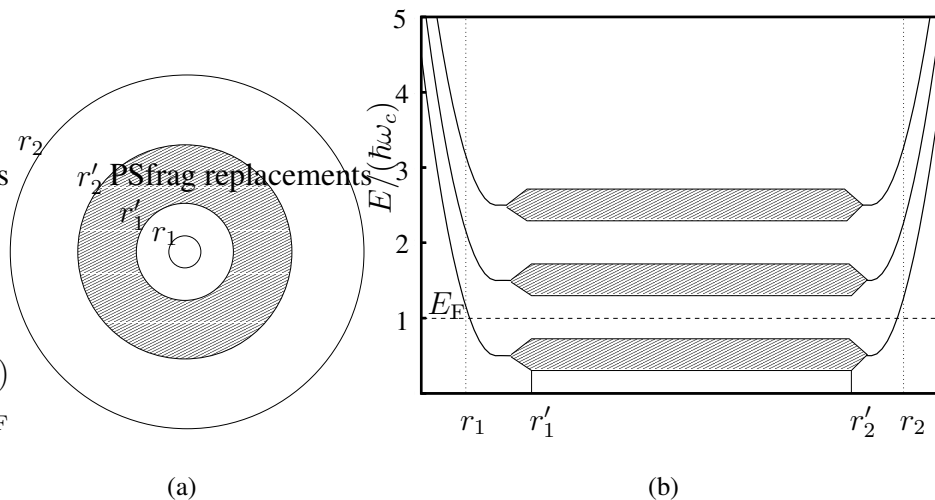
Figure 2: (a) Annulus geometry after Halperin [32]. The shaded area contains a weak disorder potential. (b) Schematic energy spectrum for the annulus in a magnetic field as a function of the distance from the center. The shaded regions indicate the disordered bulk region.

We now consider a flux piercing the center hole of the annulus. Laughlin [31] showed that if the Fermi energy is located outside the bands of extended states, and if the flux Φ threading the hole is increased by a single flux quantum $\phi_0 = h/e$, the resulting effect will be that an integral number n of electrons is transferred from the Fermi level on the outer edge to the Fermi level at the inner edge. If V is the voltage between inner and outer edge and I is the current around the ring, one has to match the work done by the flux change $-I\phi_0$ to the net energy change $-neV$ and thus finds $I/V = ne/\phi_0$. An obvious argument is now to identify the integer n with the number of bands of extended states below the Fermi level. In the following, we divide the annulus in two potential-free edge regions and a bulk region with a weak disorder potential (see Fig. 2a). At r_1 and r_2, we assume hard walls. A schematic energy spectrum for this geometry is depicted in Fig. 2b. The states are grouped in bands due to disorder around the center energies $E_\nu = (\nu + \frac{1}{2})\hbar\omega_c$. Towards the hard wall boundaries, the levels are pushed upward. Without loss of generality, we take the disorder so weak that no states between two Landau levels exist.

Concerning the localization of states in the disordered regions, there are two possibilities: Either, they are localized at all energies with a finite localization length $\xi(E)$, or there exist some delocalized states at certain energies, supposively in the band center.

Halperin [32] gave an argument leading to a caveat with the first option. Assume that the Fermi energy lies close to the cyclotron energy, then all states with energy below are

occupied. The maximal localization length $\xi_{\max}$ is supposed to be much smaller than the bulk width, $\xi_{\max} \ll r_2' - r_1'$. If the flux threading the hole in the center is now adiabatically increased by one flux quantum and no net current is flowing in the ring, this process requires no work in the limit of a very large sample. On the other hand, the wavefunctions in the ordered edge regions will slightly contract due to the change of the magnetic length, which is their characteristic width. Finally, the occupation will slightly change, with one state occupied above the Fermi level, and one state empty below. No energy is paid to achieve the shift in occupation.

However, we have imposed that all states in the disordered region are localized. Hence, there is no transport path across this area, because the localized states remain unchanged by the flux increase [31], apart from a change in phase. An electron removed from the outer edge r_2 must somehow get to a new occupied state at r_2'. Accordingly, the hole near r_1 must be related to the new electron at r_1'. The Fermi level was put far away from the band of disordered states, and, except possibly from localized impurity states resulting from a strong disorder potential with no change in occupation due to flux change, no states in the vicinity of the Fermi energy are available. As a consequence, one would have to pay energy of the order of $\hbar\omega_c$ to force a change of occupation. This would violate the law of conservation of energy. Therefore, delocalized states must exist even in the disordered region of the annulus.

The annular geometry is equivalent to a quantum wire, a quasi-two-dimensional electron gas confined in one spatial direction, with periodic boundary conditions at the open ends. We will discuss such a geometry in a later chapter and, returning to the presented argument, show that a new type of state can exist which couples the edges *without* interfering strongly with the bulk.

This work

In this thesis, we discuss the effect of electron-electron interaction and the influence of spatial confinement on the quantum Hall effect by addressing the following subjects. The first part gives an overview over important effective models for disorder and interaction, which will be used for mainly numerical investigation of the quantum Hall system. Whereas the disorder potential can be treated exactly by numerical diagonalization for reasonable system sizes, one has to find a proper effective model for the electron-electron interaction in order to make the numerics tractable. The straightforward method is the self-consistent Hartree-Fock [33] approximation. Although this kind of approximation neglects direct Coulomb correlations in the ground state, while taking the non-local exchange term exactly into account, the self-consistent quasiparticle potential can be used to extract information about charge distribution and electron-electron contribution to the ground state energy. To make this procedure transparent, we provide an explicit derivation of the Hartree-Fock equations and discuss a proper solution

scheme. We pay special attention to treat the spin degree of freedom correctly in the unrestricted Hartree-Fock approach.

The second part deals with the quantum Hall transition in interacting and non-interacting systems. We investigate the static and the dynamical critical exponent in the lowest Landau level by means of the wavefunctions of the system. The participation ratio, being proportional to the inverse second statistical moment of electron probability density, serves as a measure for localization, with similar power law scaling as the localization length ξ. Although this method is much less accurate than the usual finite-size scaling schemes based on transfer matrix or recursive Green's function methods, we find consistent results for the static critical exponent for various systems including disorder and interaction. Moreover, we treat transport in the regime of linear response by means of the Kubo formula, which grants the possibility to calculate the frequency-dependent conductivity tensor. Employing a scaling analysis of the magnetoconductivity peak width, we estimate the value for the dynamical critical exponent. We investigate if it could be altered from its expected value $z = 2$ in a zero-range white-noise potential, if a long-range disorder potential or a Hartree-Fock type interaction is present.

The third part addresses a recent experiment [34], in which the compressibility of the quantum Hall system was directly measured in dependence of the filling factor. The filling factor can be tuned independently as a function the magnetic field and the particle density in the sample. The outcome of the experiment is rather startling, since it indicates the signatures of correlation effects (Coulomb blockade) in the insulating phases and promotes a constant number of localized states in each Landau level, in contradiction to the single-particle picture with a more or less constant number of extended states at the critical energy and localized states everywhere else, with a field-dependent total number of states. This would irritate the so far consistent single particle scaling explanation of the quantum Hall effect.

We try to illuminate this discrepancy by using a Hartree-Fock approach to calculate the compressibility directly from the Hartree-Fock total energy. We calculate a separate self-consistent field for each combination of electron density and magnetic field. This gives the system the opportunity to "relax " to a new Hartree-Fock ground state and is equivalent to a charge rearrangement due to changes in magnetic field or the reentrance of an additional particle. The resulting compressibility patterns show striking similarity to the reported measurement, at least in the insulating phases. We give comments on the misfits of the Hartree-Fock approach in the band centers and conclude that electron-electron interaction is important for a comprehensive theory of the integer quantum Hall effect. Moreover, we suggest a way to match these results with the established scaling picture.

The remaining part introduces an additional lateral confinement to the system. In such modeled quantum wires, we study the quantum phase diagram as function of wire width and energy. We find zero temperature discontinuous transitions in the two-

terminal conductance between integer plateau values and (exactly) zero. Characteristic states are found which are superpositions of edge states with opposite chirality. These states have the properties of nonchiral edge states and differ significantly from bulk extended edge states, 2D localized, quasi-1D localized, and 2D critical states. The role of coupling between edge states and bulk extended states, which is omitted in Halperin's argument, is elucidated.

Finally, we comment a recent experiment [35], in which the enhancement of the electron g-factor in quantum wires is studied. It was found, according to earlier theories [36], that the enhancement is suppressed in the vicinity of transitions from the spin-polarized to the mixed state. We show that the shape of the transition is qualitatively altered, if the Hartree contribution to the self-energy is taken into account, which has been neglected before [36].

Part I

Electrons in a quantizing magnetic field: Models for disorder and interaction

Electrons in a quantizing magnetic field and disorder

In this chapter, we present a detailed discussion of models and methods we use to describe a quantum Hall system of interacting electrons.

1.1   The free electron in a quantizing magnetic field

A single electron in the x-y-plane and a perpendicular magnetic field $\mathbf{B}$ is described by the Hamiltonian

$$H_0 = \frac{(\mathbf{p} + e\mathbf{A})^2}{2m^*}, \tag{1.1}$$

where $\mathbf{p}$ is the linear momentum e the elementary charge, m^* the electron mass and $\mathbf{A}$ the magnetic vector potential. In the Landau gauge $\mathbf{A} = (0, Bx, 0)$, the Schrödinger equation

$$H_0 = |\phi\rangle = E |\phi\rangle \tag{1.2}$$

yields the solution

$$E_n = (n + \frac{1}{2})\hbar\omega_c, \quad n = 0, 1, 2, \ldots \tag{1.3}$$

for the eigenenergies which are discrete and identified by the Landau level index n and

$$\tilde{\phi}_{nX}(\mathbf{r}) \equiv \langle \mathbf{r}| \phi\rangle = \frac{1}{\left(l_B L_y \sqrt{\pi} 2^n n!\right)^{1/2}} e^{-\frac{(x-X)^2}{2l_B^2}} H_n\left(\frac{x-X}{l_B}\right) e^{-\frac{iXy}{l_B^2}} \tag{1.4}$$

for the infinitely degenerate eigenfunctions. $\omega_c = eB/m$ is the cyclotron frequency and $l_B = \hbar/(eB)$ the magnetic length. $X = -kl_B^2$ with a wavenumber $k = p/\hbar$

is often referred to as the guiding center or center-of-mass coordinate of the Landau wavefunction (1.4). $H_n(x)$ are Hermite polynomials.

We observe that the Landau wavefunction resembles an oscillatory motion in the x-direction, described by oscillator wavefunctions

$$\chi(x) \propto H_n\left((x - X)/l_B\right) \exp\left(-(x - X)^2/2l_B^2\right),\tag{1.5}$$

and a free motion in the y-direction governed by a plane wave $\exp(-iXy/l_B)$. This function can only be normalized in a system of finite length L_y.

Using periodic boundary conditions in y-direction, the wavenumber then is quantized as $k = 2\pi/L_y \times j$ with an arbitrary integer j. If one further restricts the transversal direction by requiring $X \in [-L_x/2, L_x/2]$, the number of states per Landau level n becomes finite and is given by

$$N_\phi = \frac{L_x L_y}{2\pi l_B^2} \equiv \frac{\varphi}{\varphi_0},\tag{1.6}$$

which equals the number of magnetic flux quanta $\varphi_0 = h/e$ contained in the total flux $\varphi = BL_x L_y$. One defines the filling factor of N electrons as

$$\nu = \frac{N}{N_\phi}.\tag{1.7}$$

The finite set of Landau wavefunctions serves as a suitable basis for representing additional potentials in the Hamiltonian. In cases where no lateral confinement potential is present, it is helpful to assume periodic boundary conditions also in the x-direction. These boundary conditions are met by the periodic Landau functions

$$\phi_{nX}(\mathbf{r}) = \sum_{m \in \mathbb{Z}} \tilde{\phi}_{n,X+mL_x}(\mathbf{r})\tag{1.8}$$

which remain orthonormal in the unit cell of the periodic system [37, 38].

1.2 Models of disorder

In general, real semiconductor samples are not perfect crystals. Lattice deformations, surface roughness and substitution of lattice atoms by other atoms deform the regular electrostatic potential landscape within the crystal. Electronic properties of the semiconductor thus depend on the present disorder potential, which significantly determines transport coefficients via scattering and localization processes.

In order to model effects of disorder, one often uses artificial and spatially random potentials instead of solving a complicated electrostatic problem employing doped

atoms on a grid. Within these models, scattering strength and range are well controlled and can be tuned e.g. to compare low- and high-mobility situations.

In the following, we will discuss certain models of disorder and their representation in terms of Landau functions, which is required in our investigation of the quantum Hall problem.

1.2.1   Uncorrelated disorder

A simple realization of disorder is a random distribution of N_{imp} pointlike scatterers

$$V_{\mathrm{imp}}(\mathbf{r}) = \sum_{i}^{N_{\mathrm{imp}}} V_i \, \delta(\mathbf{r} - \mathbf{r}_i) \tag{1.9}$$

with a characteristic energy amplitude $V_i \in [-V_0/2, V_0/2]$, located at random positions $\mathbf{r}_i$ in the sample. This type of disorder potential is mathematically easy to handle and has been widely studied in the literature. Applied to the 2DEG in magnetic fields, the degeneracy of the Landau levels is lifted and Landau bands are formed. The Landau level band width can be obtained in self-consistent Born approximation [39] as

$$\Gamma = \left(N_{\mathrm{imp}} V_0^2 l_B^2 \right)^{\frac{1}{2}} \tag{1.10}$$

and is independent of the Landau level index. This approximation gives the rather crude semi-circle result for the density of states:

$$D(E) = \frac{1}{\pi^2 l_B^2 \Gamma} \left[1 - \left(\frac{E - E_n}{\Gamma} \right)^2 \right]^{1/2}, \tag{1.11}$$

compared to the exact result [40]

$$D(E) = \frac{\sqrt{2}}{\pi^2 l_B V_0} \frac{e^{\varepsilon^2}}{1 + 4\pi \left(\mathrm{erf}(\varepsilon) \right)^2}, \ \varepsilon = \sqrt{2\pi} l_B (E - E_0)/V_0, \tag{1.12}$$

with $\mathrm{erf}(b) = \int_0^b dx \exp(-x^2)$. Nevertheless, equation (1.10) is often used as a characteristic disorder energy scale.

1.2.2   Correlated disorder

A disorder setup with a long-range correlation is required in modeling high mobility samples; the electron can travel without being scattered over a length d. On this scale,
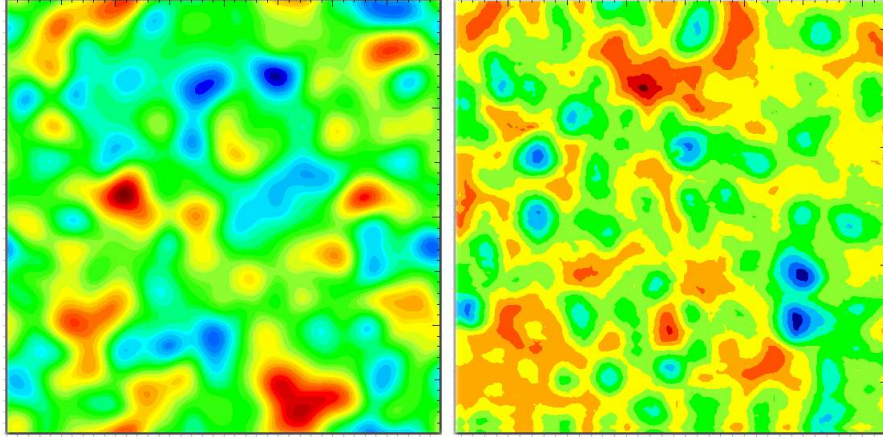
Figure 1.1: Left panel: Gaussian model of a random disorder potential after equation (1.13). Right panel: STM measurement of a potential landscape in a GaAs/GaAlAs sample. Courtesy of Jan Klijn.

the potential is only slowly varying. A convenient realization is given by a random superposition of Gaussian scatterers

$$V_{\text{imp}}(\mathbf{r}) = \sum_{i}^{N_{\text{imp}}} V_i \, e^{-(\mathbf{r}-\mathbf{r}_i)^2/d^2} \tag{1.13}$$

with a characteristic energy amplitude $V_i \in [V_0/2, V_0/2]$ located at random positions $\mathbf{r}_i$ in the sample. The Landau representation is conveniently expressed in terms of Fourier components as

$$\langle nX \mid V_{\text{imp}}(\mathbf{r}) \mid n'X' \rangle = \sum_{\mathbf{q}} V_{\text{imp}}(\mathbf{q}) \langle nX \mid e^{-i\mathbf{q}\mathbf{r}} \mid n'X' \rangle \tag{1.14}$$

The remaining matrix element $\langle nX \mid e^{i\mathbf{q}\mathbf{r}} \mid n'X' \rangle$ can be found in appendix A. For long-range scatterers, the bandwidth depends on the Landau level index [39] and is given for the lowest Landau level as

$$\Gamma_d = \frac{\Gamma}{(1 + d^2/l_B^2)^{1/2}}. \tag{1.15}$$

Fig. 1.1 shows a comparison between a random potential calculated using equation (1.13) with periodic boundary conditions, and a potential landscape measured with a scanning force microscope. We see, that the essential features of the real potential are well reproduced in the artificial model. For numerical calculations, it is helpful for correlated and uncorrelated disorder to choose equal numbers of attractive ($V_i < 0$) and

repulsive ($V_i > 0$) scatterers. This produces on the configurational average a density of states which is symmetric around the band centers E_n ("particle-hole symmetry"). This can be useful to detect the energy range in which quantum critical phenomena occur.

Electron-electron interaction

In this chapter, we discuss extensively the self-consistent Hartree-Fock approximation, which we use to treat electron-electron interaction. Although conceptually simple, it requires some effort to formulate the approximation for a given problem. In order to make the procedure transparent, we give a textbook-like derivation of the self-consistent Hartree-Fock equations and discuss the subtleties of its implementation, with a special attention to spin-dependent Hamiltonians.

2.1   Many-particle states

A generic N-particle Hamiltonian can be written

$$\mathcal{H} = \sum_{i=1}^{N} H(\mathbf{p}_i, \mathbf{r}_i) + \sum_{i=1}^{N} \sum_{j>i}^{N} V_{e-e}(\mathbf{r}_i - \mathbf{r}_j), \qquad (2.1)$$

and consists of a single-particle term $H(\mathbf{p}, \mathbf{r})$, which depends only on a single particle coordinate set $(\mathbf{r}, \mathbf{p})$, and an interaction term $V_{e-e}(\mathbf{r}_i - \mathbf{r}_j)$ describing the interaction between particles i and j. The solution of the Schrödinger equation is a complete set of many-particle eigenvalues and corresponding wavefunctions $\Psi(\mathbf{r}_1, \ldots, \mathbf{r}_N)$. A usual way of representing the many-body wavefunction for Fermions (at least in finite systems) is by means of Slater determinants. If a complete set of single-particle wave functions $\psi_i(\mathbf{r})$ is known, for instance by solving the single-particle Schrödinger equation for H, one can write

$$\Psi(\mathbf{r}_1, \ldots, \mathbf{r}_N) = c_0 \ket{\Phi_0} + \sum_{ar} c_a^r \ket{\Phi_a^r} + \sum_{arbs} c_{ab}^{rs} \ket{\Phi_{ab}^{rs}} + \ldots, \qquad (2.2)$$

where

$$\Phi = \begin{vmatrix} \psi_1(\mathbf{r}_1) & \ldots & \psi_1(\mathbf{r}_N) \\ \vdots & \ddots & \vdots \\ \psi_N(\mathbf{r}_1) & \ldots & \psi_N(\mathbf{r}_N) \end{vmatrix}. \tag{2.3}$$

In $|\Phi_0\rangle$, the N single particle functions $\psi_i(\mathbf{r})$ with the lowest energies enter. In $|\Phi_a^r\rangle$, the ast component of $|\Phi_0\rangle$ is replaced by $\psi_r(\mathbf{r})$, which is so far not present in $|\Phi_0\rangle$, and so on. The object (2.3) is called Slater determinant. A complete set of Slater determinants span the many-particle Hilbert space and fulfill the antisymmetry requirements on the wavefunction for Fermions. Unfortunately, the number of determinants to be taken into account grows exponentially with particle number and single-particle basis set size. Therefore, its use in numerical calculations is limited.

2.2 The Hartree-Fock approximation

The solution of the full many body-problem is possible for only very small systems, whose corresponding Hilbert space can be spanned by few Slater determinants, and an accordingly small number of particles . For larger systems with a variety of many-electron states and a larger number of particles involved, one is forced to make approximations.

The most systematic approximation is perturbation theory in the interaction. In this framework, approximations are well defined in any given order and can be systematically improved. The first order in perturbation theory leads naturally to the mean-field approximation, in which the two-body electron interaction is mapped onto an effective single-particle potential. This leads to corrections to the one-particle energies and wavefunctions which have to be obtained in a self-consistent manner. The corresponding single-particle Schrödinger equation is known as Hartree-Fock equation.

In this section we will derive the self-consistent Hartree-Fock equations following [41] and show that they are variational, thus leading to the minimal ground state energy in the chosen approximation. This will help in the interpretation of the results.

2.2.1 Variational derivation of the Hartree-Fock equations

The solution of the Schrödinger equation for the generic many-body Hamiltonian (2.1) can be expanded in the complete orthonormal basis of Slater determinants formed by a given complete orthonormal set of single-particle spin-orbitals $\{\chi_a\}$. The first step in the Hartree-Fock approximation is to assume that the N-electron ground state is given by a *single* Slater determinant

$$|\Psi_0\rangle = |\chi_1\chi_2\cdots\chi_a\chi_b\cdots\chi_N\rangle \tag{2.4}$$

instead of a linear combination of the complete set. Then the ground state energy

$$E_0 = \langle \Psi_0 \mid \mathcal{H} \mid \Psi_0 \rangle \tag{2.5}$$

is a functional of the spin-orbitals $\{\chi_a\}$. The ground state energy is expected to be minimal. Thus, in order to make the approximation as good as possible, we have to minimize $E_0[\{\chi_a\}]$ with the constraint

$$\langle a \mid b \rangle - \delta_{ab} = 0, \tag{2.6}$$

because the spin-orbitals are to remain orthonormal.

We use the Lagrange method of undetermined multipliers ϵ_{ab} and define the functional

$$\mathcal{L}[\{\chi_a\}] = E_0[\{\chi_a\}] - \sum_{a=1}^{N} \sum_{b=1}^{N} \epsilon_{ba} (\langle a \mid b \rangle - \delta_{ab}) \tag{2.7}$$

The expectation value E_0 is written explicitly in terms of spin-orbitals

$$E_0[\{\chi_a\}] = \sum_{a=1}^{N} \langle a \mid h \mid a \rangle + \frac{1}{2} \sum_{a=1}^{N} \sum_{b=1}^{N} (\langle ab \mid ab \rangle - \langle ab \mid ba \rangle) \tag{2.8}$$

with the single-particle Hamiltonian h and the two-electron integrals

$$\langle ij \mid kl \rangle = \int d\mathbf{r}_1 \int d\mathbf{r}_2 \; \chi_i^*(\mathbf{r}_1)\chi_j^*(\mathbf{r}_2)V_{12}\chi_k(\mathbf{r}_1)\chi_l(\mathbf{r}_2), \tag{2.9}$$

and the interaction potential $V_{12} = V(|\mathbf{r}_1 - \mathbf{r}_2|)$.

Minimizing E_0 with the constraint (2.6) is equivalent to minimizing (2.7). Therefore, for small variations $\delta\chi_a$ in the spin-orbitals, we find for the variation of (2.7)

$$\delta L = \delta E_0 - \sum_{a=1}^{N} \sum_{b=1}^{N} \epsilon_{ba}\delta\langle a \mid b \rangle \equiv 0 \tag{2.10}$$

It follows

$$\delta\langle a \mid b \rangle = \langle \delta\chi_a \mid \chi_b \rangle + \langle \chi_a \mid \delta\chi_b \rangle \tag{2.11}$$

and thus

$$
\begin{aligned}
\sum_{a=1}^{N} \sum_{b=1}^{N} \epsilon_{ba} (\langle \delta\chi_a \mid \chi_b \rangle + \langle \chi_a \mid \delta\chi_b \rangle) &= \sum_{ab} \epsilon_{ba} \langle \delta\chi_a \mid \chi_b \rangle + \sum_{ab} \epsilon_{ab} \langle \chi_b \mid \delta\chi_a \rangle \\
&= \sum_{ab} \epsilon_{ba} \langle \delta\chi_a \mid \chi_b \rangle + \sum_{ab} \epsilon_{ba}^* \langle \delta\chi_a \mid \chi_b \rangle^* \\
&= \sum_{ab} \epsilon_{ba} \langle \delta\chi_a \mid \chi_b \rangle + \text{complex conjugate.}
\end{aligned}
\tag{2.12}
$$

For the variation of the ground state energy we get

$$
\begin{aligned}
\delta E_0 &= \sum_{a=1}^{N} \langle \delta\chi_a \mid h \mid \chi_a \rangle + \langle \chi_a \mid h \mid \delta\chi_a \rangle \\
&+ \frac{1}{2} \sum_{a=1}^{N} \sum_{b=1}^{N} \langle \delta\chi_a\chi_b \mid \chi_a\chi_b \rangle + \langle \chi_a\chi_b \mid \delta\chi_a\chi_b \rangle + \langle \chi_a\delta\chi_b \mid \chi_a\chi_b \rangle + \langle \chi_a\chi_b \mid \chi_a\delta\chi_b \rangle \\
&- \frac{1}{2} \sum_{a=1}^{N} \sum_{b=1}^{N} \langle \delta\chi_a\chi_b \mid \chi_b\chi_a \rangle + \langle \chi_a\chi_b \mid \delta\chi_b\chi_a \rangle + \langle \chi_a\delta\chi_b \mid \chi_b\chi_a \rangle + \langle \chi_a\chi_b \mid \chi_b\delta\chi_a \rangle \\
&= \sum_{a=1}^{N} \langle \delta\chi_a \mid h \mid \chi_a \rangle + \sum_{a=1}^{N} \sum_{b=1}^{N} \left(\langle \delta\chi_a\chi_b \mid \chi_a\chi_b \rangle - \langle \delta\chi_a\chi_b \mid \chi_b\chi_a \rangle \right) + \text{compl. conj.}
\end{aligned}
$$

$$\tag{2.13}$$

The linear variation in $\mathcal{L}$ now becomes

$$
\begin{aligned}
\delta\mathcal{L} &= \sum_{a=1}^{N} \langle \delta\chi_a \mid h \mid \chi_a \rangle + \sum_{a=1}^{N} \sum_{b=1}^{N} \langle \delta\chi_a\chi_b \mid \chi_a\chi_b \rangle - \langle \delta\chi_a\chi_b \mid \chi_b\chi_a \rangle \\
&- \sum_{a=1}^{N} \sum_{b=1}^{N} \epsilon_{ba} \langle \delta\chi_a \mid \chi_b \rangle + \text{complex conjugate} \\
&\equiv 0
\end{aligned}
$$

$$\tag{2.14}$$

We now introduce the notation

$$\chi_a(\mathbf{r}_1, s_1) \equiv \chi_a(1) \tag{2.15}$$

for a spin-orbital depending on position $\mathbf{r}$ and spin s. The Coulomb operator due to a particle in spin-orbital $\chi_b(2)$ which interacts via the potential V_{12} with a particle in spin-orbital $\chi_a(1)$ can be written as

$$\mathcal{J}_b(1)\chi_a(1) = \left[\sum_{s_2} \int d\mathbf{r}_2 \chi_b^*(2) V_{12} \chi_b(2) \right] \chi_a(1), \tag{2.16}$$

the non-local exchange operator as

$$\mathcal{K}_b(1)\chi_a(1) = \left[\sum_{s_2} \int d\mathbf{r}_2 \chi_b^*(2) V_{12} \chi_a(2) \right] \chi_b(1). \tag{2.17}$$

Using these operators, equation (2.14) becomes

$$
\begin{aligned}
\delta L &= \sum_{a=1}^{N}\sum_{s_1}\int d\vec{r}_1 \delta\chi_a^*(1)\left[h(1)\chi_a(1) + \sum_{b=1}^{N}(\mathcal{J}_b(1) - \mathcal{K}_b(1))\chi_a(1) - \sum_{b=1}^{N}\epsilon_{ba}\chi_b(1)\right] \\
&+ \quad \text{complex conjugate} \\
&= \quad 0
\end{aligned} \tag{2.18}
$$

The variation $\delta\chi_a^*(1)$ is infinitesimal small, but arbitrary. Therefore, the expression in square brackets must vanish for all a:

$$
\left[h(1) + \sum_{b=1}^{N}\mathcal{J}_b(1) - \mathcal{K}_b(1)\right]\chi_a(1) = \sum_{b=1}^{N}\epsilon_{ba}\chi_b(1) \quad a = 1, 2, \ldots, N \tag{2.19}
$$

The quantity in square brackets is called Fock operator $f(1)$; the equation for the spin-orbitals takes the form

$$
f(1)\left|\chi_a\right\rangle = \sum_{b=1}^{N}\epsilon_{ba}\left|\chi_b\right\rangle . \tag{2.20}
$$

This result is not a standard eigenvalue equation and thus difficult to solve. The reason is in the variational ansatz, since any single-determinant wavefunction is not uniquely determined by minimizing the energy expectation value; mixing the spin-orbitals among themselves, for instance, does not change the expectation value (2.5). Consequently, we have to find a canonical form of the Hartree-Fock equation, which can be achieved by unitary transformations.

2.2.2 The canonical Hartree-Fock equations

We define a new set $\{\chi_a'\}$

$$
\chi_a' = \sum_b \chi_b U_{ba} \tag{2.21}
$$

by a unitary transformation $\mathbf{U}$. Since $\mathbf{U}^\dagger = \mathbf{U}^{-1}$, orthonormality is conserved. The single-determinant many-body wavefunction $\left|\Psi_0\right\rangle$ can be written as

$$
\left|\Psi_0\right\rangle = (N!)^{-1/2}\det(\mathbf{A}) \tag{2.22}
$$

with

$$
\mathbf{A} = \begin{pmatrix} \chi_1(1) & \cdots & \chi_N(1) \\ \vdots & \ddots & \vdots \\ \chi_1(N) & \cdots & \chi_N(N) \end{pmatrix} \tag{2.23}
$$

The matrix $\mathbf{A}'$ of transformed spin-orbitals has thus the determinant

$$\det(\mathbf{A}') = \det(\mathbf{U})\det(\mathbf{A}) \tag{2.24}$$

and also

$$|\Psi_0'\rangle = \det(\mathbf{U})\,|\Psi_0\rangle \tag{2.25}$$

The determinant of a unitary matrix is at most a phase factor $e^{i\beta}$, because

$$\det(\mathbf{U}^\dagger\mathbf{U}) = \det(\mathbf{U}^\dagger)\det(\mathbf{U}) = \det(\mathbf{U})^*\det(\mathbf{U}) = |\det(\mathbf{U})|^2 = \det(\mathbf{1}) = 1 \tag{2.26}$$

Any expectation value of a single Slater determinant is accordingly invariant under a unitary transformation of the spin-orbitals it is constructed from.

We will now use this invariance to simplify equation (2.20) by choosing a particular set of spin-orbitals, in which equation (2.20) appears as an eigenvalue equation.

The Coulomb operator is transformed as

$$
\begin{aligned}
\sum_a \mathcal{J}_a' &= \sum_a \sum_{s_2} \int d\mathbf{r}_2 \chi_{a'}^*(2) V_{12} \chi_{a'}(2) \\
&= \sum_{bc} \left[\sum_a U_{ba}^* U_{ca}\right] \sum_{s_2} \int d\mathbf{r}_2 \chi_b^*(2) V_{12} \chi_c(2) \\
&= \sum_b \sum_{s_2} \int d\mathbf{r}_2 \chi_b^*(2) V_{12} \chi_b(2) \\
&= \sum_b \mathcal{J}_b
\end{aligned}
\tag{2.27}
$$

and thus invariant under unitary transformations of the spin-orbitals. The same holds in equivalent manner also for the exchange operator and the Fock operator. Therefore, the spectral properties also remain unchanged.

We now investigate the effect on the Hartree-Fock equation. According to (2.20), the matrix elements of the Fock operator can be written as

$$\langle\chi_c\mid f\mid\chi_a\rangle = \sum_{b=1}^{N} \epsilon_{ba}\langle\chi_c\mid\chi_b\rangle = \epsilon_{ca} \tag{2.28}$$

In terms of the transformed spin-orbitals we have

$$
\begin{aligned}
\epsilon_{ab}' &= \sum_{s_1} \int d\mathbf{r}_1 \chi_a^{*\,'}(1) f(1) \chi_b'(1) \\
&= \sum_{cd} U_{ca}^* U_{db} \sum_{s_1} \int d\mathbf{r}_1 \chi_c^*(1) f(1) \chi_d(1) \\
&= \sum_{cd} U_{ca}^* \epsilon_{cd} U_{db}
\end{aligned}
\tag{2.29}
$$

This is in matrix form

$$\epsilon' = \mathbf{U}^\dagger \epsilon \mathbf{U} \tag{2.30}$$

By default, ϵ is Hermitian, and there always exists a unique unitary matrix $\mathbf{U}$ which diagonalizes ϵ. Then there must exist a set of spin-orbitals $\{\chi'_a\}$ such that ϵ is diagonal. This set is called *canonical* and uniquely determined via

$$f\,|\chi'_a\rangle = \epsilon'_a\,|\chi'_a\rangle \tag{2.31}$$

In the following, we will drop the primes and refer to (2.31) as the Hartree-Fock equations. Due to the complicated form of the Fock operator, the Hartree-Fock equations are coupled integro-differential equations which in most cases cannot be solved in closed form. Instead, one tries to expand the spin-orbitals into a suitable set of basis functions consistent with given boundary conditions in order to transform (2.31) into an algebraic matrix equation. The matrix equation can be solved numerically. The appropriate procedure will be outlined in section 2.3.

2.3   The self-consistent field procedure

2.3.1   Restricted and unrestricted spin orbitals

Following the above discussion, one can assume the one-particle wavefunctions as spin orbitals. The most simple approach is to assume

$$\chi_i(\mathbf{x}) = \begin{cases} \psi_i(\mathbf{r})\alpha(s) \\ \psi_i(\mathbf{r})\beta(s) \end{cases} \tag{2.32}$$

In that case, a spin-up orbital differs from a spin-down orbital only in the spinor, but not in the spatial part of the wavefunction. In other words, each spatial orbital with a certain energy is doubly occupied with a spin-up and a spin-down orbital. These wavefunctions are often referred to as restricted spin-orbitals (or RHF-wavefunctions).

This description holds well if no spin-dependent operators appear in the Hartree-Fock Hamiltonian. However, if some kind of symmetry break occurs, the calculation in the RHF picture may not be sufficient. Such a symmetry breaking effect is for instance the Zeeman splitting adding a spin dependent part to the one-particle Hamiltonian, which produces a spin-polarized fine structure in the Fock spectrum. In such a situation, one can introduce unrestricted spin orbitals or UHF-wavefunctions:

$$\chi_i(\mathbf{x}) = \begin{cases} \psi_i^\uparrow(\mathbf{r})\langle s\,|\uparrow\rangle \\ \psi_i^\downarrow(\mathbf{r})\langle s\,|\downarrow\rangle \end{cases} \tag{2.33}$$

The next task is to solve

$$f^s\chi_i = \varepsilon_i\chi_i \tag{2.34}$$

Inserting (2.33) yields for the spin-up case

$$f\psi_i^\uparrow(\mathbf{r})\langle s\,|\!\uparrow\rangle = \varepsilon_i^\uparrow\psi_i^\uparrow(\mathbf{r})\langle s\,|\!\uparrow\rangle \tag{2.35}$$

and for the spin-down case

$$f^\downarrow\psi_i^\downarrow(\mathbf{r})\langle s\,|\!\downarrow\rangle = \varepsilon_i^\downarrow\psi_i^\downarrow(\mathbf{r})\langle s\,|\!\downarrow\rangle \tag{2.36}$$

By multiplying with $\langle\uparrow|\,s\rangle$ (or $\langle\downarrow|\,s\rangle$, respectively) and integrating over the spin coordinate s, one obtains

$$F^{\uparrow,\downarrow}\psi_i^{\uparrow,\downarrow}(\mathbf{r}) = \varepsilon_i^{\uparrow,\downarrow}\psi_i^{\uparrow,\downarrow}(\mathbf{r}) \tag{2.37}$$

Here, the spatial Fock operators are defined as

$$F^{\uparrow,\downarrow}(\mathbf{r}) = \sum_s \langle\uparrow,\downarrow|\,s\rangle f(\mathbf{r},s)\langle s\,|\!\uparrow,\downarrow\rangle \tag{2.38}$$

According to the agreeing structure of both operators, it is possible to concentrate on $F^\uparrow(\mathbf{r})$. Inserting (2.33) into (2.38), we get

$$
\begin{aligned}
(F^\uparrow - h)(\mathbf{r})\psi_j^\uparrow(\mathbf{r}) \;=\; & \sum_a^{N_\uparrow}\int d\mathbf{r}'\psi_a^{\uparrow*}(\mathbf{r}')V(|\mathbf{r}-\mathbf{r}'|)\psi_a^\uparrow(\mathbf{r}') \\
& \sum_{ss'}\langle\uparrow|\,s\rangle\,\langle\uparrow|\,s'\rangle\,\langle s|\uparrow\rangle\,\langle s'|\uparrow\rangle\psi_j^\uparrow(\mathbf{r}) \\
+\; & \sum_a^{N_\downarrow}\int d\mathbf{r}'\psi_a^{\downarrow*}(\mathbf{r}')V(|\mathbf{r}-\mathbf{r}'|)\psi_a^\downarrow(\mathbf{r}') \\
& \sum_{ss'}\langle\uparrow|\,s\rangle\,\langle\downarrow|\,s'\rangle\,\langle s|\uparrow\rangle\,\langle s'|\downarrow\rangle\psi_j^\uparrow(\mathbf{r}) \\
-\; & \sum_a^{N_\uparrow}\int d\mathbf{r}'\psi_a^{\uparrow*}(\mathbf{r}')V(|\mathbf{r}-\mathbf{r}'|)\psi_a^\uparrow(\mathbf{r}) \\
& \sum_{ss'}\langle\uparrow|\,s\rangle\,\langle\uparrow|\,s'\rangle\,\langle s|\uparrow\rangle\,\langle s'|\uparrow\rangle\psi_j^\uparrow(\mathbf{r}') \\
-\; & \sum_a^{N_\downarrow}\int d\mathbf{r}'\psi_a^{\downarrow*}(\mathbf{r}')V(|\mathbf{r}-\mathbf{r}'|)\psi_a^\downarrow(\mathbf{r}) \\
& \sum_{ss'}\langle\uparrow|\,s\rangle\,\langle\downarrow|\,s'\rangle\,\langle s'|\uparrow\rangle\,\langle s|\downarrow\rangle\psi_j^\uparrow(\mathbf{r}') \tag{2.39}
\end{aligned}
$$

Now the integration over the spin variables can be carried out explicitly, leading to

$$F^\uparrow(\mathbf{r})\psi_j^\uparrow(\mathbf{r}) = h(\mathbf{r})\psi_j^\uparrow(\mathbf{r}) \;\; + \;\; \sum_a^{N_\uparrow} \int d\mathbf{r}' \psi_a^{\uparrow*}(\mathbf{r}')V(|\mathbf{r}-\mathbf{r}'|)\psi_a^\uparrow(\mathbf{r}')\psi_j^\uparrow(\mathbf{r})$$

$$+ \;\; \sum_a^{N_\downarrow} \int d\mathbf{r}' \psi_a^{\downarrow*}(\mathbf{r}')V(|\mathbf{r}-\mathbf{r}'|)\psi_a^\downarrow(\mathbf{r}')\psi_j^\uparrow(\mathbf{r})$$

$$- \;\; \sum_a^{N_\uparrow} \int d\mathbf{r}' \psi_a^{\uparrow*}(\mathbf{r}')V(|\mathbf{r}-\mathbf{r}'|)\psi_a^\uparrow(\mathbf{r})\psi_j^\uparrow(\mathbf{r}')$$

$$\tag{2.40}$$

The last equation can be written as

$$F^\uparrow(\mathbf{r}) = h + \sum_a^{N_\uparrow} \left[J_a^\uparrow - K_a^\uparrow \right] + \sum_a^{N_\downarrow} J_a^\downarrow, \tag{2.41}$$

where Coulomb and exchange operator are defined in agreement with (2.16) and (2.17).

The formal result reflects the Pauli principle: the effective interaction of an electron with a certain spin includes the Coulomb interaction with all electrons independent on their spin and the exchange interaction with only those electrons with the same spin as the test particle.

In (2.41), the sum over the $N^\uparrow$ states $\psi_a^\uparrow$ includes the interaction of a spin-up electron with itself. However, with (2.16) and (2.17) it can be verified that

$$\left[J_a^\uparrow - K_a^\uparrow \right] \psi_a^\uparrow = 0, \tag{2.42}$$

i.e. the self-interaction is cancelled.

The spatial Fock operator for spin-down electrons is accordingly given as

$$F^\downarrow(\mathbf{r}) = h + \sum_a^{N_\downarrow} \left[J_a^\downarrow - K_a^\downarrow \right] + \sum_a^{N_\uparrow} J_a^\uparrow \tag{2.43}$$

The expressions for the Fock operators (2.41) and (2.43) shows that the corresponding eigenequations (2.37) are coupled and thus cannot be solved independently, since both operators depend as well on the occupied spin-up and spin-down orbitals. The equations must therefore be solved in a simultaneous iterative process.

Of particular interest is the total electronic energy, which can now be determined from proper expectation values.

The kinetic energy and the potential energy resulting from external potentials for an electron in the unrestricted orbital $\psi_i^\uparrow$ or $\psi_i^\downarrow$ is given by the expectation values

$$h_{ii}^\uparrow = \left\langle \psi_i^\uparrow \right| h^\uparrow \left| \psi_i^\uparrow \right\rangle \; \text{ or } \; h_{ii}^\downarrow = \left\langle \psi_i^\downarrow \right| h^\downarrow \left| \psi_i^\downarrow \right\rangle \tag{2.44}$$

The Coulomb interaction between two electrons with spins s and s' ($s, s' \in \{|\!\uparrow\rangle, |\!\downarrow\rangle\}$) in the orbitals ψ_i^s and $\psi_j^{s'}$ reads

$$J_{ij}^{ss'} = \langle\psi_i^s| J_j^{s'} |\psi_i^s\rangle = \left\langle\psi_j^{s'}\middle| J_i^s \middle|\psi_j^{s'}\right\rangle = J_{ji}^{s's} \equiv \langle\psi_i^s \psi_i^s|\psi_j^{s'}\psi_j^{s'}\rangle \tag{2.45}$$

The exchange energy between two electrons of parallel spin is

$$K_{ij}^{ss} = \langle\psi_i^s| K_j^s |\psi_i^s\rangle = \left\langle\psi_j^s\middle| K_i^s \middle|\psi_j^{s'}\right\rangle \equiv \langle\psi_i^s \psi_j^s|\psi_j^s\psi_i^s\rangle \tag{2.46}$$

whereas electrons with opposite spin do not feel any exchange interaction. The total energy can finally be written as

$$E_0 = \sum_a^{N_\uparrow} h_{aa}^\uparrow + \sum_a^{N_\downarrow} h_{aa}^\downarrow + \frac{1}{2}\sum_a^{N_\uparrow}\sum_b^{N_\uparrow}(J_{ab}^{\uparrow\uparrow} - K_{ab}^{\uparrow\uparrow}) \tag{2.47}$$

$$+ \frac{1}{2}\sum_a^{N_\downarrow}\sum_b^{N_\downarrow}(J_{ab}^{\downarrow\downarrow} - K_{ab}^{\downarrow\downarrow}) + \sum_a^{N_\uparrow}\sum_b^{N_\downarrow} J_{ab}^{\uparrow\downarrow} \tag{2.48}$$

The factors $\frac{1}{2}$ in the third and fourth term occur in order to remove the double counting in the summation. Again, the self-interaction is eliminated via

$$J_{aa}^{\uparrow\uparrow} - K_{aa}^{\uparrow\uparrow} = J_{aa}^{\downarrow\downarrow} - K_{aa}^{\downarrow\downarrow} = 0 \tag{2.49}$$

2.3.2 The Pople-Nesbet equations

In the last sections, the Hartree-Fock equations have been reduced by eliminating the spin degrees of freedom in a suitable way.

It still remains to solve the coupled eigenequations (2.37). As mentioned before, this will be done by transforming the integro-differential equations into matrix equations.

Introduction of a basis

Every quantum mechanical state can be formally expressed as a vector in a Hilbert space, whose dimension depends on the problem to be treated. The coordinates of this vector depend on the basis used to span the Hilbert space. The choice of the basis is not unique, but in most problems infinitely many basis functions are required for an exact description of the states. In numerical calculations, an infinite dimension cannot be handled. It is thus necessary to approximate the wavefunctions by expansion into a finite basis set $\{\phi_\mu(\mathbf{r})|\mu = 1, 2, \ldots, N_\phi\}$:

$$\psi_i^s = \sum_{\mu=1}^{N_\phi} C_{\mu i}^s \phi_\mu, \tag{2.50}$$

with $s = \uparrow, \downarrow$. It is obvious that the approximation gets better for large values of N_ϕ. The choice of the basis functions is therefore important for the accuracy of the approximation, since the magnitude of N_ϕ can be very limited due to available computational power.

Matrix equations

Matrix equations to obtain the expansion coefficients are generated by inserting (2.50) into (2.37). This yields

$$\sum_\nu C^s_{\nu j} f^s \phi_\nu = \varepsilon^s_j \sum_\nu C^s_{\nu j} \phi_\nu \tag{2.51}$$

Multiplying these equations from the left with ϕ^*_μ and integrating over the spatial coordinates gives

$$\sum_\nu f^s_{\mu\nu} C^s_{\nu j} = \varepsilon^s_j \sum_\nu S_{\mu\nu} C^s_{\nu j} \tag{2.52}$$

The new matrices

$$F^s_{\mu\nu} = \int d\mathbf{r}\, \phi^*_\mu(\mathbf{r}) f^s(\mathbf{r}) \phi_\nu(\mathbf{r}) \tag{2.53}$$

are called Fock matrices , whereas

$$S_{\mu\nu} = \int d\mathbf{r}\, \phi^*_\mu(\mathbf{r}) \phi_\nu(\mathbf{r}) \tag{2.54}$$

is known as overlap matrix or metric matrix. It is not needed for a basis set to be orthonormal. The formal discussion therefore includes the presence of the overlap matrix. If an orthonormal basis set is chosen, the metric matrix becomes the unity matrix, which we will assume from now on.

A compact way of writing the eigenequations including all possible values of the index μ is

$$\mathbf{F}^\uparrow \mathbf{C}^\uparrow = \mathbf{S}\mathbf{C}^\uparrow \epsilon^\uparrow \tag{2.55}$$

$$\mathbf{F}^\downarrow \mathbf{C}^\downarrow = \mathbf{S}\mathbf{C}^\downarrow \epsilon^\downarrow \tag{2.56}$$

The columns of the $N_\phi \times N_\phi$-matrices $\mathbf{C}^{\uparrow,\downarrow}$ contain the expansion coefficients for $\psi^\uparrow$ and $\psi^\downarrow$. The matrices $\epsilon^{\uparrow,\downarrow}$ are diagonal and contain the orbital energies, i.e. the requested eigenvalues. Equations (2.55) and (2.56) are known as *Pople-Nesbet equations*. They form a generalized eigenproblem; in case of orthonormal basis functions, the Hartree-Fock problem is projected on finding the eigenvalues and eigenvectors of the Fock matrix. This is usually done by numerical diagonalization. The first step, however, is to find an explicit expression for the Fock matrices.

2.3.3   Density matrices

It turns out to be helpful to develop the concept of density matrices before continuing the evaluation of Fock matrix elements. The charge density contribution of N_s electrons in N_s orbitals ψ_a^s is given by

$$\rho^s(\mathbf{r}) = \sum_a^{N_s} |\psi_a^s(\mathbf{r})|^2 \tag{2.57}$$

The total charge density reads

$$\rho^T(\mathbf{r}) = \rho^\uparrow(\mathbf{r}) + \rho^\downarrow(\mathbf{r}) \tag{2.58}$$

It is also convenient to introduce the spin density

$$\rho^S(\mathbf{r}) = \rho^\uparrow(\mathbf{r}) - \rho^\downarrow(\mathbf{r}) \tag{2.59}$$

to gain access to the spin distribution in a system: in regions of space where $\rho^S(\mathbf{r}) > 0$ it is more probable to find a spin-up electron than a spin-down electron and vice versa. Inserting the basis set expansion (2.50) into (2.57) results in

$$\rho^s(\mathbf{r}) = \sum_a^{N_s} |\psi_a^s(\mathbf{r})|^2 = \sum_\mu \sum_\nu \sum_a^{N_s} \phi_\nu^*(\mathbf{r}) C_{\nu a}^{s*} C_{\mu a}^s \phi_\mu(\mathbf{r}) = \sum_\mu \sum_\nu \rho_{\mu\nu}^s \phi_\nu^*(\mathbf{r}) \phi_\mu(\mathbf{r}) \tag{2.60}$$

Here,

$$\rho_{\mu\nu}^s = \sum_a^{N_s} C_{\nu a}^{s*} C_{\mu a}^s \tag{2.61}$$

is recognized as the matrix representation of the density operator

$$\hat{\rho} = \sum_a^{N_s} |\phi_a\rangle \langle\phi_a| \tag{2.62}$$

in the basis of orbitals ψ_a^s. As eigenfunctions of a Hermitian matrix, these orbitals are orthonormal and form a complete basis set of the finite-dimensional Hilbert subspace.

The use of these density matrices opens a possibility to write down concise expressions for the Fock matrices.

2.3.4   Expressions for the Fock matrices

Returning to the matrices (2.53), one can continue by inserting the matrix elements for Coulomb and exchange operator (2.45) and (2.46):

$$F^\uparrow = H_{\mu\nu}^{\uparrow,\text{core}} + \sum_a^{N_\uparrow} \left[\langle \phi_\mu \phi_\nu | \psi_a^\uparrow \psi_a^\uparrow \rangle - \langle \phi_\mu \psi_a^\uparrow | \psi_a^\uparrow \phi_\nu \rangle \right] + \sum_a^{N_\downarrow} \langle \phi_\mu \phi_\nu | \psi_a^\downarrow \psi_a^\downarrow \rangle \tag{2.63}$$

$$F^\downarrow = H_{\mu\nu}^{\downarrow,\text{core}} + \sum_a^{N_\downarrow} \left[\langle \phi_\mu \phi_\nu | \psi_a^\downarrow \psi_a^\downarrow \rangle - \langle \phi_\mu \psi_a^\downarrow | \psi_a^\downarrow \phi_\nu \rangle \right] + \sum_a^{N_\uparrow} \langle \phi_\mu \phi_\nu | \psi_a^\uparrow \psi_a^\uparrow \rangle \qquad (2.64)$$

where

$$H_{\mu\nu}^{s,\text{core}} = \int d\mathbf{r} \phi_\mu^*(\mathbf{r}) h(\mathbf{r}) \phi_\nu(\mathbf{r}) \qquad (2.65)$$

is the matrix representation of all single-particle operators in the selected basis. This matrix will be referred to as the core Hamiltonian . It has to be remarked, that all energy contributions resulting from spin-dependent single-particle operators are included in this matrix; occasionally, it might then be required to calulate two diffferent core Hamiltonians $\mathbf{H}^{\uparrow,\text{core}}$, $\mathbf{H}^{\downarrow,\text{core}}$.

Now one can substitute the basis set expansion of $\psi_a^\uparrow$ and $\psi_a^\downarrow$ and get, e.g. for the spin-up Fock operator

$$
\begin{aligned}
F^\uparrow &= H_{\mu\nu}^{\text{core},\uparrow} + \sum_\lambda \sum_\sigma \sum_a^{N_\uparrow} C_{\lambda a}^\uparrow C_{\sigma a}^{\uparrow *} \left[\langle \mu\nu | \lambda\sigma \rangle - \langle \mu\lambda | \sigma\nu \rangle \right] \\
&\quad + \sum_\lambda \sum_\sigma \sum_a^{N_\downarrow} C_{\lambda a}^\downarrow C_{\sigma a}^{\downarrow *} \langle \mu\nu | \sigma\lambda \rangle \\
&= H_{\mu\nu}^{\text{core},\uparrow} + \sum_\lambda \sum_\sigma \rho_{\lambda\sigma}^\uparrow \left[\langle \mu\nu | \lambda\sigma \rangle - \langle \mu\lambda | \sigma\nu \rangle \right] \\
&\quad + \sum_\lambda \sum_\sigma \rho_{\lambda\sigma}^\downarrow \langle \mu\nu | \sigma\lambda \rangle \\
&= H_{\mu\nu}^{\text{core},\uparrow} + \sum_\lambda \sum_\sigma \rho_{\lambda\sigma}^T \langle \mu\nu | \sigma\lambda \rangle - \rho_{\lambda\sigma}^\uparrow \langle \mu\lambda | \sigma\nu \rangle \qquad (2.66)
\end{aligned}
$$

where

$$\langle \mu\nu | \sigma\lambda \rangle = \int d\mathbf{r} \int d\mathbf{r}' \phi_\mu^*(\mathbf{r}) \phi_\nu(\mathbf{r}) V(|\mathbf{r} - \mathbf{r}'|) \phi_\sigma^*(\mathbf{r}') \phi_\lambda(\mathbf{r}') \qquad (2.67)$$

The same steps as above can be carried out for the spin-down Fock matrix to obtain

$$F^\downarrow = H_{\mu\nu}^{\text{core}} + \sum_\lambda \sum_\sigma \rho_{\lambda\sigma}^T \langle \mu\nu | \sigma\lambda \rangle - \rho_{\lambda\sigma}^\downarrow \langle \mu\lambda | \sigma\nu \rangle \qquad (2.68)$$

The coupling of both matrix equations is performed implicitly, because

$$\mathbf{F}^\uparrow = \mathbf{F}^\uparrow(\rho^\uparrow, \rho^\downarrow) \qquad (2.69)$$

$$\mathbf{F}^\downarrow = \mathbf{F}^\uparrow(\rho^\uparrow, \rho^\downarrow) \qquad (2.70)$$

so that both Fock matrices depend on the spin-up and spin-down orbitals. Furthermore, one can insert the basis expansion into the formula for the total energy (2.48) and find

$$E_0 = \frac{1}{2} \sum_\mu \sum_\nu \left[\rho^T_{\nu\mu} H^{\text{core}}_{\mu\nu} + \rho^\uparrow_{\nu\mu} F^\uparrow_{\mu\nu} + \rho^\downarrow_{\nu\mu} F^\downarrow_{\mu\nu} \right] \qquad (2.71)$$

2.3.5   Solution to the unrestricted Hartree-Fock equations

The dependence of the Fock matrices on their own eigenvectors requires a solution of the Pople-Nesbet equations by iteration: a guess for the density matrices is made and used to build the Fock matrices. The latter are diagonalized and new density matrices are formed from their eigenvectors. These new density matrices are used to construct new Fock operators and so on, until the density matrices do not change any more. The resulting density matrices give an approximation to the charge density formed by the interacting electrons. This method of defining an effective potential for a many-particle system, which can be used to rely on a single-particle picture for the electron motion, is known as the method of self-consistent fields (SCF).

This section provides a detailed description of the unrestricted SCF procedure. The main steps are listed below, see also [37]:

SCF procedure

1. Specify the Hamiltonian with all external potentials, the number of electrons N and a basis set of adequate size N_ϕ, which in general depends on the system geometry

2. Set up the overlap matrix, the core Hamiltonians and, if possible, the two-electron matrix

3. Make an initial guess for the density matrices

4. Calculate the Fock matrices from the density matrices and the matrix elements

5. Solve $\mathbf{F}^s \mathbf{C}^s = \mathbf{S} \mathbf{C}^s \epsilon^s$, $s \in \{\uparrow, \downarrow\}$ by numerical diagonalization

6. Select the lowest N eigenenergies ϵ^s and their eigenvectors $\mathbf{C}^s$ from the $2N_\phi$ levels obtained from the diagonalization

7. Form new density matrices from the selected eigenvectors

8. Check for convergence, i.e. check if the difference between the new total density matrix and the one from the previous iteration step is smaller than a specified limit; if the procedure has not converged, return to step 4. with the new density matrices

9. After convergence, perform the analysis, i.e. calculate exspectation values and wavefunctions

Comments

1. This chapter dealt extensively with matrix representations of operators and difficulties in the spin dependent formulations. Naturally, the procedure only works for $N < 2N_\phi$. The proper choice of the basis set may help to include symmetries and certain properties of the system.

2. Depending on the basis size, it could be difficult to store the complete two-electron matrix; note however that there exist certain symmetries in the two-electron integral which make it obsolete to calculate every element.

3. The initial choice of the density matrices, i.e. the initial occupation configuration may influence the convergence and accuracy of the SCF procedure, especially in badly conditioned systems. One possibility is, for instance, to diagonalize the single-particle Hamiltonian (without interaction) in a first run and construct the density matrices by defining certain numbers of spin-up and spin-down electrons occupying single-particle states. This corresponds to "switching on" the interaction in the following step.

4. The Fock matrices are determined as described in the previous section. This is the most time consuming step in the procedure.

5. The diagonalization is efficiently done by a standard library; platform-optimized LAPACK-routines quickly produce good results.

6. The density matrices are determined as described in the previous section.

7. Convergence is not guaranteed in the SCF procedure. Sometimes so called metastable states in the iteration are reached, where the system oscillates between to possible configurations. One can try to avoid these states by refining the convergence criterion, e.g check if the standard deviation

$$\left[N_\phi^{-2} \sum_\mu \sum_\nu [P_{\mu\nu}^{(i)} - P_{\mu\nu}^{(i-1)}]^2 \right]^{1/2} < \delta \qquad (2.72)$$

It is also possible to extrapolate the density matrices from different iteration steps i. The simplest way to do this is a weighted average

$$\rho = \alpha \rho^{(i)} + (1 - \alpha)\rho^{(i-1)} \qquad (2.73)$$

for $0 \leq \alpha \leq 1$. A common value is $\alpha = 0.1$.

8. After convergence, one has access to the Fock levels and expansion coefficients of the wavefunctions. These can be used to perform further analysis.
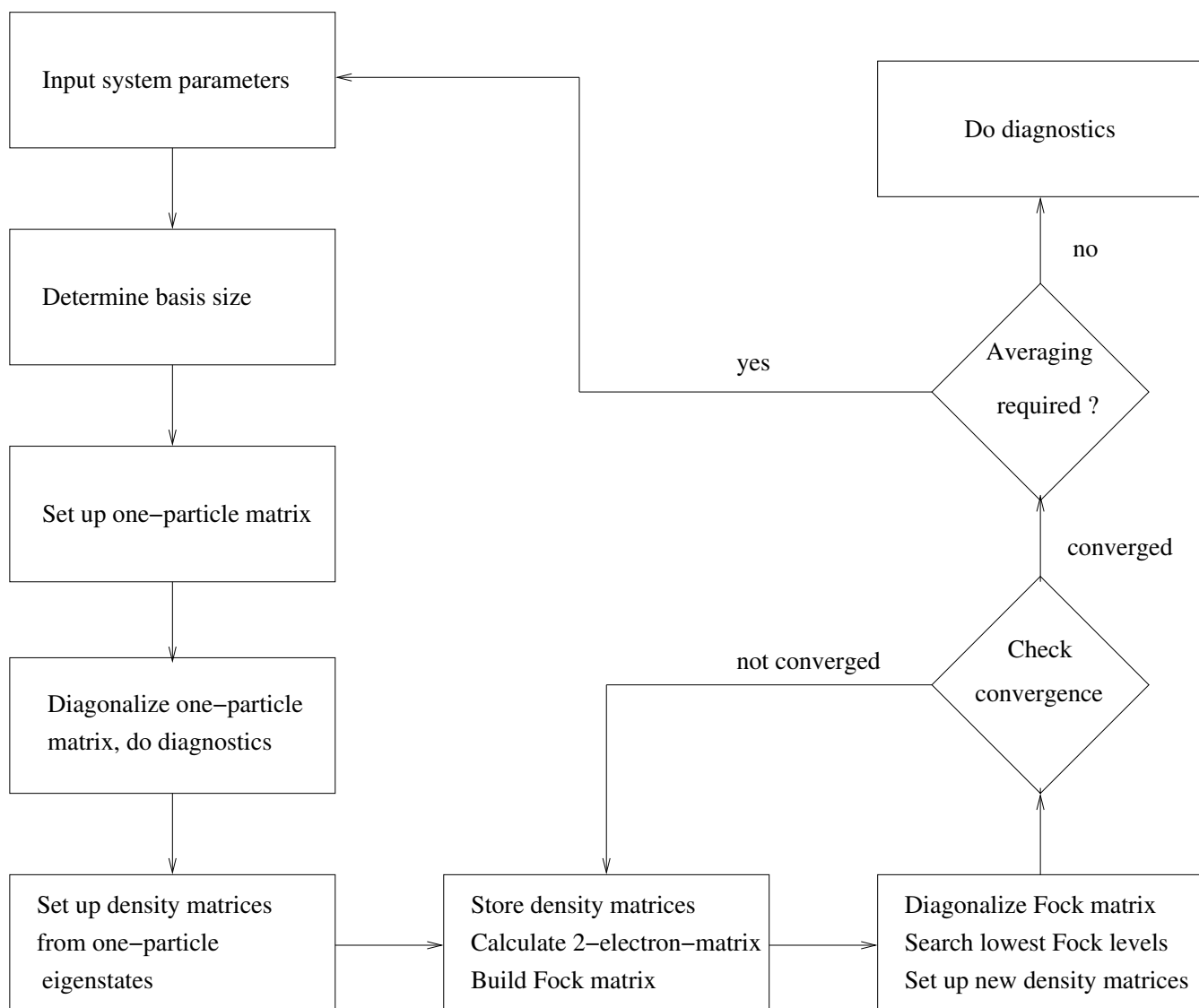
Figure 2.1: Structogram of the SCF program (from [37]).

Part II

Coulomb interaction in the integer quantum Hall effect

Localization

3.1 Localization and the metal-insulator transition

The integer quantum Hall transition can be understood as the expansion of the electron wavefunction in dependence of the magnetic field. The degeneracy of the Landau levels is lifted in the presence of disorder, and the single-particle energy levels form a band around the Landau energy $E_C = (n + \frac{1}{2})\hbar\omega_c$. Knowing the density of states, one can map the increase of the magnetic field onto an increase of the Fermi energy E. States far away from the band center are localized; for long-range correlated disorder, one can show that the wavefunctions follow equipotential lines [18, 42] corresponding to their energy. Localized wavefunctions encircle local potential pits, whereas states with energies closer to the band center follow equipotential lines which circumvent larger areas. At the critical energy, there is a percolating equipotential line which connects opposite sides of the sample. It has been shown (see [43] for a recent review) that this transition from localized to delocalized states is governed by the power law

$$\xi(E) \propto |E - E_C|^{-\tilde{\nu}}, \tag{3.1}$$

where $\xi(E)$ is the correlation length of the percolating line and called localization length. However, one has to include quantum corrections when trying to calculate the critical exponent from a percolation model [16].

The critical exponent for the lowest Landau level has been determined with high numerical precision as [10]

$$\tilde{\nu} = 2.34 \pm 0.04. \tag{3.2}$$

The critical exponent for this transition is only weakly dependent on type and range of disorder and is regarded as universal for the integer quantum Hall transition of non-interacting electrons.

The standard methods to determine the localization length and the conductance use either a refined transfer-matrix method [4, 10] or the method of recursive Green's function [44]. Both techniques operate with a tight-binding Hamiltonian; the sample is discretized, and a random disorder potential is assigned to each grid point. One can now calculate the probability for hopping between the lattice sites and devise the required quantities from this information. In case of uncorrelated disorder, it is not necessary to treat the system in toto.

In case of a correlated potential, or in the presence of mean field interaction, this is no longer possible. Instead, one has to know the corresponding potentials at every lattice site simultaneously. This makes the calculation of large systems, required for these types of calculations, infeasible.

In this chapter, we take a different approach and investigate the localization directly from the wavefunctions. By this approach, we are also limited to small system sizes, but long-range disorder and interaction can be included in a natural way. We start with the definition of a suitable quantity to be extracted from the wavefunction, the participation ratio.

3.2 Participation ratio and multifractality

If access to the wavefunctions ψ_α of a disordered system is provided, it is possible to investigate localization properties via the second statistical moment of the density $|\psi_\alpha|^2$, the inverse participation number

$$\wp = \int\limits_{\text{Vol.}} d^d r |\psi_\alpha(\mathbf{r})|^4, \tag{3.3}$$

where d is the spatial dimension.

Following the argument of Aoki [45, 46], the participation ratio

$$P_\alpha = \frac{1}{L^d \int\limits_{\text{Vol.}} d^d r |\psi_\alpha(\mathbf{r})|^4} \tag{3.4}$$

is constant for a uniformly distributed wavefunction in a volume L^d, because in this case $\wp \propto L^{-d}$. In the localized regime, the inverse participation number is related to the localization length as $\wp \approx \xi^{-d}$. Therefore, $P_\alpha \to 0$ for $L \to \infty$. In the transition region, where the wavefunction is extended, $P_\alpha \lesssim 1$. Hence, P_α mimics the localization length and can be calculated directly from spectral information.
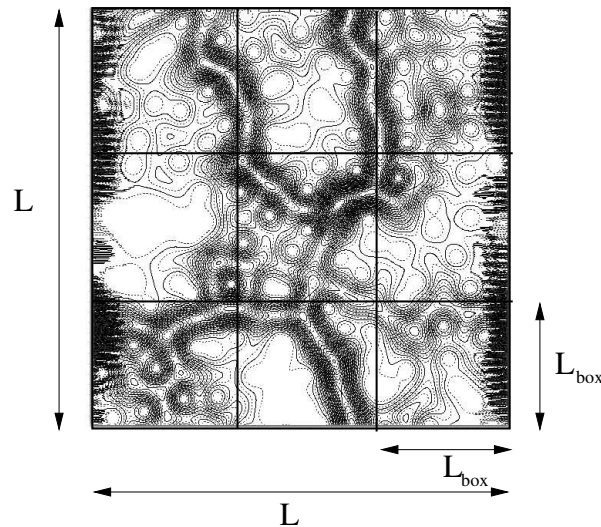
Figure 3.1: Self-similar partitioning of the density as a tool to calculate the fractal dimension.

However, the critical exponents describing the metal-insulator transition differ for participation ratio and localization length. This is due to the fact that P_α vanishes also in the transition region in the thermodynamic limit, although the wavefunction is extended. Accordingly, $\wp$ scales with a power $d^* < d$. The correct exponent for the scaling of the participation ratio can be calculated by considering the scaling of statistical moments of a given local field (in our case the wavefunction) on general grounds. As a further difficulty for quantum Hall critical states, it has been shown [47] that they are multifractals. As any multifractal object [48], the scaling of the moments is described by a whole spectrum of critical exponents. In the following, we summarize the important steps for the analysis of a self-similar, multifractal object which lead to the relevant critical exponent.

We consider a finite two-dimensional quantum Hall system of linear size L at fixed magnetic field with a disorder correlation length larger than the magnetic length. The probability to find an electron within a box of linear size L_{box} is given by the box probability

$$P(L_{\text{box}}) = \int_{\text{box}} d^2r |\psi(\mathbf{r})|^2 \tag{3.5}$$

Dividing the quadratic sample into a grid of $N(L, L_{\text{box}})$ boxes (see Fig. 3.1), one defines the fractal dimension D as

$$N(\lambda) \propto \lambda^{-D}. \tag{3.6}$$

$N(\lambda)$ is the number of boxes in which the probability to find the electron is non-zero, and $\lambda = L_{\text{box}}/L$.. Since the wavefunction is nowhere exactly zero, $N(L, L_{\text{box}}) = N(\lambda)$.

Therefore, $D = d = 2$. Somewhat more interesting is the scaling of the box probability [49]. Using the normalization condition

$$\sum_i^{N(\lambda)} P_i(L_{\text{box}}) \equiv 1 \equiv N(\lambda)\langle P(L_{\text{box}})\rangle_L, \tag{3.7}$$

we obtain the scaling law for the average

$$\langle P(L_{\text{box}})\rangle_L \propto \lambda^D, \tag{3.8}$$

where the average is as usual defined as

$$\langle P(L_{\text{box}})\rangle_L := \frac{1}{N(\lambda)} \sum_i^{N(\lambda)} P_i(L_{\text{box}}). \tag{3.9}$$

We now assume that also the higher moments

$$P^{(q)}(L_{\text{box}}) = \int_{\text{box}} d^2r |\psi(\mathbf{r})|^{2q} \tag{3.10}$$

of the box probability obey power law scaling. This assumption is reasonable if length scales are absent, as given at the quantum Hall transition [50], as long as

$$l_B \ll L_{\text{box}} < L \ll \xi_C, \tag{3.11}$$

where ξ_C is the localization length in the critical regime. In this case, the scaling relation

$$\langle P^{(q)}(L_{\text{box}})\rangle_L \propto \lambda^{D+\tau(q)} \tag{3.12}$$

holds. In the thermodynamical limit $L \to \infty$, critical states only exist at the critical energy E_C. In this limit,

$$\tau(q) = \lim_{\lambda \to 0} \frac{\ln(\langle P^{(q)}(L_{\text{box}})\rangle_L)}{\ln \lambda} - D. \tag{3.13}$$

In finite systems,

$$\tau(q) \approx \frac{\Delta \ln(\langle P^{(q)}(L_{\text{box}})\rangle_L)}{\Delta \ln \lambda} - D, \tag{3.14}$$

as long as equation (3.11) holds.

The normalization condition (3.7) implies $\tau(0) = -D$ and $\tau(1) = 0$. We can also write

$$D(q)(q-1) := \tau(q) \tag{3.15}$$

with the generalized dimension $D(q)$ and $D(0) = D$. Specifically, for the inverse participation ratio $q = 2$ and thus $\tau(2) = D(2)$. With

$$P^{(q)} \propto \xi_C^{-\tau(q)} \tag{3.16}$$

and

$$\xi_C \propto |E - E_C|^{-\tilde{\nu}}, \tag{3.17}$$

we have

$$P^{(q)} \propto |E - E_C|^{\pi(q)}, \tag{3.18}$$

where

$$\pi(q) = \tilde{\nu}\,\tau(q). \tag{3.19}$$

We therefore expect that the participation ratio increases with an exponent $\pi(2) = \tilde{\nu}\,D(2)$ when the Fermi energy approaches the critical energy.

3.3 Finite size scaling

The power law scaling of the localization-delocalization transition implies a divergence of the localization length at the critical energy and thus characterizes a second-order phase transition. However, if the localization length is viewed as a correlation length defining the range in which the particle is likely to be found, the overall volume has to diverge accordingly. In other words, for finite systems of linear size L a "divergence" in the localization length ξ is granted for $\xi > L$. Scaling relations like (3.1) or (3.18) hold, if the corresponding observable compensates the rescaling of the system size. Quantitatively, the size dependence of phase transitions is expressed via scaling functions. For the localization-delocalization transition, one calculates the localization length $\xi_L(E)$ in the finite system and relates it to the localization length in the infinite system $\xi(E)$ via a scaling conjecture

$$\frac{\xi_L(E)}{L} = \mathcal{F}\left(\frac{L}{\xi(E)}\right). \tag{3.20}$$

A similar scaling function Π is taken for the participation ratio [51, 52] away from the critical point:

$$\Pi(L^{1/\tilde{\nu}}|E - E_C|) = P_\alpha(E, L)\,L^{2-D(2)} \tag{3.21}$$

Employing generic results for finite size scaling techniques [4, 11], the correctness of an estimation of the single scaling parameter $\tilde{\nu}$ requires the collapse of scaling functions Π in dependence of the scaling variable onto a single curve.

3.4 Critical exponents for non-interacting and Hartree-Fock systems

We will now investigate how to extract critical exponents from the spectrum of a quantum Hall system, which contains no interparticle interaction, and also for a system including Coulomb interactions on Hartree-Fock level. We choose a long-range disorder potential of the form (1.13) with a correlation length $d = 2l_B$ and fix the magnetic field to $B = 8$ T. The spin-dependent single-particle Hamiltonian

$$H^s = \frac{1}{2m^*} \left(\mathbf{p} + e\mathbf{A} \right)^2 + \frac{1}{2} s g \mu_B B + V_{\text{dis}}(\mathbf{r}) \tag{3.22}$$

with the vector potential $\mathbf{A} = (0, Bx, 0)$, flux density B and spin $s = \pm 1$ enters the Fock matrix

$$F^s_{nXn'X'} \equiv F^s_{ij} = H^s_{0,ij} + \sum_a \sum_b \rho_{ab} M_{ijab} - \rho^s_{ab} M_{iabj}, \tag{3.23}$$

which has to be determined selfconsistently by an iterative solution of the unrestricted Hartree-Fock equations

$$\sum_b F^s_{ab} C^{\alpha s}_b = E^{\alpha s} C^{\alpha s}_a. \tag{3.24}$$

m^* is the effective electron mass, μ_B is the Bohr magneton and g the effective electron g-factor. $\langle nX | \alpha s \rangle = C^{\alpha s}_{nX} \equiv C^{\alpha s}_a$ are the expansion coefficients of the Hartree-Fock states $|\alpha s\rangle$ and $E^{\alpha s}$ the energy eigenvalues. The interaction matrix elements

$$M_{ijab} = \frac{\gamma l}{L^2} \sum_{q_x, q_y} V(q) \langle i | e^{i\mathbf{qr}} | j \rangle \langle a | e^{-i\mathbf{qr}} | b \rangle \tag{3.25}$$

are elucidated in Appendix A.2. The spin-resolved density matrix $\rho_{ij} = \sum_s \rho^s_{ij}$ is given as

$$\rho^s_{ij} = \sum_{\alpha(\text{occ})} C^{\alpha s *}_i C^{\alpha s}_j. \tag{3.26}$$

As a first step, we estimate the fractal dimension $D(2)$ by calculating

$$P^{(2)}(\lambda, \alpha) = \sum_i \left(\int_{\mathbf{r} \in \Omega_i(\lambda)} d^2r |\psi_\alpha(\mathbf{r})|^2 \right)^2 \tag{3.27}$$

Here, the area of the system with length L is covered with quadratic boxes of size $L_{\text{box}} = \lambda L$ and area $\Omega = L^2_{\text{box}}$. The probability to find the electron in each of the boxes
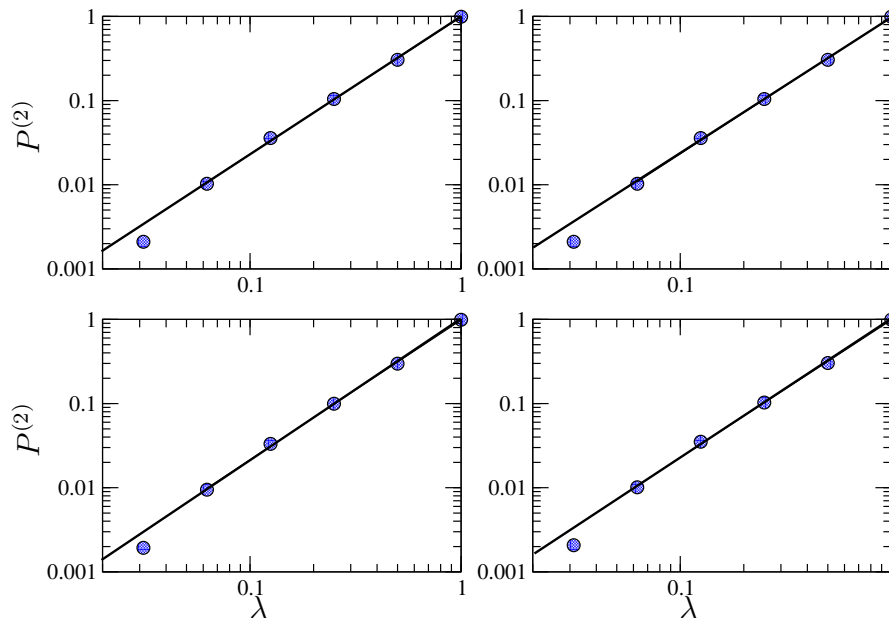
Figure 3.2: Average values for $P^{(2)}$ according to equation (3.27) for different box sizes. Upper left: Spin up, noninteracting. Upper right: Spin down, noninteracting. Lower left: Spin up, interacting. Lower right: Spin down, interacting. A power law fit yields an average exponent $D(2) = 1.63$ for all curves. The value for $\lambda = 0.0325$ has been omitted for the fit, since it is beyond the validity region of equation (3.11). The solid lines are guides to the eye.

is calculated, squared and summed up for all the boxes. For states in the critical region, the participation ratio is considerably larger than for states in the insulating region (see Fig. 3.3). $D(2)$ is then obtained using equation (3.14) and averaged boxed probabilities for a few critical states. Results are shown in Fig. 3.2. For all types of interaction and disorder we found

$$D(2) = 1.63 \pm 0.03, \tag{3.28}$$

in agreement with earlier results reported in [52]. A notable result is thus that the multifractality of the wavefunction is not modified in the presence of interactions.

Results for the participation ratio are shown in Fig. 3.3.

A power law fit according to equation (3.18) in the tails of the curves give the critical exponents $\pi(2)$ for the participation ratio and accordingly $\tilde{\nu}$ for the localization length.
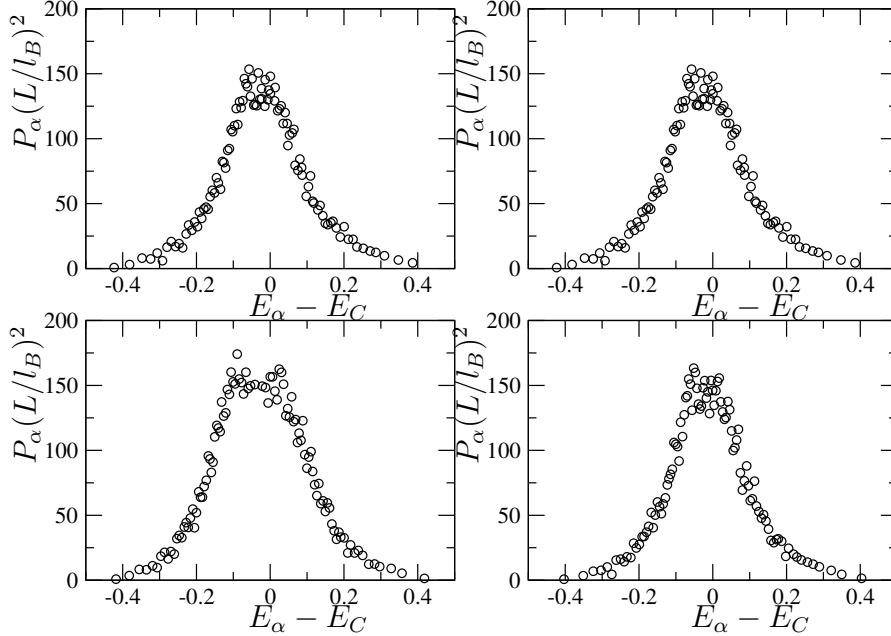
Figure 3.3: Averaged participation ratio for a system of size $L = 30 \ l_B$ at $B = 8$ T, averaged over 60 realizations of Gaussian disorder with correlation length $d = 2l_B$, $V_0 = 10$ meV and $N_{\mathrm{imp}} = 200$.

The estimated critical exponents are shown in Table 3.1. Within the accuracy provided by the relatively small system size, we do not find significant deviations from the expected values even in presence of Hartree-Fock-like interaction. This supports the conjecture of a universal critical exponent at least in the lowest Landau level. However, the Hartree-Fock spectrum has to be treated with some care, because certain correlation effects are negleced it this approximation. The participation ratio is evaluated at fixed filling factor. Nevertheless, the fitting has been performed over the Hartree-Fock single particle energies approaching the critical region. Thus, the single-particle spectrum is assumed to be stable against adding or removing a particle, and the levels depict the correct Fermi energy. No possibility is given for charge rearrangement and renormalization of the Fermi energy. We return to this point in chapter 5 and note that our results are consistent with those presented in Ref. [52], and remain unchanged also for spin-split Landau levels. For the sake of completeness, results for the scaling function are

Table 3.1: Results for the critical exponents $\pi(2)$ and $\tilde{\nu}$ for a system as in Fig. 3.3.

spin	d	ν_f	γ	$\pi(2)$	ν
0	$2l$	$1/N_\phi$	0	3.96 ± 0.41	2.43
$\uparrow$	$2l$	1	1	3.64 ± 0.38	2.23
$\downarrow$	$2l$	1	1	3.74 ± 0.39	2.29

PSfrag replacements
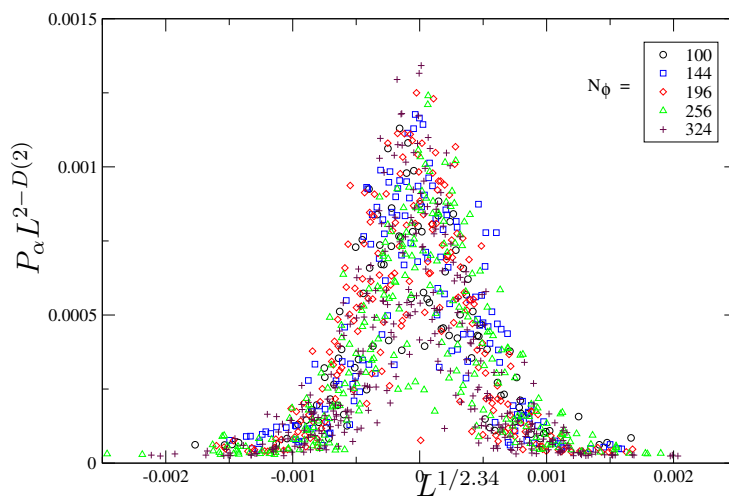
Figure 3.4: Scaling function for systems with parameters as in Fig. 3.3, but different linear sizes L. At constant magnetic field, $L^2 = 2\pi N_\phi l_B^2$ with the total number N_ϕ of magnetic flux quanta in the system.

shown in Fig. 3.4, using $\tilde{\nu} = 2.34$. A reasonable collapse onto a single scaling curve is observed for different system sizes.

3.5 Conclusions

In summary, we have derived a procedure to extract information about the metal-insulator transition from spectral data of a single-particle Hamiltonian. We investigated the localization properties of electrons in a quantum Hall system by calculating the participation ratio for eigenstates of a suitable Hamiltonian with and without Coulomb interaction.

Specifically, we have elucidated that a multifractal analysis (in particular, the determination of the correlation dimension $D(2)$) of the wavefunctions is required to obtain the correct critical exponent. We found, that for fixed filling factor the transition from localized states in the Landau band tails to extended states in the vicinity of the band center remains quantitatively unchanged even in the presence of mean field Coulomb interaction.

Frequency-dependent transport of disordered electrons

4.1 Introduction

Experimental determination of the resistance and conductivity of a two-dimensional electron system in a strong perpendicular magnetic field and disorder along ("xx-direction") and perpendicular to ("xy-direction") the direction of the applied external electric field is the central issue in the exploration of the quantum Hall phase transition[1, 25, 53]. A characteristic result is that in dependence of filling factor the Hall conductivity σ_{xy} is quantized to integer multiples of the conductivity quantum e^2/h over a certain range of filling factors, with sharp transitions between these plateaux. Simultaneously, the longitudinal conductivity σ_{xx} exhibits peaks at position of the plateau transition and vanishes elsewhere. Width of the Hall plateaus and slope of the transition between as well as width and height of the longitudinal peaks depend on temperature T and frequency ω of a stimulating external electric field. The additional energy scales $k_B T$ and $\hbar\omega$ make a single parameter power law scaling like equation (3.1) unlikely. In fact, it represents the dynamics of the system, which is expected to decelerate when the system approaches criticality. In other words, the divergence of the localization length ξ is accompanied by a divergence of a characteristical correlation time τ_C for $E \to E_C$. The finite-size scaling theory predicts power law scaling also for the transport coefficients. This behaviour is reflected in the scaling of the conductivity tensor [54]

$$\sigma_{\alpha\beta} = \frac{e^2}{h} S_{\alpha\beta} \left[L_{\text{eff}}^{1/\tilde{\nu}} (E - E_C) \right] \tag{4.1}$$

with the effective system size L_{eff} and the critical exponent for the localization length $\tilde{\nu}$ (see equation (3.1)). At temperature $T = 0$, $L_{\text{eff}} = L$, whereas at $T > 0$, the effective system size is given by the phase coherence length L_ϕ [55]. It is then argued that

$$\frac{d\sigma_{\alpha\beta}}{dB} \propto L_{\text{eff}}^{1/\tilde{\nu}} \propto T^{-\gamma}, \tag{4.2}$$

with $\gamma = \tilde{\nu}\, z$. z is the dynamical critical exponent, which can be obtained by temperature dependent measurements of the Hall conductivity.

A similar effect on scaling is expected, if the system is stirred up by an externally applied AC field of angular frequency ω. With increasing ω, the peak width ΔE of the σ_{xx}-peaks increases. Above a temperature-dependent saturation frequency, the width is expected to scale as

$$\Delta E \propto \omega^{\tilde{\kappa}} \tag{4.3}$$

The dynamical scaling assumption for the longitudinal conductivity can then be written as

$$\sigma_{xx}(L, \omega) = \frac{e^2}{h} S_{xx}\left[L/\xi(E), \omega\tau_0(E)\right], \tag{4.4}$$

where

$$\tau_0(E) \propto \xi(E)^z \propto |E - E_C|^{-\tilde{\nu}z}, \tag{4.5}$$

For frequencies high enough, the scaling function S_{xx} is mainly determined by $\omega\tau_0(E)$. Thus ΔE scales as $\omega^{1/\tilde{\nu}z}$, which implies $\tilde{\kappa} = 1/z\tilde{\nu}$.

We now set $T = 0$ and concentrate on the case of frequency scaling. Experiments using a coplanar waveguide to excite the 2DEG in a GaAs/GaAlAs heterostructure [25] revealed power law scaling with an exponent $\tilde{\kappa} = 0.41$ for the broadening of the lowest conductivity peak. With $\tilde{\nu} = 2.34$, this value is consistent with a dynamical exponent $z = 1$. Other experiments [21, 23, 53] found $\tilde{\kappa} = 0.21$ and accordingly $z = 2$ for spin-unresolved Landau levels and $z = 1$ for spin-split Landau levels. The value of $z = 2$ for dynamical scaling is anticipated for non-interacting electron systems in the diffusive limit; it has been shown [56] that correlations in the two-particle spectral function resulting from eigenfunction correlations with a correlation length shorter than the localization length leads to anomalous scaling with a reduced dynamical exponent $z = 1$.

Theoretical attempts have been made on a semiclassical basis [57] and quantum mechanically [58]. The latter intended to explain the experimental results by calculating the frequency-dependent conductivity in time-dependent Hartree-Fock approximation via the Einstein relation. This involves the calculation of the irreducible susceptibility, which is connected to the polarization function. As a result, the exponent $z = 1$ was validated for the interacting system.

However, the reported calculation was not free of systematic errors, because vertex corrections linking the disorder potential to local exchange fields had to be neglected

in order to make the calculation numerically possible. These corrections are crucial for the density-density response function, and their omission leads to spurious results in the screening properties [59]. Therefore, it is yet unknown if interactions between the electrons emerge as the observed behaviour.

Another approach [60] used the Kubo formula [61] with a spatially long-range correlated disorder potential to calculate the longitudinal conductivity from disordered eigenstates. In order to handle only a single Landau level, the full current operator entering the Kubo formula (which is in fact a current-current correlation function) was replaced by velocity matrix elements of the guiding center coordinates [39] (see Appendix A.4.2). Finite-size scaling leads to $z = 1.19$. This result is surprising; although the finite-range disorder potential may have an effect, it seems more likely that the semiclassical approximation used here is not suitable. It was demonstrated later [62] for δ-like scatterers using the recursive Green function method, that the conductivity follows diffusive scaling with $z = 2$.

The issue of frequency-dependent transport in the quantum Hall regime remains therefore unclear. In this chapter, we try to contribute some insight by deriving an expression for the frequency-dependent conductivity tensor of a non-interacting system using the complete quantum mechanical current density operator and compare scaling results to the earlier works in order to understand the validity of the Kubo approach to address frequency scaling.

4.2   Transport and linear response

We start with a brief review of linear response theory. In particular, we study the calculation of the conductivity tensor in terms of energy spectrum and eigenstates and the special cases of single-particle and Hartree-Fock Hamiltonians [63, 64] . Measurements of electrical conductivity in solid state devices involves the response of its charge carriers to an external electromagnetic field, which is defined by the potentials $\mathbf{A}(\mathbf{r}, t)$ an $\Phi(\mathbf{r}, t)$. The many-particle Hamiltonian for N two-dimensional electrons in the external potential V

$$H = \sum_{i=1}^{N} \left(\frac{(\mathbf{p}_i + e\mathbf{A}(\mathbf{r}_i, t))}{2m^*} + e\Phi(\mathbf{r}_i, t) \right) + V(\mathbf{r}_1, \ldots, \mathbf{r}_n) \tag{4.6}$$

can alternatively be written in position representation

$$H = \int d^2 r' \left(\mathbf{j}(\mathbf{r'})\mathbf{A}(\mathbf{r}', t) + en(\mathbf{r}')\Phi(\mathbf{r}', t)) + \frac{e^2}{2m^*}n(\mathbf{r}')\mathbf{A}^2(\mathbf{r}', t)\right) + H_0, \tag{4.7}$$

where H_0 is the N-electron Hamiltonian without electromagnetic field,

$$\mathbf{j}(\mathbf{r}, t) = \frac{e^2}{2m} \sum_{i=1}^{N} \left[(\mathbf{p}_i - e\mathbf{A}(\mathbf{r}_i, t)) \, \delta(\mathbf{r} - \mathbf{r}_i) + \delta(\mathbf{r} - \mathbf{r}_i) \, (\mathbf{p}_i - e\mathbf{A}(\mathbf{r}_i, t)) \right] \tag{4.8}$$

is the symmetrized current density operator and

$$n(\mathbf{r}) = \sum_{i=1} N\delta(\mathbf{r} - \mathbf{r}_i) \tag{4.9}$$

the particle density operator. The electromagnetic field thus couples via particle and current density with a system of charged particles. This is known as *diamagnetic* coupling due to the charge, in contrast to the Zeeman coupling via magnetic moments.

Transport is described by the expectation value of the current operator (4.8). In linear order in the perturbation due to the electric field its α-component given as

$$
\begin{aligned}
\langle j_\alpha(\mathbf{r})\rangle_{\rho(t)} &= \frac{e^2}{m} A_\alpha(\mathbf{r}, t)\langle n(\mathbf{r})\rangle_{\rho_0} \\
&- \int d^2 r' \int dt' \left(\sum_{\gamma=1}^{2} \chi_{j_\alpha^0(\mathbf{r}), j_\gamma^0(\mathbf{r}')}(t - t') A_\gamma(\mathbf{r}', t') \right. \\
&+ \left. e\chi_{j_\alpha^0(\mathbf{r}), n(\mathbf{r}')}(t - t')\Phi(\mathbf{r}', t') \right),
\end{aligned}
\tag{4.10}
$$

where $\mathbf{j}^0$ is the current density for $\mathbf{A} = \mathbf{0}$ and

$$\chi_{j_\alpha^0(\mathbf{r}), j_\gamma^0(\mathbf{r})}(t - t'), \chi_{j_\alpha^0(\mathbf{r}), n(\mathbf{r}')}(t - t') \tag{4.11}$$

are current-current and current-density response functions, respectively [64, 65].

In the following, we restrict ourselves to a spatially independent AC electric field

$$\mathbf{E}(t) = \mathbf{E}_0 \, e^{-i(\omega + i\delta)t}. \tag{4.12}$$

Here, ω is the frequency of the AC field $\mathbf{E}_0$ a constant amplitude and δ an infinitesimal convergence factor, which turns out to be helpful later. The spatial homogeneity implies wavelength larger than the mean characteristic length scale of the sample. Note, that the choice of a monochromatic field does not require an additional restriction, since arbitrary fields can be decomposed into Fourier components, which are additive in linear response theory.

The time-dependent vector- and scalar potentials can now be chosen as

$$\mathbf{A}(t) = -i\frac{1}{\omega + i\delta}\mathbf{E}_0 e^{-i(\omega + i\delta)t} \quad \Phi = 0, \tag{4.13}$$

which satisfied $\dot{\mathbf{E}} \propto -\dot{\mathbf{A}}$.

Moreover, the spatial homogeneity allows to neglect the spatial dependence of the expectation value, which can be replaced by its average

$$\langle \mathbf{j}\rangle = \frac{1}{L^2} \int d^2 r \langle \mathbf{j}(\mathbf{r})\rangle. \tag{4.14}$$

Substituting the particle density

$$n = \frac{1}{L^2} \int d^2r \langle n(\mathbf{r}) \rangle, \tag{4.15}$$

we get

$$\langle j_\alpha \rangle = i \frac{ne^2}{m(\omega + i\delta)} E_{0,\alpha} e^{-i(\omega + i\delta)t} + \frac{1}{V} \frac{i}{\omega + i\delta} \sum_{\gamma=1}^{2} \chi_{j_\alpha^0(\mathbf{r}), j_\gamma^0(\mathbf{r})}(\omega + i\delta) E_{0,\gamma} e^{-i(\omega + i\delta)t}. \tag{4.16}$$

The conductivity σ relates current density and electric field as $\mathbf{j} = \sigma \mathbf{E}$. From (4.16) follows

$$\sigma_{\alpha,\gamma}(\omega + i\delta) = \frac{i}{\omega + i\delta} \frac{1}{V} \chi_{j_\alpha^0(\mathbf{r}), j_\gamma^0(\mathbf{r})}(\omega + i\delta) + i \frac{ne^2}{m(\omega + i\delta)} \delta_{\alpha\gamma} \equiv \tilde{\sigma}_{\alpha,\gamma} + \sigma^{\text{dia}}. \tag{4.17}$$

This expression is referred to as Kubo formula [61] for the frequency-dependent conductivity.

On general grounds, one can write the response function of an arbitrary operator A to the action of another operator B in spectral representation using (many-particle) eigenstates $|m\rangle$ of the unperturbed Hamiltonian H_0 as [63, 64]

$$\chi_{B,A}(\omega + i\delta) = -\frac{1}{Z_0} \sum_{lm} \frac{\langle l \mid B \mid m \rangle \langle m \mid A \mid l \rangle}{\hbar\omega + i\delta + E_l - E_m} \left(e^{-\beta E_l} - e^{-\beta E_m} \right), \tag{4.18}$$

where $Z_0 = \sum_l e^{-\beta E_l}$ is the partition function orresponding to H_0 and $\beta^{-1} = k_B T$. This leads obviously to

$$\sigma_{\alpha,\gamma}(\omega + i\delta) = \frac{-i}{\omega + i\delta} \frac{1}{V} \frac{1}{Z_0} \sum_{lm} \frac{\langle l \mid j_\alpha \mid m \rangle \langle m \mid j_\gamma \mid l \rangle}{\hbar\omega + i\delta + E_l - E_m} \left(e^{-\beta E_l} - e^{-\beta E_m} \right) + \frac{ine^2 \delta_{\alpha\gamma}}{m(\omega + i\delta)}. \tag{4.19}$$

This formula grants the possibility to calculate the conductivity as linear transport coefficient, if the complete spectrum of the corresponding Hamiltonian and the current density matrix elements in its many-particle eigenbasis are known. Therefore, the usability is limited to systems which can be exactly diagonalized. In particular, it is well applicable for single-particle systems.

4.3   Kubo formula for single-particle systems

The αth component of the current density operator can be written in second quantization as

$$j_\alpha = \sum_{il} \frac{e}{m} \langle i \mid p_\alpha + eA_\alpha \mid l \rangle c_i^\dagger c_l := \sum_{il} j_{il;\alpha} c_i^\dagger c_l, \tag{4.20}$$

where $|i\rangle$, $|l\rangle$ are arbitrary one-particle basis kets and c_i ($c_i^\dagger$) the corresponding annihilation (creation) operators. We have included a time-independent vector potential $\mathbf{A}$ in the kinetic momentum, which is suitable to model a constant external magnetic field. This does not qualitatively alter the considerations in the previous section.

This leads immediately to an expression for the conductivity in a single-particle system. Starting from equation (4.19), and assuming

$$H_0 = \sum_i \epsilon_i c_i^\dagger c_i, \tag{4.21}$$

we obtain

$$\frac{1}{Z_0} \sum_{lm} \left\langle l \mid c_i^\dagger c_n \mid m \right\rangle \left\langle m \mid c_j^\dagger c_k \mid l \right\rangle \left(e^{-\beta E_l} - e^{-\beta E_m} \right) = \delta_{nj}\delta_{ik}(f_i - f_n), \tag{4.22}$$

where $f_i = f(\epsilon_i)$ is the usual Fermi factor. This leads to the frequency-dependent conductivity for a single-particle model

$$\sigma_{\alpha\gamma}(\omega + i\delta) = \frac{i}{L^2(\omega + i\delta)} \sum_{lk} j_{lk;\alpha} j_{kl;\gamma} \frac{f_l - f_k}{\hbar\omega + i\delta + \epsilon_l - \epsilon_k} + i\frac{ne^2}{m(\omega + i\delta)}\delta_{\alpha\gamma} \tag{4.23}$$

4.4 Frequency scaling of the integer quantum Hall transition

With the help of equation (4.23) we can calculate the frequency-dependent conductivity tensor, neglecting Coulomb interaction between the electrons for the moment. We determine the eigenvalues and eigenfunctions using periodic boundary conditions via exact diagonalization and the corresponding current density matrix elements as shown in Appendix A.4.1. The use of equation (4.23) requires some attention in the quantum Hall system. The current density matrix elements couple disordered eigenstates belonging to adjacent Landau levels. Therefore, the spectrum for at least $m \pm 1$ Landau levels has to be evaluated if one is interested in the current response of m Landau levels. Moreover, the $\sigma_{xx} = \sigma_{yy}$-component diverges in the band center for $\delta \to 0$, a behaviour, which is unsuitable for numerical evaluation. To overcome this obstacle, one chooses a finite value for δ of the order of a few times the mean level spacing. The observable conductivity $\text{Re}(\sigma_{xx})$ then depends on δ, which must not be selected too large. As usual in linear response theory, $\mathbf{E}_0 \to \mathbf{0}$ has been tacitly assumed. In the following, we calculate σ_{ab} separately for several (≈ 10) disorder configurations and frequencies and perform the disorder average afterwards.

4.4.1   Short-range disorder

We diagonalize the Hamiltonian

$$H = \frac{(\mathbf{p} + e\mathbf{A})^2}{2m} + \sum_{i}^{N_{\text{imp}}} V_i \, \delta(\mathbf{r} - \mathbf{r}_i), \tag{4.24}$$

assuming $N_{\text{imp}} = 200$ zero-range scatterers at positions $\mathbf{r}_i$, with amplitudes $|V_i| \leq V_0 = 5$ meV and a magnetic flux density of $B = 7$ T. The linear system size is $L = 30l_B$. All other parameters are set to the material values of GaAs (see Appendix B). We use the Landau representation as described in Chapter 1. We found acceptable results for $\delta = 8\Gamma/N_\phi$ in equation (4.23), where $\Gamma = 0.2\hbar\omega_c$ is the bandwidth of the lowest Landau level. A disorder-averaged result for short-range scatterers is shown in Fig. 4.4.1 for different driving frequencies ω. $\sigma_{xx}(E, \omega)$ shows peaks around $E = E_C = \hbar\omega_c(n + \frac{1}{2})$. The width of the peaks ΔE is enlarged towards higher frequencies ω. The peak maximum decreases with increasing frequency. This observation has been the central issue of the dynamical scaling theory of the quantum Hall plateau transition.

To quantify the relation between ω and ΔE, we have fitted each peak in the lowest Landau level to a Gaussian

$$f(E) = A \, e^{-(E-E_C)^2/\Delta E^2} + C, \tag{4.25}$$

where all energies are taken in units of $\hbar\omega_c$ and C compensates the offset of the conductivity curve, which is a finite-size effect depending on the frequency.

The results for the width are plotted against the frequency in Fig. 4.2. A power-law fit of the form

$$\Delta E = A\omega^{\tilde{\kappa}} + C \tag{4.26}$$

yields

$$\tilde{\kappa} = 0.24 \pm 0.16 \tag{4.27}$$

which leads to the dynamical critical exponent

$$z = \frac{1}{\tilde{\kappa}\tilde{\nu}} = 1.78 \approx 2 \quad \text{for } \tilde{\nu} = 2.34. \tag{4.28}$$

The constant C has been used as an additional fitting parameter in order to compensate the finite width at $\omega = 0$, which is solely determined by the artificial parameter δ in the Kubo formula. These results are within the limits imposed by the small system size and numerical accuracy close to the values $\tilde{\kappa} = 0.21$ and $z = 2$ expected for noninteracting systems. We conclude that the dissipative component of the Kubo formula for the electrical conductivity is able to describe qualitatively and even quantitatively the integer quantum Hall transition in the presence of magnetic field and disorder, but so far without interaction between the electrons.
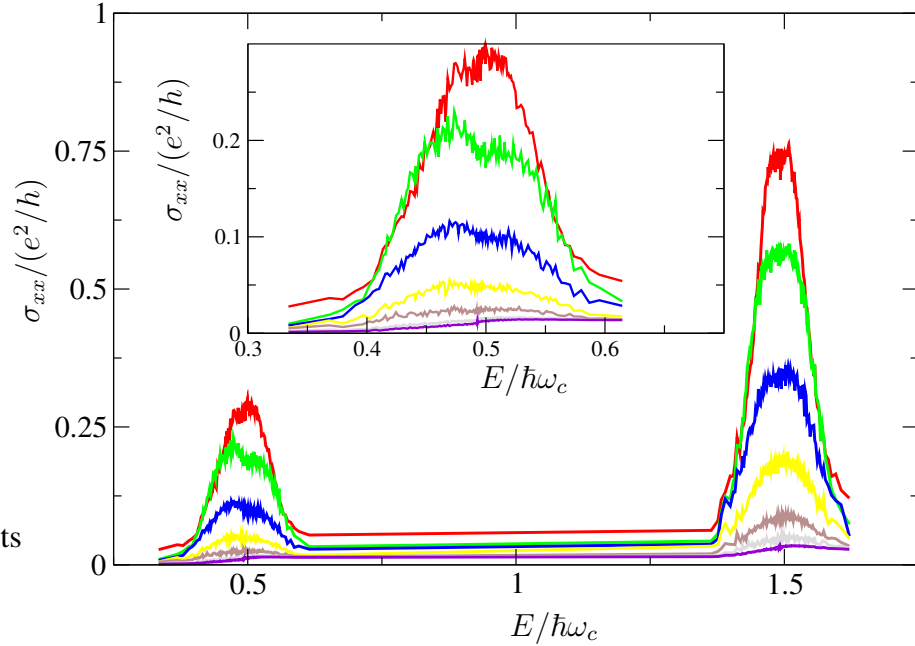
Figure 4.1: Real part of the magnetoconductivity for a system of size $L = 30l_B$ with 200 δ-impurities at $B = 7$ T. The disorder strength is $\Gamma = 0.2\hbar\omega_c$. The curves show results for different external frequencies ω. External frequencies are color coded: $\omega/\omega_c = 0.0342$ (red), 0.0684 (green), 0.1026 (blue), 0.1369 (yellow), 0.1711 (brown), 0.2053 (grey), 0.2396 (violet). The inset shows a magnification of the lowest Landau level peak.

The frequency-dependent Hall conductivity $\sigma_{xy}(\omega)$ for the same system is shown in Fig. 4.4.1 for the first two Landau levels. The slope around the critical points is depending on the frequency. The DC conductivity $\sigma_{xy}(0)$ (black curve) matches integer multiples of e^2/h exactly around integer filling factors. For $\omega > 0$, the plateaux differ from these values. This is probably due to an increasing localization length in higher Landau bands.

4.4.2   Long-range disorder

We now discuss the effect of long-range disorder on dynamical scaling. The Hamiltonian

$$H = \frac{(\mathbf{p} + e\mathbf{A})^2}{2m} + \sum_i^{N_{\text{imp}}} V_i \, e^{-(\mathbf{r}-\mathbf{r}_i)^2/d^2}, \tag{4.29}$$
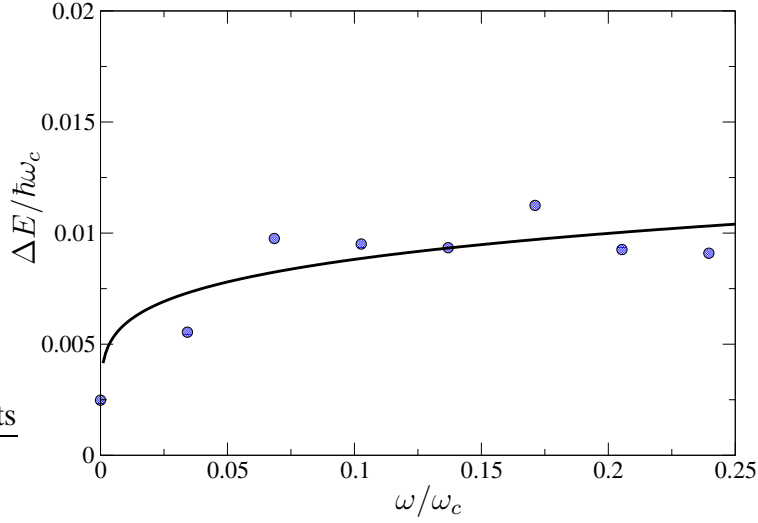
Figure 4.2: Scaling of the width for the peaks in Fig. 4.4.1 as a function of frequency. The solid line is a least-square fitted function $\Delta(E) = A\omega^{\tilde{\kappa}} + C$, with $\tilde{\kappa} = 0.24$.

is diagonalized with $N_{\mathrm{imp}} = 200$ scatterers of range $d = l_B$ at positions $\mathbf{r}_i$, with amplitudes $|V_i| \leq V_0 = 15$ meV and a magnetic flux density of $B = 7$ T. The linear system size is $L = 30l_B$. All other parameters as before are set to the material values of GaAs (see Appendix B). Again, we use $\delta = 8\Gamma/N_\phi$ in the Kubo formula (4.23), where $\Gamma = 0.2\hbar\omega_c$ is the bandwidth of the lowest Landau level. As for the case of δ-impurities, the spectrum and eigenfunctions for the lowest three Landau levels have been calculated.

Fig. 4.4.2 shows disorder-averaged results for $\sigma_{xx}(E, \omega)$ and $\sigma_{xy}(E, \omega)$ in the lowest Landau level, without qualitative difference to the features of zero-range scatterers. The frequency dependence of the peak widths Δ has been investigated with the help of the Gaussian fitting function (4.25). Δ as a function of ω is shown in Fig. 4.5. We find

$$\tilde{\kappa} = 0.49 \pm 0.24, \tag{4.30}$$

and therefore

$$z = 0.87 \approx 1. \tag{4.31}$$

Again, these results are contaminated with relatively large statistical errors, as discussed in the previous section. Within these limits, our results for long-range impurities with $d = 1$ seem to be consistent with earlier works [60]. This leads to the conclusion that the critical exponent z governing dynamical scaling is strongly influenced by the microscopic properties of the sample. This seems reasonable, since the motion of the

PSfrag replacements

$\sigma_{xy}/(e^2/h)$
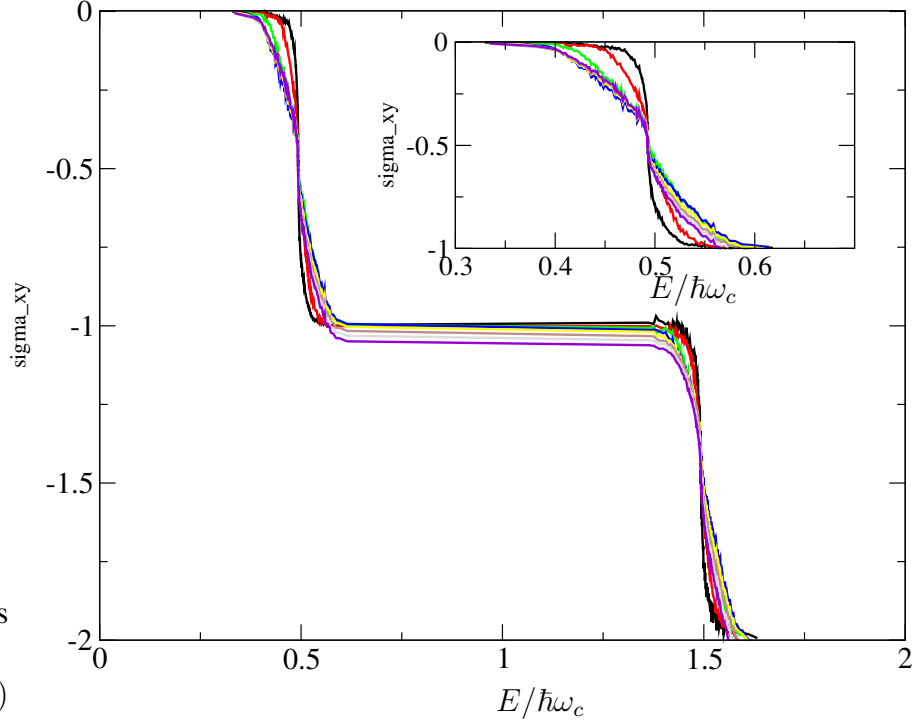
Figure 4.3: Results for the Hall conductivity at various frequency. System parameters are the same as in Fig. 4.4.1. External frequencies are color coded: $\omega/\omega_c = 0$ (black), 0.0342 (red), 0.0684 (green), 0.1026 (blue), 0.1369 (yellow), 0.1711 (brown), 0.2053 (grey), 0.2396 (violet). The inset shows a magnification of the lowest Landau level curvature.

electron in the presence of a smooth disorder potential exhibits a considerably different, diffusive behaviour compared to the free, ballistic motion or the motion in presence of zero-range scatterers. We therefore expect also a strong dependence of dynamical scaling on electron-electron interaction.

4.4.3 The effect of Coulomb interaction

We finally discuss the influence of Coulomb interaction in the Hartree-Fock approximation. Starting with

$$H = \sum_i \frac{(\mathbf{p}_i + e\mathbf{A})^2}{2m} + \sum_i \sum_j^{N_{\text{imp}}} V_i \, \delta(\mathbf{r}_i - \mathbf{r}_j) + V_{e-e}, \qquad (4.32)$$
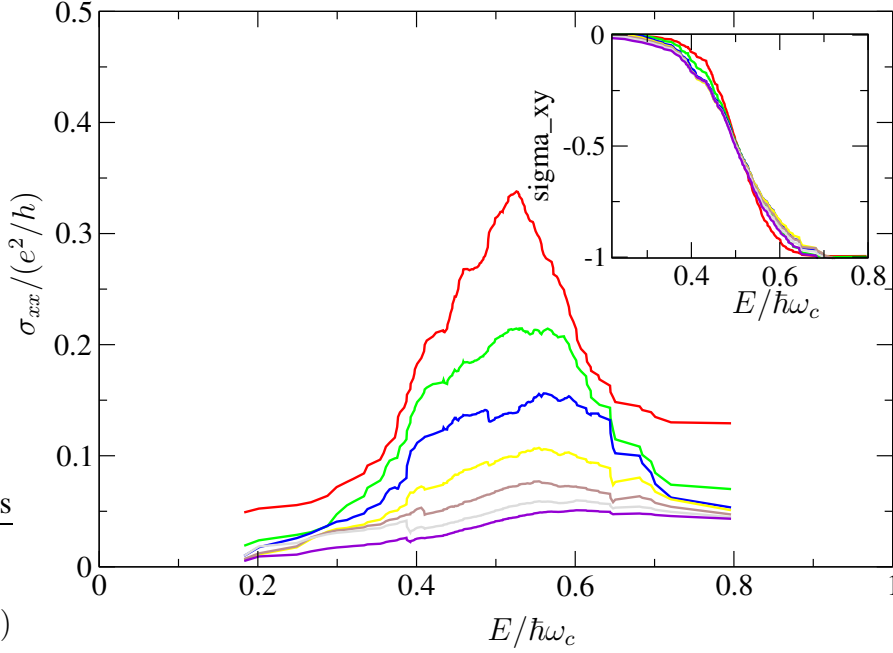
Figure 4.4: Real part of the magnetoconductivity for a system of size $L = 30l_B$ with 200 Gaussian impurities of range $d = l_B$ at $B = 7$ T. The disorder strength is $\Gamma = 0.6\hbar\omega_c$. The curves show results for different external frequencies ω. The inset shows the Hall conductivity σ_{xy}. External frequencies are color coded: $\omega/\omega_c = 0.0342$ (red), 0.0684 (green), 0.1026 (blue), 0.1369 (yellow), 0.1711 (brown), 0.2053 (grey), 0.2396 (violet).

where

$$V_{e-e} = \frac{1}{4\pi\epsilon\epsilon_0} \sum_{i>j} \frac{1}{|\mathbf{r}_i - \mathbf{r}_j|}, \tag{4.33}$$

we solve the Hartree-Fock equations as devised in chapter 2 and elaborated in section 3.1. We will show results for a system of linear size $L = 25l_B$ containing 400 δ-impurities of strength $V_0 = 15$ meV with random sign and position. The magnetic flux density is $B = 7$ T, material parameters have been set as usual to the bulk values of GaAs. The infinitesimal parameter δ in equation 4.23 was chosen eight times the mean level spacing in presence of interaction. Figs. 4.6, 4.7 and 4.8 show results for the conductivity in the lowest Landau level for filling factors 0.05, 0.5 and 0.96, respectively.

PSfrag replacements
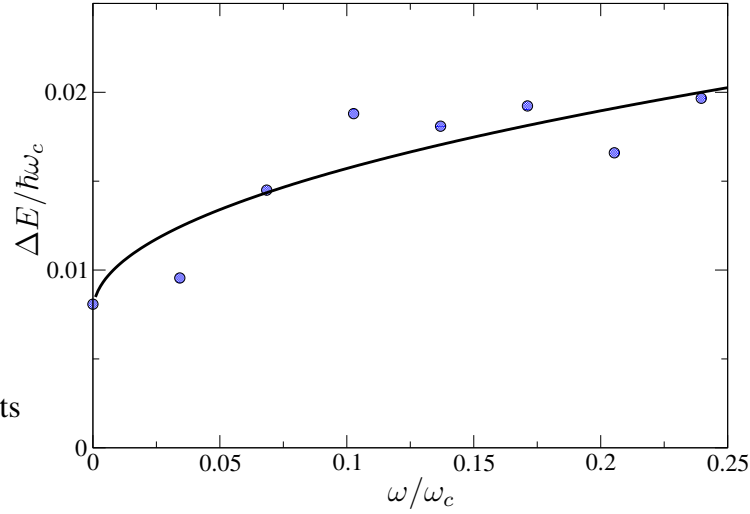
Figure 4.5: Scaling of the width for the peaks in Fig. 4.4.2 as a function of frequency. The solid
line is a least-square fitted function $\Delta(E) = A\omega^{\tilde{\kappa}} + C$, with $\tilde{\kappa} = 0.49$.

We observe that the peak values of the magnetoconductivity is raised in the presence
of electron-electron interaction. The high-energy tail is lifted, and thus the conductivity
peak deformed, although the Coulomb interaction strength is smaller than the Landau
level gap, thus prohibiting a cyclotron resonance signature. It is difficult to decide,
what exactly the origin of this behaviour is. The most probable is connected to a severe
shortcoming in the Kubo formula we used. The expression (4.23) resembles a response
function obtained in time dependent Hartree or random phase approximation (RPA). On
the other hand, the self-energies entering the spectrum of the effective Hamiltonian are
calculated in Hartree-Fock theory. The latter is not conserved in the RPA, because di-
rect particle-hole interactions ("ladder contributions") during the polarization process (a
moving electron leaves a positively charged zone behind) are omitted. If these contribu-
tions are important, spurious results in the RPA response functions can occur. However,
including the ladders leads to a much more involved problem, which is so far beyond
the scope for our considerations. Anyway, we can conclude that the scaling of the peak
width is likely to be changed by electron-electron interactions.

4.5   Conclusions

We have derived a Kubo formula which enables us to calculate the four-terminal con-
ductivity obtained in quantum Hall measurements directly from eigenstates and eigen-
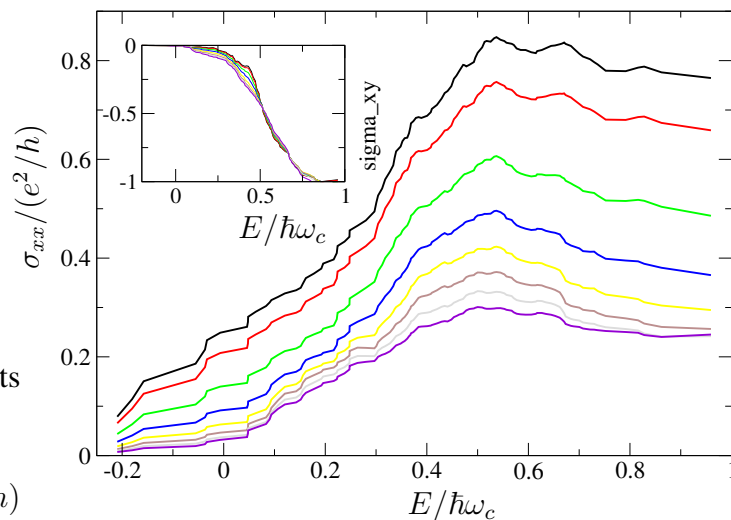
Figure 4.6: Real part of the magnetoconductivity for a system of size $L = 25l_B$ with 400 zero-range impurities at $B = 7$ T. The disorder strength is $\Gamma = \hbar\omega_c$, the Coulomb interaction strength is $\gamma = 0.5\Gamma$. The curves show results for different external frequencies ω at filling factor $\nu = 0.05$. The inset shows the Hall conductivity σ_{xy}. External frequencies are color coded: $\omega/\omega_c = 0$ (black), 0.0342 (red), 0.0684 (green), 0.1026 (blue), 0.1369 (yellow), 0.1711 (brown), 0.2053 (grey), 0.2396 (violet).

values of the Hamiltonian. The conductivity depends also on the frequency of an externally applied electromagnetic field. We have investigated the frequency dependence of the magnetoconductivity peak width and found that the expected power law scaling $\Delta E \propto \omega^{\tilde{\kappa}}$ is not governed by a universal exponent $\tilde{\kappa}$. The exponent $\tilde{\kappa} = 1/(z\tilde{\nu})$ is strongly dependent on the type of disorder and interaction. On the other hand, we have shown in section 3.1 that the static exponent $\tilde{\nu}$ is robust against microscopic properties in the range of the parameters we have assumed. This implies, that the time-dependent transport properties must be handled with care. Within our quite corsegrained model, we can quantitatively support earlier theoretical work and experiments. Especially concerning the correct treatment of mutual electron interaction, further work is desirable to identify the role of correlation in comparison to effective field treatment of the integer plateau transition.
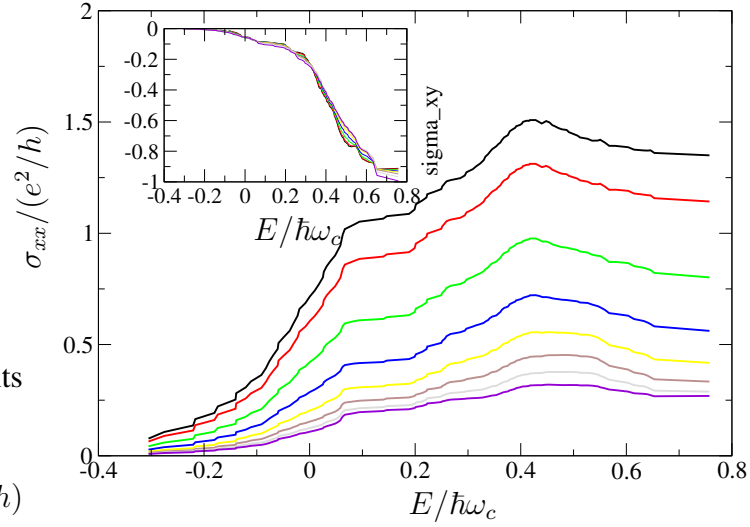
Figure 4.7: Real part of the magnetoconductivity for the system of Fig. 4.6 at filling factor $\nu = 0.5$. The curves show results for different external frequencies ω. The inset shows the Hall conductivity σ_{xy}. External frequencies are color coded: $\omega/\omega_c = 0$ (black), 0.0342 (red), 0.0684 (green), 0.1026 (blue), 0.1369 (yellow), 0.1711 (brown), 0.2053 (grey), 0.2396 (violet).
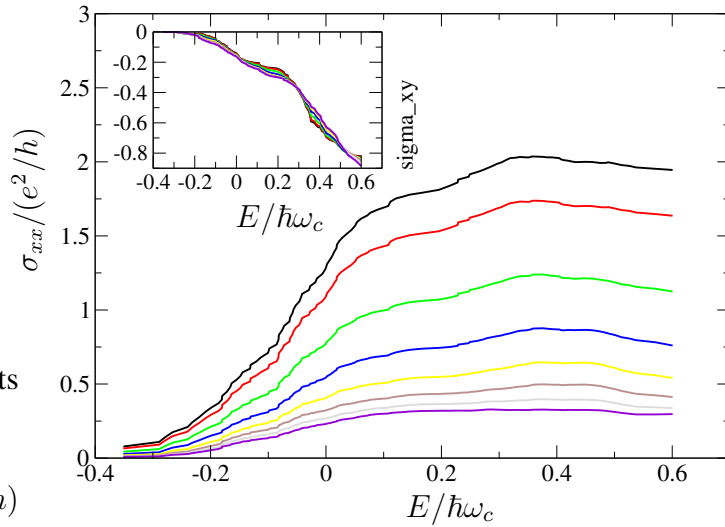
Figure 4.8: Real part of the magnetoconductivity for the system of Fig. 4.6 at filling factor $\nu = 0.96$. The curves show results for different external frequencies ω. The inset shows the Hall conductivity σ_{xy}. External frequencies are color coded: $\omega/\omega_c = 0$ (black), 0.0342 (red), 0.0684 (green), 0.1026 (blue), 0.1369 (yellow), 0.1711 (brown), 0.2053 (grey), 0.2396 (violet).

Coulomb blockade in the integer quantum Hall effect

In this chapter, the compressibility of a two-dimensional electron system with spin in a spatially correlated random potential and a quantizing magnetic field is investigated. Electron-electron interaction is treated in Hartree-Fock approximation. Numerical results for the influences of interaction and disorder on the compressibility as a function of the particle density and the strength of the magnetic field are presented. Localization-delocalization transitions associated with highly compressible region in the energy spectrum are found at half-integer filling factors. Interaction-induced g-factor enhancement is clearly detected. Coulomb blockade effects are found near integer fillings in the regions of low compressibility. Results are compared with recent experiments.

The unique features of the 2DEG discussed in the previous chapters are determined by the quantization of the energy into Landau levels in the absence of disorder and interaction, the broadening of these levels into bands in the presence of disorder and the energy gaps between the spin-split bands in the presence of interaction.

Information about the energy spectrum and thus the relevant single-/many-particle processes in a given sample can be gathered by measuring thermodynamic properties like entropy, compressibility or magnetization[34, 66–70]. These equilibrium quantities are expected to reveal the significance of Coulomb interactions. In this chapter we focus on calculating the chemical potential and the compressibility in the limit where Coulomb interaction prevails and discuss a charging pattern required for a thorough understanding of the integer quantum Hall transition.

5.1 Thermodynamic properties of the electron gas in magnetic fields

5.1.1 The model

The Hamiltonian of the 2DEG is $H_0^s + V_C$ with

$$H_0^s = \frac{1}{2m^*}\left(\mathbf{p} + e\mathbf{A}\right)^2 + \frac{1}{2}sg\mu_B B + V_{\text{dis}}(\mathbf{r}) \tag{5.1}$$

with the vector potential $\mathbf{A} = (0, Bx, 0)$, flux density B and spin $s = \pm 1$. m^* is the effective electron mass μ_B is the Bohr magneton and g the effective electron g-factor. The impurity potential is assumed as $V_{\text{dis}}(\mathbf{r}) = \sum_{i=1}^{N_i}(V_i/\pi d^2)\exp\left[(\mathbf{r} - \mathbf{r}_i)^2/d^2\right]$ with N_i the number of scatterers at random positions $\mathbf{r}_i$ with random strengths V_i, $-V_0 < V_i < V_0$. The range d of the impurity potential is the spatial correlation length of the randomness, $d = 0$ corresponds to uncorrelated disorder, $d > l_B$ ($l_B = \sqrt{\hbar/m\omega_c}$ magnetic length, $\omega_c = eB/m$ cyclotron frequency) yields a slowly varying potential which is believed to be adequate for high mobility samples. The disorder introduces the energy scale $\Gamma = (N_i V_0^2/l_B^2 L^2)^{1/2}$ (L^2 area of the 2DEG). The Coulomb interaction

$$V_C(\mathbf{r} - \mathbf{r}') = \frac{e^2}{4\pi\epsilon\epsilon_0}\frac{1}{|\mathbf{r} - \mathbf{r}'|} \tag{5.2}$$

introduces an energy scale $\gamma = e^2/4\pi\epsilon\epsilon_0 l_B$ (e elementary charge, dielectric constant $\epsilon = 12.4$ for GaAs). Periodic boundary conditions are assumed [39, 71]. Neglecting disorder and interaction, the Schrödinger equation yields the Landau wavefunctions $|mX\rangle$ ($X = -k_j l_B^2$ guiding center coordinate, $k_j = 2\pi j/L$ wavenumber) that are used for the construction of the Hartree-Fock basis.

The Hartree-Fock equation is

$$\sum_b F_{ab}^s C_b^{\alpha s} = E^{\alpha s} C_a^{\alpha s} \tag{5.3}$$

where $\langle mX|\alpha s\rangle = C_{NX}^{\alpha s} \equiv C_a^{\alpha s}$ are the expansion coefficients of the Hartree-Fock states $|\alpha s\rangle$ and $E^{\alpha s}$ the energy eigenvalues. The Fock matrix

$$F_{mXm'X'}^s \equiv F_{ij}^s = H_{0,ij}^s + \sum_a\sum_b \rho_{ab}M_{ijab} - \rho_{ab}^s M_{iabj} \tag{5.4}$$

has to be determined self-consistently. It contains the interaction matrix elements

$$M_{ijab} = \frac{\gamma l}{L^2}\sum_{q_x,q_y} V(q)\langle i|e^{i\mathbf{qr}}|j\rangle\langle a|e^{-i\mathbf{qr}}|b\rangle \tag{5.5}$$

and the density matrix $\rho_{ij} = \sum_s \rho_{ij}^s$,

$$\rho_{ij}^s = \sum_{\alpha(\text{occ})} C_i^{\alpha s *} C_j^{\alpha s}. \tag{5.6}$$

5.1.2 The chemical potential

The chemical potential μ at $T = 0$ is defined as the energy required to add a particle to a system with already N particles present:

$$\mu = E(N+1) - E(N), \tag{5.7}$$

where $E(N)$ the ground state energy for the N-particle system. The ground state energy in Hartree-Fock approximation is given as

$$E_{\text{HF}}^{B,N} = \frac{1}{2} \sum_{ab} \left[(\rho_{ab}^\uparrow + \rho_{ab}^\downarrow) H_{0,ab} + \rho_{ba}^\uparrow F_{ab}^\uparrow + \rho_{ba}^\downarrow F_{ab}^\downarrow \right] \tag{5.8}$$

with the Fock operators $F^{\uparrow,\downarrow}$ (see equations (2.41) and (2.43)) and the density matrices $\rho^{\uparrow,\downarrow}$ (equation (2.61). Figure 5.1 shows the dependence of the chemical potential on the magnetic field for a sample system with and without mutual electron interaction. The curves are obtained at fixed electron density $n = N/L^2$ and varying magnetic field, which results in different fillings of the Landau bands. The filling factor $\nu = N/N_\phi = n\frac{h}{e} B^{-1}$ decreases with increasing magnetic field, whereas the Landau level width Γ increases proportional to $\sqrt{B}$. The energy of the occupied single-particle states thus evolves with the magnetic field. In the case of non-interacting electrons, the chemical potential grows linear with the magnetic field. The Zeeman splitting is negligible, which results in equal occupation of spin-up and spin-down levels. Effectively, there are $2N_\phi$ states per Landau level. With increasing magnetic field, the number of states per Landau level increases. This leads to a depletion of the Landau levels. Close to even integer fillings, levels are completely drained of electrons, which results in sharp discontinuities in the chemical potential which drops to the next lowest Landau level.

The effect of interaction on this behaviour is twofold. The quantum mechanical interaction consists of the repulsive direct term and the attractive exchange term, which lowers the energy expectation value accounting for the fact that the Pauli principle prohibits particle to be in the same quantum state. The Coulomb energy contributions of these configuration are thus subtracted. The most severe shortcoming of the Hartree-Fock approximation used in the present calculations is the neglect of all Coulomb correlations whereas exchange correlation is treated exactly. This results in a strong renormalization of the ground state energy. The μ-B-curve for interacting electrons therefore is shifted towards smaller values, when plotted on the same energy scale.
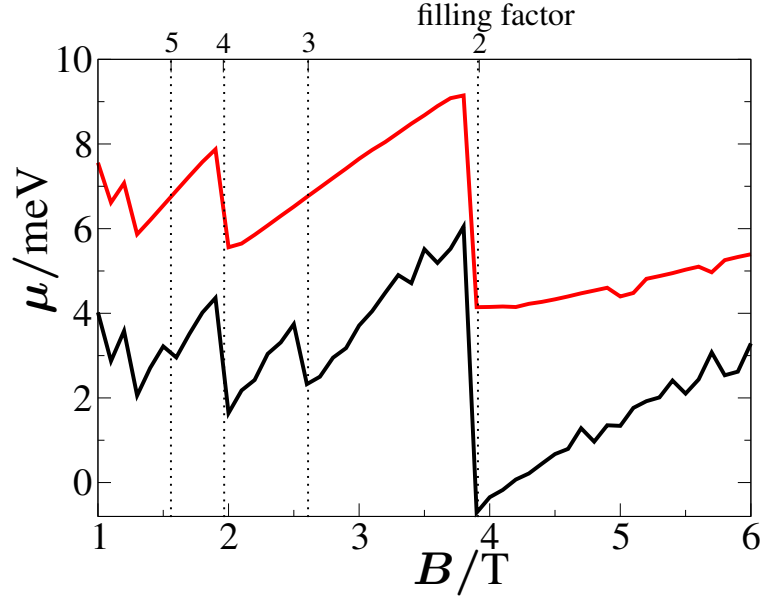
Figure 5.1: Chemical potential μ as a function of the magnetic field B for interacting (black) and noninteracting (red) electrons. The system contains 170 electrons (density $n = 18.9 \cdot 10^{10}$ cm^{-2}) with $\Gamma = 0.41\sqrt{B/\mathrm{T}}$meV.

Furthermore, one observes additional discontinuities at odd integer fillings. They resemble the interaction-induced g-factor enhancement. The different spin subbands are now well separated and subsequently filled (see Figure 5.2). The depletion of Landau levels therefore happens at every integer filling factor. The slope of the chemical potential remains linear, but is larger than for non-interacting electrons.

5.1.3   Tunneling and thermodynamic density of states

The density of states $D(E)$ can be regarded as the number of particle eigenstates available in an energy range $[E, E + dE]$ and is normalized for an N-particle system with Fermi energy ϵ_F by requiring

$$N = \int\limits_{-\infty}^{\epsilon_F} dE D(E), \tag{5.9}$$

with

$$D(E) = \sum_{\text{states } i} \delta(E - \epsilon_i). \tag{5.10}$$
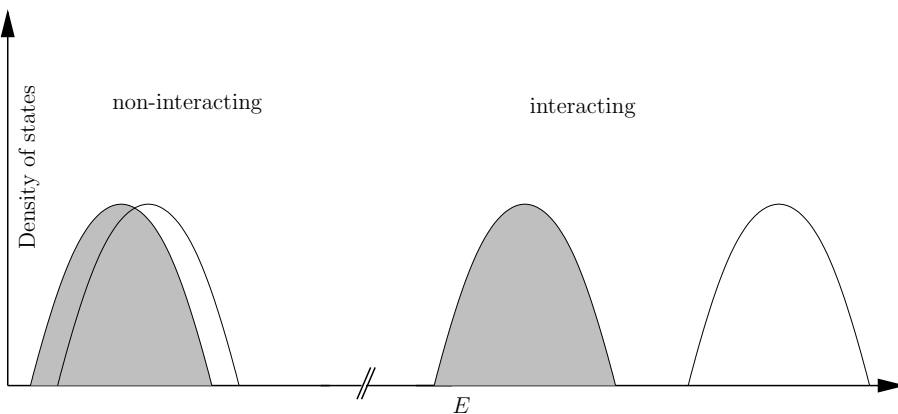
Figure 5.2: Schematic tunneling density of states for non-interacting and interacting electrons.

This quantity can be used to determine the probability for a new particle to tunnel into the system without changing the energy level structure and is therefore known as the tunneling density of states (TDOS).

Figure 5.3 shows an example of the TDOS for a disordered system of non-interacting (red) and interacting electrons (blue). In the presence of Hartree-Fock interaction, the TDOS shows a gap at the Fermi level (dashed lines). This gap indicates a clear separation of occupied and unoccupied energy levels, which is not related to criticality, because it occurs at every Fermi energy, regardless of the corresponding localization length. An astonishing similarity is observed with the Efros-Shklovskii-gap [72], which is an interaction induced linear decrease of the TDOS on two-dimensional systems. However, it has been shown [59] that the Hartree-Fock TDOS differs significantly from the thermodynamical density of states $d\mu/dn$, which specifies the change in the chemical potential as a response to changes in the particle density n. It is the latter which has to be used in order to determine quantum transport behaviour in the presence of disorder and interaction.

5.2   Coulomb blockade in the integer quantum Hall effect

In this section, we discuss a recent experiment giving evidence for charging effects in the integer quantum Hall regime and present an effective single-particle theory which aims to integrate these results into the consistent single-particle theory describing the metal-insulator transition in this regime.

In a recent attempt to identify localized states of a two-dimensional electron gas in a high mobility GaAs/GaAlAs sample, Ilani and coworkers [34] measured the change

PSfrag replacements
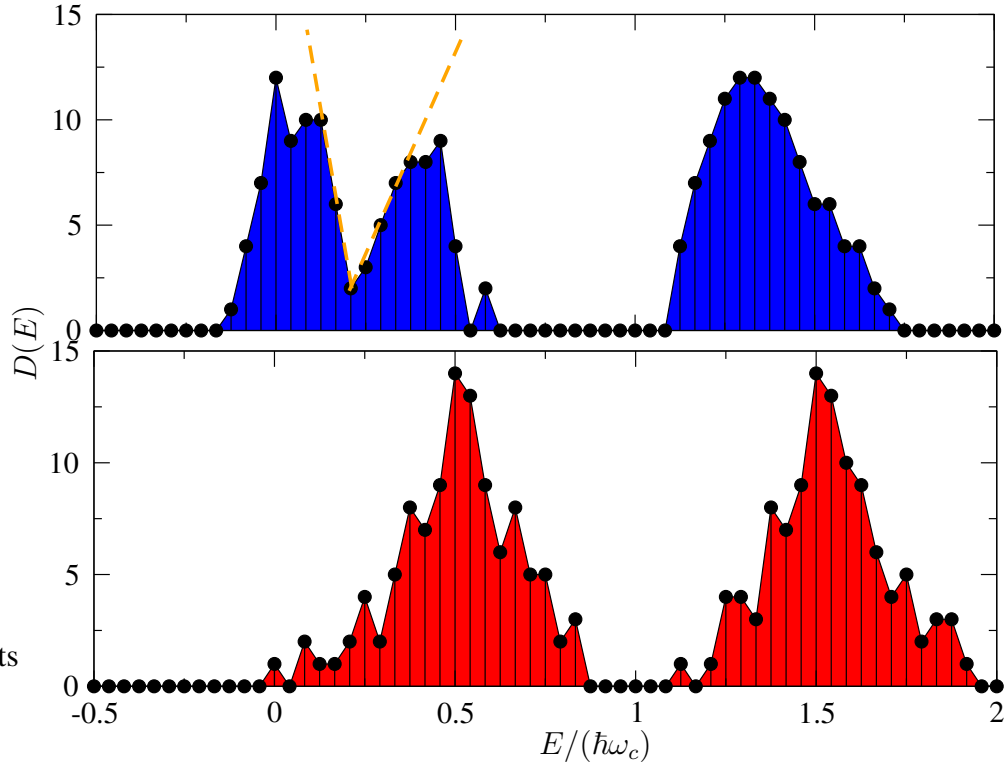
Figure 5.3: Tunneling density of states for non-interacting (red) and interacting (blue)electrons in a fixed realization of disorder at $B = 7$ T. The histogram for the interacting spectrum shows a linear Coulomb gap at the Fermi energy. Dashed lines are guides to the eye.

of the chemical potential with respect to the particle density n and magnetic field B, which is proportional to the voltage V_{bg} applied to a metallic back gate mounted onto the sample.

Consistent with the expectations discussed in the previous section, the results exhibit incompressible lines in the n-B-plane along integer filling factors. In addition, a pattern of alternating compressible and incompressible lines parallel to these filling factors appear, also in the insulating phase parallel to $\nu = 0$. These regions are of constant width with a constant number of states belonging to them, the states evolve in the n-B-plane with exactly the slope of the corresponding quantum Hall phase $\nu = 0, 1, 2, \ldots$. In particular, the constant width of the stripes indicate a constant number of localized states, which is in clear contradiction to the common understanding of the quantum Hall transition, since the number of states per Landau level grows linearly with B and only a few states (one in the thermodynamical limit) are expected to be extended and thus com-
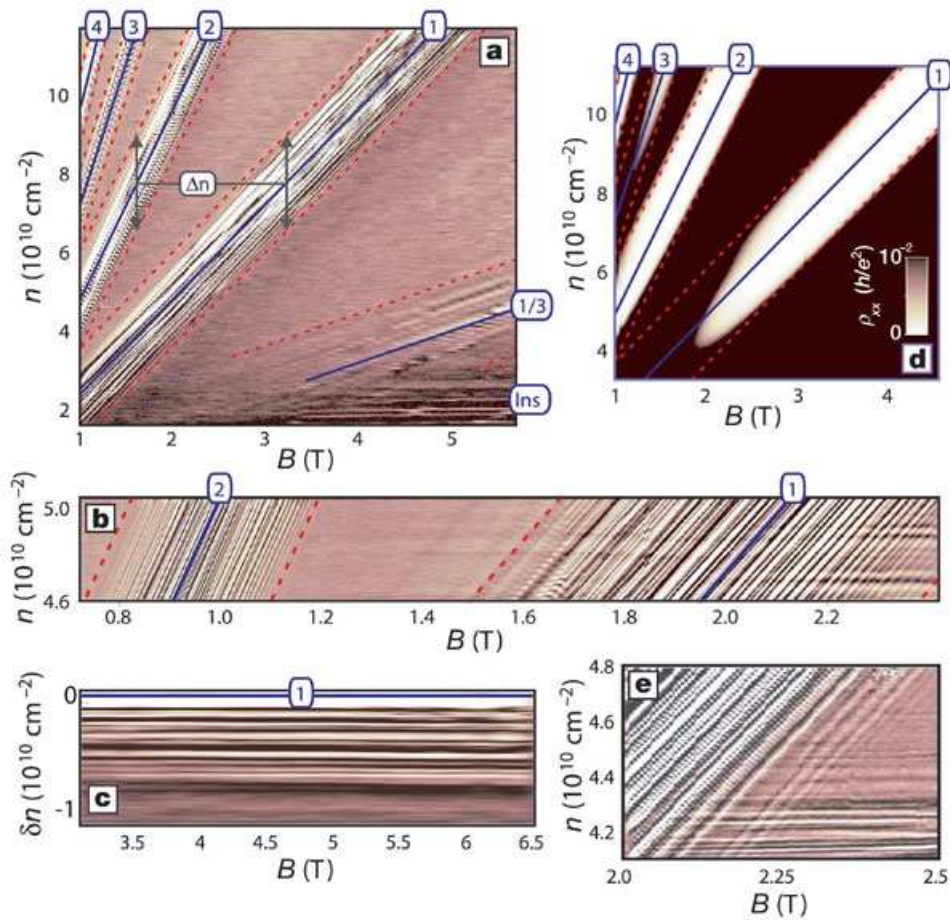
Figure 5.4: Compressibility measurements in dependence of filling factor as function of magnetic field and particle density. Picture taken from Ilani *et. al.*, Nature 2004 [34].

pressible. Therefore, a mechanism must be active which keeps the number of localized states constant. This must apparently be attributed to Coulomb interactions.

Single electron transport through quantum dots is a standard setup to study the effect of inter-electron relations in confined geometries. A central observation in this case is the emergence of periodic oscillation in transmission conductivities, related to a similar oscillation in the chemical potential. This phenomenon is known as Coulomb blockade [73].

The underlying mechanism is related to strong Coulomb interaction between the electrons in the dot and the entering electron: The energy required to add an electron to the dot is given by the chemical potential. If this energy is paid, the additional charge within the dot is screened by the rearrangement of charges in the dot. The resulting

electrostatic potential is flat and gives rise to a lower chemical potential, which favors the entry of another charge. In this manner, the observed oscillatory behaviour of the chemical potential is created. The related charging patterns are surprisingly similar to those shown in Fig. 5.4.

From these results, one can conclude, that each line corresponds to the charging of an individual localized state, governed by a Coulomb blockade of localized states.

The appearance of Coulomb blockade in integer quantum Hall phases demonstrates the presence and importance of Coulomb interaction in this regime. As a consequence, the nature of the integer quantum Hall transition must be characterized by the properties of an interacting, strongly correlated electron system. On the other hand, single-particle physics yields a qualitatively and quantitatively convincing description of the localization-delocalization transition and is supported by many experiments. In the remainder of this chapter, we discuss the Hartree-Fock approach for Coulomb interaction in the quantum Hall system and try to connect the two competing interpretations of the transition.

5.3   Compressibility patterns in the Hartree-Fock approximation.

5.3.1   Introduction

The integer quantum Hall Effect occurs when a two-dimensional electron system (2DEG) is subject to a strong perpendicular magnetic field [1]. The integer quantization of the Hall conductance can be understood in terms of quantum phase transitions near the centres of the Landau bands associated with disorder-induced localization-delocalization transitions of single-electron states which can be described within the frame of a one parameter scaling model. Neglecting the Coulomb interaction, the localization length has been found to diverge, $\xi \propto |E - E_C|^{-\tilde{\nu}}$, where E_c corresponds to the critical energy. The universal value of the critical exponent, $\tilde{\nu} = 2.34 \pm 0.04$ [10, 11], is widely accepted. In this model, peaks in the magneto-conductance are associated with the critical energies E_c in the Landau bands. The localized states in the band tails are associated with zero conductance at zero temperature [74].

Despite this picture has been found to be consistent with several transport experiments [21–23, 53], the validity of the one-parameter scaling model has been controversely discussed during the past decade, on the basis of both experimental and theoretical results. Modifications due to Coulomb interaction have been suggested [56, 58] referring to results of frequency-dependent scaling [25]. Whether or not interactions are of importance for understanding the experiments has been debated theoretically [59, 75]. Other experimental findings [76] suggest the influence of interactions on the tunneling density of states. In recent experiments, mesoscopic conductance fluctuations found in

Table 5.1: Cyclotron energy $\hbar\omega_c$, disorder strength $\Gamma = (N_{\mathrm{i}}V_0^2/l_B^2 L^2)^{1/2}$, Coulomb energy $\gamma_0 = (e^2/4\pi\epsilon_0\epsilon_{\mathrm{GaAs}}l_B)$ and number of flux quanta N_ϕ used in the calculations with material parameters for GaAs..

	$\hbar\omega_c$/meV	Γ/meV	γ_0/meV	N_ϕ
$B = 1\,\mathrm{T}$	1.728	0.412	4.526	21
$B = 6\,\mathrm{T}$	10.367	1.01	11.087	131

silicon MOSFETs in dc-transport show regular patterns which have been interpreted as due to charging effects [77]. Regular patterns associated with Coulomb blockade in localized states have also been found in measurements of the shift $d\mu/dn$ of the chemical potential μ with a scanning SET probe when changing the particle density n [34]. The latter results have been interpreted very convincingly in a model in which the quantum Hall transition appears as a consequence of the strong and complete screening of the disorder potential near half-integer filling factors. The absence of screening in the incompressible regions of the energy spectrum leads to localized states that account for the observed charging effects. In this model, the phase transition has been interpreted as a percolation threshold between incompressible and compressible regions at certain concentrations of localized charge islands. It is obvious that this is not consistent with the non-interacting one-parameter scaling scenario.

We report results of an extensive unrestricted Hartree-Fock study of the 2DEG with spin in the presence of long-range correlated disorder and a strong perpendicular magnetic field that can contribute towards more detailed understanding of the experiments. We have studied the change $d\mu/dn$ of the chemical potential μ with the particle density n as a function of n and the magnetic field strength B. This quantity is proportional to the inverse compressibility $\kappa^{-1} \propto d\mu/dn$. We find evidence for strong interaction-induced enhancement of the g-factor. We also find strong evidence for charging effects in regions near integer filling factors. At the same time, however, analyzing the shapes of the Hartree-Fock quasiparticle wave functions indicates that the localization behavior does not seem to be significantly changed as compared to the non-interacting limit. Most of our results are fully consistent with the picture that has been deduced from recent experimental data [34]. However, from the participation number corresponding to the wave functions we deduce strong evidence that the critical behavior near the quantum Hall transition is the same as the one for non-interacting electrons. This is due to quantum corrections which modify the simple percolation mechanism [43].

5.3.2   The delta-SCF approach

We have performed self-consistent calculations for B in the range of $1 \ldots 6$T and $n = (2 \ldots 200)/L^2$ in a square of length $L = 30a$ for $a = 10$ nm. This yields electron densities $n = (0.22 \ldots 22) \, 10^{10} \, \text{cm}^{-2}$. We used 250 impurities with $d = 2a$ and $V_0 = 2$ meV to model a high mobility sample. Table 5.1 summarizes the energy scales used in the calculations.

In order to study the effect of Coulomb interactions, it is useful to control its strength with respect to the other energy scales. We therefore set $\gamma = c\gamma_0$, so that $c = 0$ corresponds to the noninteracting system, and $c = 1$ to the non-screened Coulomb interaction in a GaAs/GaAlAs heterostructure. For each combination of parameters, the self-consistent field and related quantities like total energy and chemical potential are determined separately. Therefore, the self-consistent field can relax and the ground state, the Fock spectrum and the quasiparticle wavefunctions are optimized to the given set of parameters N and B. The chemical potential is then calculated as the difference $\mu = E(B, N + 1) - E(B)$. This method is sometimes referred to as the "delta-SCF-method" [78, 79]. As pointed out, the difference between total energies is calculated successfully in Hartree-Fock approximation, because the response of the N-particle system to the addition of another electron or hole -the screening of the additional or missing particle- is contained in the calculation of the $N \pm 1$-particle wavefunction.

Interband coupling due to interaction and disorder has been taken into account. The number of Landau levels per spin direction included in the calculation has been chosen as $1 + L^2 n_{\max}/N_\phi$ in order to provide enough states available during the self-consistent field calculations.

5.3.3   Localization of Hartree-Fock particles

At the energies in the band tails, the wave functions are localized and located roughly near equipotential lines, at least for strong magnetic fields. In the center of the band, the wave function is delocalized (for an example, see Fig. 5.5).

The quantitative analysis of the participation number P of the wavefunctions near the Fermi energy E, $P^{-1} = \int \mathrm{d}^2 r |\psi^4(\mathbf{r})|^4 \propto \xi^{-2}(E)$ as a function of the filling factor at the Fermi energy (Fig. 5.6) has been tested by its scaling function [52], using the method described in section 3.2.The exponent $\tilde{\nu} = 2.3$ yields a reasonable collapse of the data for different system sizes to a single curve consistent with the critical behavior of the localization length without interaction taken into account. The curve also resembles the scaling of Hartree-Fock wave functions obtained at *fixed* filling factor using occupied and empty Hartree-Fock orbitals [52].
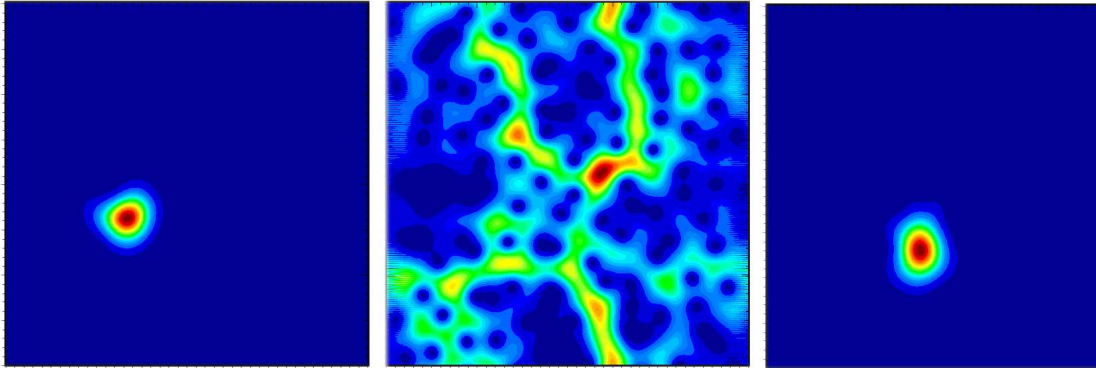
Figure 5.5: Absolute square of wavefunctions at the Fermi level for an interacting system in the lowest Landau level. Left panel: State in the low-energy tail. Central panel: State in the band center. Right panel: State in the high-energy tail.

5.3.4 Compressibility and localization

In the following, we will investigate the localization from a different point of view. It can be argued, that localized wavefunctions are much less sensitive to volume changes than wavefunctions with a localization length of the order of the system size. Therefore, extended states are more "compressible" than localized states.

The compressibility κ is related to the total energy E as follows. Being an extrinsic quantity, the total energy is proportional to the number of particles N in a volume V. The pressure P is the change of energy with respect to change in volume at fixed particle number,

$$P = -\left(\frac{dE}{dV}\right)_N. \tag{5.11}$$

Likewise, the inverse compressibility is the rate of change of P at constant N,

$$\frac{1}{\kappa} = -V\left(\frac{dP}{dV}\right)_N. \tag{5.12}$$

If $E_g = E/N$ is the ground state energy per particle, the only volume dependence of the energy is given by the density $n = N/V$. Thus we get

$$P = -N\frac{dE_g}{dV} = n^2\frac{dE_g}{dn}, \tag{5.13}$$

and

$$\frac{1}{\kappa} = n^2\frac{d^2}{d^2n}(nE_g(n)). \tag{5.14}$$
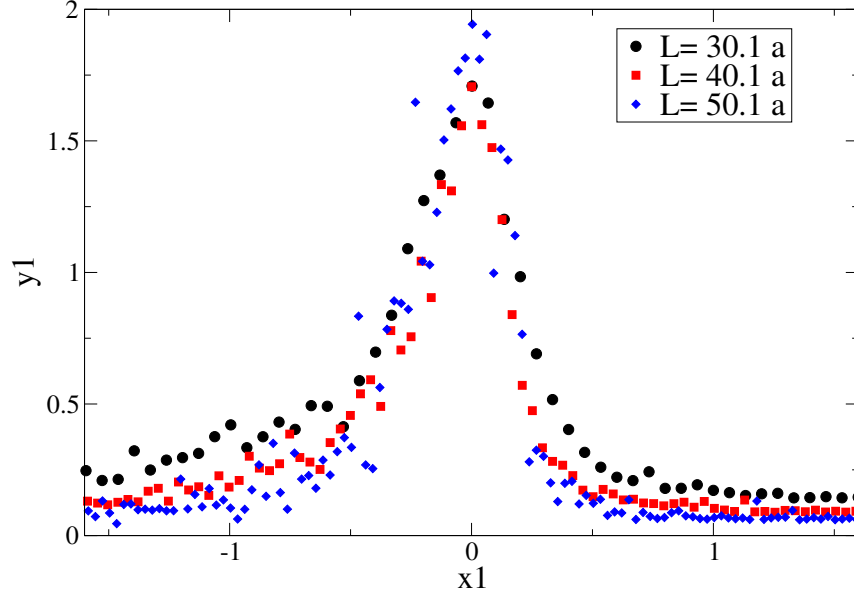
Figure 5.6: Scaling function $\Pi = L^{2-D(2)}P$ as a function of filling factor $(\nu - \nu_c)L^{1/\tilde{\nu}}$, averaged over a few realizations of the disorder potential for each system length L [52]. Parameter values $\tilde{\nu} = 2.3$ (critical exponent) and $D(2) = 1.6$ (correlation dimensions of wavefunctions [80]) give the shown data collapse. The inset shows the dependence of P_ν at the Fermi level on the filling factor ν for spin-up (solid line) and spin-down (dashed line) electrons for a system of length $L = 30.1a$, averaged over a few realizations of disorder. The g-factor enhancement for the illustrated system is so large, that a subsequent filling of the spin-split Landau level is observed.

On the other hand, an $N + 1$-particle system with density $(N + 1)/V = n + 1/V$ has the total energy

$$
\begin{aligned}
E(N + 1) &= (N + 1)E_g\left(n + \frac{1}{V}\right) = (N + 1)\left(E_g(n) + \frac{1}{V}\frac{\partial E_g}{\partial n}\right) \\
&= E(N) + E_g(N) + \frac{n\partial E_g}{\partial n} + \mathcal{O}\left(\frac{1}{V}\right),
\end{aligned}
\tag{5.15}
$$

and, using equation (5.7), we get

$$
\mu = \frac{d}{dn}(nE_g),
\tag{5.16}
$$

a result known as Seitz theorem, and accordingly

$$
\frac{1}{\kappa} = n^2\frac{d\mu}{dn}.
\tag{5.17}
$$
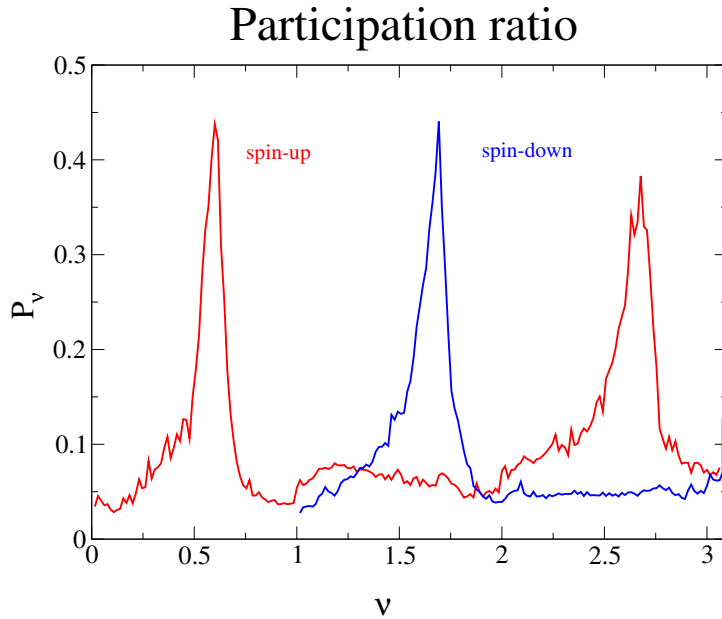
Figure 5.7: Dependence of P_ν at the Fermi level on the filling factor ν for spin-up (solid line) and spin-down (dashed line) electrons for a system of length $L = 30.1a$, averaged over a few realizations of disorder. The g-factor enhancement for the illustrated system is so large, that a subsequent filling of the spin-split Landau level is observed.

Therefore, the inverse compressibility and thus the localization can be related to the change of the chemical potential with particle number, and this is what was measured in the experiment presented above.

We will continue with an investigation of the role of Coulomb interactions on this quantity.

5.3.5 Results

The total Hartree-Fock energy for N particles

$$E_{\mathrm{HF}}^{B,N} = \frac{1}{2} \sum_{ab} \left(\rho_{ab} H_{0,ab} + \rho_{ba}^\uparrow F_{ab}^\uparrow + \rho_{ba}^\downarrow F_{ab}^\downarrow \right) \tag{5.18}$$

is used to determine the chemical potential $\mu = E_{\mathrm{HF}}^{N+1,B} - E_{\mathrm{HF}}^{N,B}$ and accordingly

$$\frac{d\mu}{dn} = L^2 \left(E_{\mathrm{HF}}^{N+1,B} - 2E_{\mathrm{HF}}^{N,B} + E_{\mathrm{HF}}^{N-1,B} \right) \propto \frac{1}{\kappa} \tag{5.19}$$

Figures 5.8, 5.9 and 5.10 show $d\mu/dn$ for various particle numbers and magnetic fields without and with interaction. Without interaction (Fig. 5.8), the pattern indicates

compressible states everywhere except near lines that correspond to even integer filling factors $\nu = N/N_\phi$ and some deviations for small particle numbers. This is the expected behaviour, since every new particle that enters finds many states at energies close to the Fermi level. Therefore, the Fermi energy remains almost unchanged with respect to the particle number, as long as the actual Landau level is not completely filled. Near even integer filling, the Fermi level jumps to the next Landau level due to vanishingly small level density. In the presence of Zeeman splitting, there exist N_ϕ states per spin alignment in each Landau level. Since the Zeeman energy in GaAs is very small in comparison to the other energies (the effective electron g-factor in GaAs is $g = -0.44$), the levels overlap strongly and are equally occupied. Therefore, lines marking incompressible states are only obtained for even fillings. With interaction, the Zeeman splitting is large due to exchange enhancement of the g-factor [81]. Spin-up levels and spin-down levels are now well separated, resulting in additional incompressible lines at odd filling factors. This effect is exaggerated in our spin-unrestricted Hartree-Fock-approximation [82], which treats the exchange term exactly but neglects other correlations.

Figures 5.9 and 5.10 show compressibility patterns for different interaction strengths. The compressibility of the interacting electrons exhibit several regular structures. Horizontal lines of equal compressibility parallel to the B-axis appear below $\nu = 1/2$, enclosed by lines of low or even negative compressibility. At $\nu \approx 1/2$, a region of high compressibility exists. At filling factors close to $\nu = 1$, lines of low compressibility parallel to the line $n = \nu n_B = j/2\pi l_B^2 = jeB/h$ corresponding to this filling factor are observed. The width of region of electron density where this happens is independent of B. The number of the strongly localized states must therefore be independent of B. This has been ascribed before to Coulomb blockade in strongly localized states associated with deep potential wells [34]. Localized electrons block the entrance of another electron and require a jump in the chemical potential, until the potential landscape is completely screened, which then makes the addition of a further electron more favorable. This can even result in a negative compressibility, which in this case is not related to a thermodynamic instability, but rather to the fact that a positive impurity can be screened and even overcompensated by an entering electron, which in turn causes a depletion of electronic charge afterwards in this region [83]. Structures resembling charging effects are repeated in the higher Landau levels, although less prominent, because the localization length of the electrons in high Landau increases with the Landau level index, thus making the interacting system more sensitive to compression. We emphasize that the behavior of the Hartree-Fock total energy with n and B provides the correct charging pattern in the strongly localized region.

In addition to these Coulomb interaction-dominated features related to the charging of localized states, we observe highly compressible regions around half integer filling factors $\nu = j/2$, $n_B = jeB/2h$. These correspond to the centers of the Landau bands where the disorder is considerably screened. The width of these regions, Δn_ext is con-
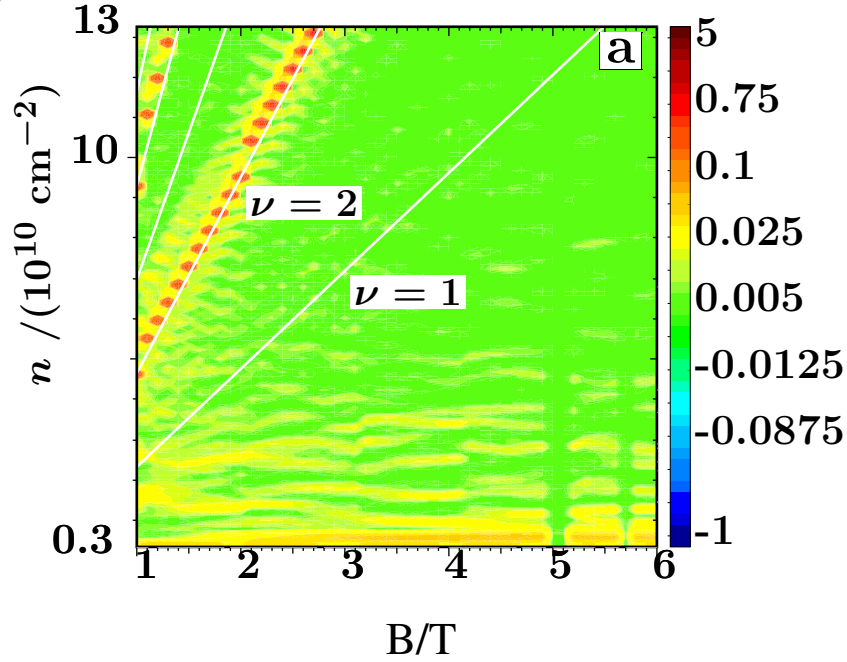
Figure 5.8: $d\mu/dn$ (in units of meV/L^2) in the (n, B)-plane for non-interacting electrons with $\gamma/\gamma_0 = 0$. Dark (blue) regions high, bright (red) regions low compressibility. Solid white lines are guide to the eyes.

stant as a function of B. The total number of the effectively extended states (states with diameters larger than the system size) in a Landau band must be considered as independent of B although the total number of single-electron states per Landau band increases linearly with B. This can be qualitatively understood by noticing that in the one-band approximation the single particle density of states $D(E)$ scales as [84]

$$D(E/\Gamma) = (N_\phi/\Gamma)f(EB/\Gamma). \tag{5.20}$$

The energy interval $\Delta E = |E - E_c|$ in which the localization length exceeds the system size is defined by

$$\xi(E) = \xi_0|E - E_0|^{-\tilde{\nu}} > L. \tag{5.21}$$

Thus,

$$\Delta E = (L/\xi_0)^{-1/\tilde{\nu}} \propto B^{-1/\tilde{\nu}}, \tag{5.22}$$
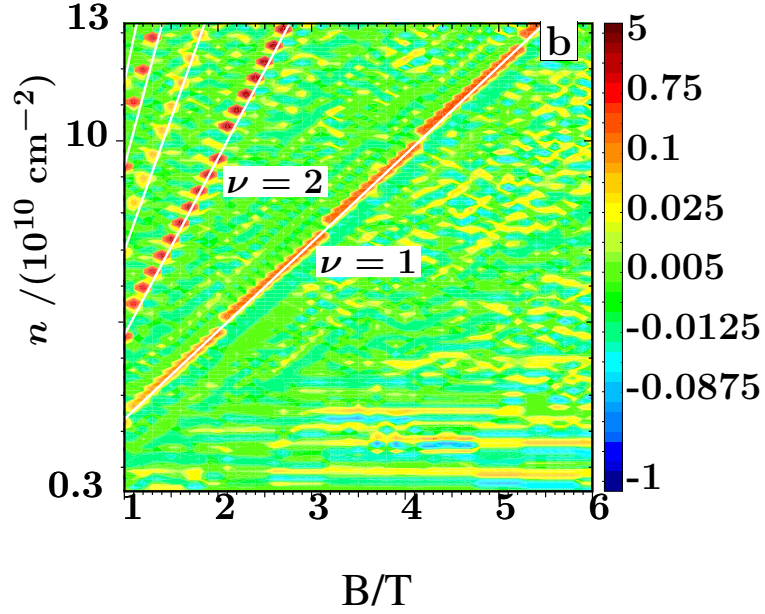
Figure 5.9: $d\mu/dn$ (in units of meV/L^2) in the (n, B)-plane for interacting electrons with $\gamma/\gamma_0 = 0.1$. Dark (blue) regions high, bright (red) regions low compressibility. Solid white lines are guide to the eyes.

since $\xi_0 \propto \Gamma^{-2} \propto B^{-1}$. Thus,

$$\delta n_{\text{ext}} \approx D(0)\Delta E \propto B^{1/2-1/\tilde{\nu}} = B^{0.065} \approx \text{const.}, \tag{5.23}$$

with $\nu \approx 2.3$.

Between the low-compressibility regions of Coulomb blockade in the strongly localized states and the high compressibility regions of delocalization, there are large regions of intermediate statistically fluctuating compressibility. These correspond to localized states that cover larger spatial regions with randomly fluctuating areas. The charging energies of these states, if applicable at all, should be much smaller than in the regimes of strongly localized states, and also strongly fluctuating. As a consequence, one would not expect regular compressibility patterns in these intermediate regions, and this is what is observed in Fig. 5.10. In these regions, the localization properties are determined by the competition of tunneling *between*, and destructive interference *along* the percolating equipotential lines, and it is this competition that is responsible for the critical behavior [43]. The regimes of strong localization and extended states are clearly observed, separated by regions of intermediate states.
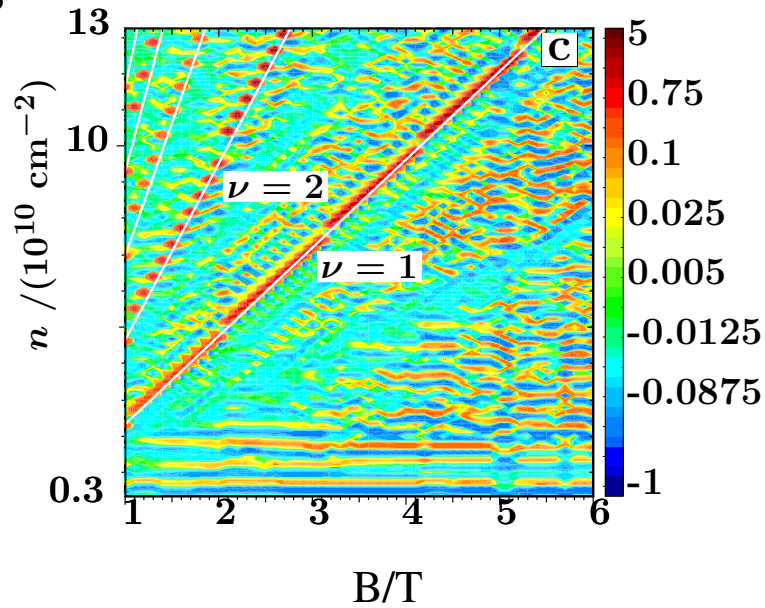
Figure 5.10: $d\mu/dn$ (in units of meV/L^2) in the (n, B)-plane for interacting electrons with $\gamma/\gamma_0 = 0.5$. Dark (blue) regions high, bright (red) regions low compressibility. Solid white lines are guide to the eyes.

The appearance of charging lines parallel to integer filling factors raises the question if correlations beyond the Hartree-Fock approximation can affect the compressibility pattern. Rigorous calculations are very demanding from a computational point of view and will not be reported here. It remains an open issue if correlated ground states can suppress the strong fluctuations in the critical region as indicated in the experiment [34]. However, the Hartree-Fock results reproduce the charging effects in the domain of localized states very well and support the assumption that the critical behaviour of the integer quantum Hall transition can be understood within an effective single particle picture.

5.4   Conclusions

In conclusion, we have investigated quantitatively the density dependence of the chemical potential as a function of electron density and magnetic field for a quantum Hall system. We have shown that electron-electron interactions –treated in Hartree-Fock

approximation, but with the possibility for the ground state to respond to changes in magnetic field or electron density – modify the corresponding compressibility pattern. The appearance of regular structures can be interpreted as charging of localized states. This is in agreement with recent experiments and suggests that interactions are important for the understanding of the integer quantum Hall effect especially in the plateau regions. It is important to note that the latter results are not contradictory to the conjecture that the critical behaviour of the metal-insulator transition remains unaffected from interaction and microscopic details of the disorder potential. The scaling of the participation number of the wavefunction at the Fermi energy is consistent with the results for single-particle wavefunctions, although for each electron density the effective potential changes in response to the charge rearrangement due to the entrance of a new particle.

Our results therefore imply that an effective one-particle approximation can be used to study the critical behaviour at the quantum Hall phase transition, although interaction effects are important for understanding the behaviour in the band tails.

Part III

On the effects of spatial confinement

The chiral metal-insulator transition

The quantum phase diagram of disordered wires in a strong magnetic field is studied as function of wire width and energy. The two-terminal conductance shows zero temperature discontinuous transitions between *exactly* integer plateau values and zero. In the vicinity of this transition, the chiral metal insulator transition (CMIT), peculiar states are identified which are superpositions of edge states with opposite chirality. The bulk contribution of such states is found to decrease with increasing wire width. Based on exact diagonalization results for the eigenstates and their participation ratios, we conclude that these state are characteristic for the CMIT, have the appearance of nonchiral edges states, and are thereby distinguishable from other states in the quantum Hall wire, namely, extended edge states, two-dimensionally (2D) localized, quasi-1-D localized, and 2D critical states.

This chapter has been published as a scientific paper [85].

6.1 Introduction

Recently, there has been renewed interest in quantum Hall bars of finite width, where the interplay between localized states in the bulk of the two-dimensional electron system (2DES) and edge states with energies lifted by the confinement potential above the energies of centers of bulk Landau bands, E_{n0} [32], results in the quantization of the Hall conductance. The study of mesoscopically narrow quantum Hall bars [86], revealed new types of conductance fluctuations [87–89], edge state mixing [81, 90–100], the breakdown of the quantum Hall effect [101], and the quenching of the Hall effect due to classical commensurability effects [102]. In the presence of white noise disorder

the edge states do mix with the bulk states when the Fermi energy is moved into the center of a Landau band. It had been suggested that this might result in localization of edge states [94–96, 99, 100, 103]. Recently, it has been shown that at zero temperature the two-terminal conductance of a quantum wire in a magnetic field exhibits for uncorrelated disorder and hard wall confinement discontinuous transitions between integer plateau values and zero [104]. These transitions have been argued to be due to sharp localization transitions of chiral edge states, where the localization length of the edge states jumps from *exponentially large* to finite values, driven by the dimensional crossover of localized bulk states, and are accordingly called chiral metal insulator transitions (CMIT).

In this article, we will study the nature of this transition in more detail, and in particular find that at this transition there exists a new type of state, with properties distinguishable from both localized and extended bulk states, and extended edge states. This new state is a superposition of edge states with opposite chirality. Since it is still located mainly close to the edges, we will call this state *nonchiral edge state*.

The article is organized in the following way. In the next section, we present transfer matrix calculations of the quantum phase diagram of a quantum Hall bar with uncorrelated disorder, being characterized by the two–terminal conductance G as function of energy E and width w of the wire. Sharp jumps in the conductance from integer values to zero are found as function of energy. These CMITs are seen to become more pronounced with increasing wire widths w.

In the third section we will study with exact diagonalization the eigenstates of a disordered quantum Hall wire. We will classify these states into five classes, the edge states, the 2D localized states, the quasi-1-D localized states, 2D extended states, and the new nonchiral edge states at the chiral metal insulator transition. These states are characterized by their specific participation ratio as function of energy and wire width w, their distribution of coefficients in an expansion in eigenstates of the clean 2DES, and the spatial distribution of the eigenfunction amplitudes. This allows us to identify the state at the transition as a superposition of edge states of opposite chirality.

The final section contains our conclusions, and a discussion on how the CMIT could be observed experimentally.

6.2   The Quantum Phase Diagram of the CMIT

Using the transfer matrix method[1] [4], we have calculated the two-terminal conductance [105] G as function of energy E in a tight binding model with band width $8t$, where t is the hopping amplitude, of a disordered quantum wire in a perpendicular magnetic field (Fig. 6.1), with hard wall boundary conditions at $y = \pm L_{\text{bulk}}/2$ and finite length

---

[1]All results on localization length and two-terminal conductance used in this section are based on programs by courtesy of Prof. Tomi Ohtsuki, Sophia University, Japan.
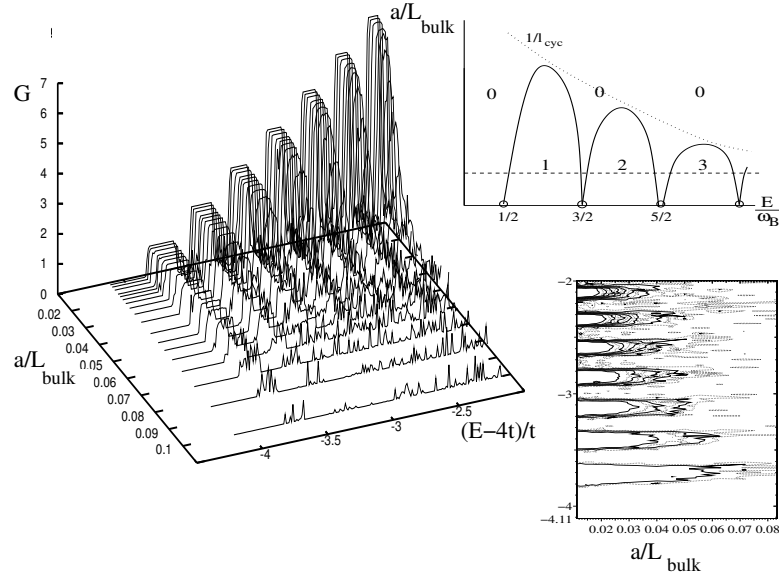
Figure 6.1: The conductance as function of energy for increasing values of the width L_{bulk}
(left), and in a contour plot as function of energy and L_{bulk} (lower right), as com-
pared with the schematic phase diagram (upper right). Finite integer values of the
conductance correspond to the number of extended edge states. The disorder is uni-
formly distributed in an interval of width $W = 0.8t$. There are $x = 0.025$ magnetic
flux quanta per elementary cell of area a^2.

$L = 2000a$ [104]. Here we have assumed a square lattice with lattice spacing a. The
disorder potential is uniformly distributed in an interval $[-W/2, W/2]$. These results
are summarized in the phase diagram (Fig. 6.1), where the value of G, in units of e^2/h,
is given as function of bulk width L_{bulk} and energy E in units of $\hbar\omega_B$, for a disorder
strength $W = 0.8t$. As expected, $G = m$, where m is the number of extended edge
states between the Landau bands. Close to the middle of the Landau bands, however,
the conductance plateaus collapse abruptly to $G = 0$.

When the wires are so narrow, that the edge states cannot form, as it is the case when
the width is smaller than the cyclotron length, or when edge states of opposite chirality
are mixed by backscattering, then all the states become localized and the conductance
is vanishing with only small mesoscopic fluctuations due to the finite length L of the
wire. Previously, it has been pointed out that, when the bulk localization length ξ is
smaller than the physical wire width w, backscattering between edges is exponentially
suppressed. As a result, the localization length of edge states increases strongly.
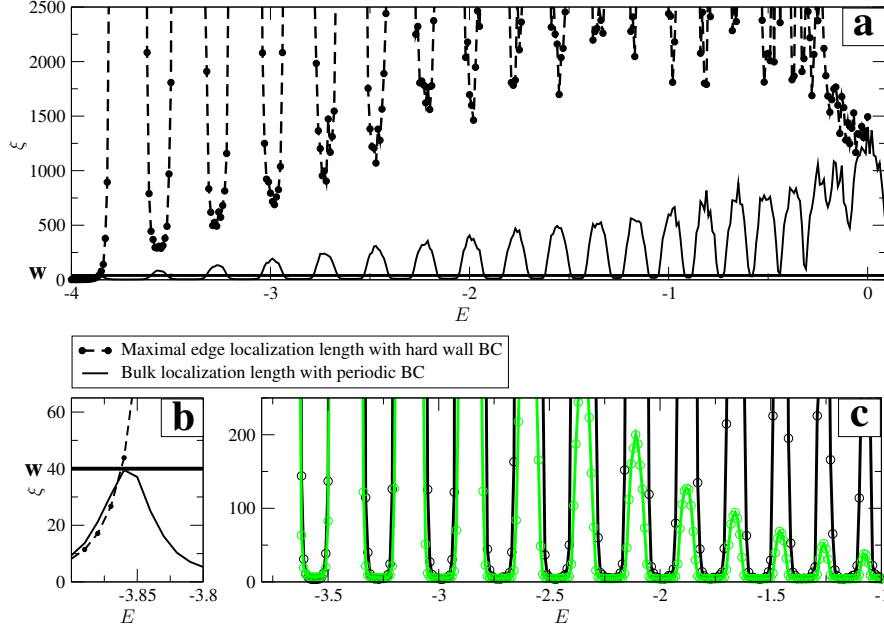
Figure 6.2: (a) The localization length for a disordered wire calculated with the transfer matrix method with periodic boundary conditions (full line) and with hard wall boundary conditions (dashed line) for uniformly distributed uncorrelated disorder in an interval of width $W = 0.8t$. The straight line indicates the bulk width $w = 40a$. There are $x = 0.025$ magnetic flux quanta per elementary cell of area a^2. (b) Enlargement of the low-energy region of (a). Edge and bulk localization length coincide as long as no edge state is present. (c) The functions $\xi_{\text{edge}}/\xi(E)$ (black) and $e^{2w/\xi}$ (green).

The overlap of opposite edge states is known to decrease exponentially with increasing wire width w [91–93]. Thus, the backscattering rate between edges, being proportional to the square of the overlap integral is $1/\tau \sim \exp(-2w/\xi)$. Since the edge states are one-dimensional, their localization length due to the back scattering is given by $\xi_{edge} = 2v_F\tau$, with Fermi velocity v_F. On the other hand, when the bulk localization length ξ becomes equal to the wire width, one expects that the edge states become mixed with the bulk states, and localized with a length proportional to the bulk localization length ξ. Therefore, we conjectured the edge localization length to behave like [104]

$$\xi_{\text{edge}} = \xi \exp(2w/\xi), \tag{6.1}$$

In Fig. 6.2a, the localization length is plotted as function of energy, as obtained with the transfer matrix method in a tight binding model of a disordered quantum wire in a perpendicular magnetic field with hard wall boundary conditions, dashed line. Since the edge states are the most extended states in the wire, this localization length can be identified with the edge localization length ξ_{edge}.

Using the transfer matrix method [4], we have also calculated the localization length ξ as function of energy E for a disordered quantum wire with identical properties, but with periodic boundary conditions, Fig. 6.2a, solid curve. Since there are no edge states this bulk localization length is small in the tails of Landau bands, and has maxima, which are seen to increase linearly with n.

Indeed the behavior of the edge state localization length follows qualitatively the behaviour suggested by Eq. (6.1). The edge localization length does increase sharply, whenever the bulk localization length becomes smaller than the wire width w (full straight line). Note that the minima in the middle of the Landau bands do increase linearly with the Landau band number n. In Fig. 6.2c, we have explicitly plotted ξ_{edge}/ξ and $\exp(2w/\xi)$, using the numerically calculated values for ξ_{edge} and ξ, as function of E. We find that both functions coincide for all energies above the lowest Landau band and for $l_{cyc} < w$, so that edge states exist in the tails of the Landau bands.

An abrupt decrease of the inverse localization length has been found before for energies in the upper tail of the lowest Landau level and the tails of the second Landau level in Ref. 8. In agreement with our above results, it has been found there, that the inverse localization length decays exponentially in the tails, like $1/\xi_{edge} \sim \exp(-\beta(E)w)$. The fitted values of β have been found there to depend weakly on energy, whereas we identified it directly with the energy dependent inverse bulk localization length $1/\xi(E)$.

From these results we can conclude that the energy at which edges states backscatter and become localized, is, given by the condition that the bulk localization length is on the order of the wire width, $\xi(E_{m,p}) = w$. At this energy, m edge states mix and transitions from extended edge states to insulating states occur. This causes sharp jumps of G from finite integer to vanishingly small values, as seen in Fig. 6.1. This can be explained by the exponential decrease of the edge state localization length, Fig. 6.2. We note that $m = n$ when the energy is above the n-th Landau band , whereas $m = n - 1$, if it is below.

A more detailed understanding of this drastic behaviour of the conductance can be obtained by considering the dimensional crossover of the bulk localization length in disordered wires [104, 106, 107]. In a 2DES with broken time reversal symmetry, scaling theory [7, 40, 108–110] and numerical scaling studies [4, 44, 111] find that the bulk localization length ξ is independent of the wire width, $\xi_{2D} = l_0 \exp(\pi^2 g^2)$. Here, g, is the 2D conductance parameter per spin channel. l_0 is the short distance cutoff, the elastic mean free path $l = 2g(B = 0)/k_F$ (k_F Fermi wave number) at weak magnetic fields, $b \equiv \omega_c \tau < 1$. For stronger magnetic fields, $b > 1$, the short length scale l_0

becomes the cyclotron length l_{cyc}. The conductance parameter g exhibits Shubnikov-de-Haas oscillations as function of magnetic field for $b > 1$. Maxima occur when the Fermi energy is in the center of Landau bands. The localization length in tails of Landau bands, where $g \ll 1$ is very small, is of the order of the cyclotron length $l_{\text{cyc}} = v_F/\omega_B = \sqrt{2n+1}l_B$. It increases towards the centers of the Landau bands, $E_{n0} = \hbar\omega_B(n + 1/2)$ $(n = 0, 1, 2, ...)$, with $\omega_B = eB/m^*$ the cyclotron frequency (e elementary charge, m^* effective mass), v_F the Fermi velocity, and $l_B^2 = \hbar/eB$ defines the magnetic length. In an *infinite* 2DES in perpendicular magnetic field, the localization length at energy E diverges as $\xi \sim |E - E_{n0}|^{-\nu}$. The critical exponent ν is known from numerical finite size scaling studies for the lowest two Landau bands, $n = 0, 1$, to be $\nu = 2.33 \pm 0.04$ for spin-split Landau levels [11, 56, 112], in agreement with analytical [113, 114] and experimental studies [21–26]. In a *finite* 2DES, a region of state exists in the centers of disorder broadened Landau-bands, which cover the whole system of size L. The width of these regions is given by $\Delta E = (l_{\text{cyc}}/L)^{1/\nu}\Gamma$, where $\Gamma = \hbar(2\omega_B/\pi\tau)^{1/2}$ is the band width, with elastic scattering time τ.

However, the 2D localization length is seen to increase strongly from band tails to band centers, even when the wire width w is so narrow, that it is far from the critical point at $w \to \infty$. One can estimate the noncritical localization length for uncorrelated impurities, by inserting g, as obtained within self consistent Born approximation [81, 97, 98]. Its maxima are $g(E = E_{n0}) = (2n+1)/\pi = g_n$. Thus, $\xi_{2D}(E_{n0}) = l_{\text{cyc}} \exp(\pi^2 g_n^2)$ are macroscopically large in centers of higher Landau bands, $n > 1$ [11, 115]. When the width of the system w is smaller than ξ_{2D}, electrons in centers of Landau bands can diffuse between the edges of the system. In long wires, however, the electrons are localized due to quantum interference along the wire with a localization length that is found to depend linearly on g and w [104, 116–120],

$$\xi_{1D} = 2g(B)w. \tag{6.2}$$

The conductance per spin channel, $g(b) = \sigma_{xx}(B)/\sigma_0$, is given by the Drude formula $g(b) = g_0/(1 + b^2)$, ($g_0 = E\tau/\hbar$, $b = \omega_B\tau$) for weak magnetic field, $b < 1$. For $b > 1$, when the cyclotron length l_{cyc} is smaller than the mean free path l, disregarding the overlap between Landau bands, g is obtained in SCBA [81, 97, 98], $g(B) = (1/\pi)(2n + 1)(1 - (E_F - E_n)^2/\Gamma^2)$, for $|E - E_n| < \Gamma$. One obtains the localization length for $b > 1$ and $|\epsilon/b - n - 1/2| < 1$ by inserting g. It oscillates between maximal values in centers of Landau bands, and minimal values in band tails. For $n > 1$, one finds in band centers,

$$\xi_n = \frac{2}{\pi}(2n + 1)w\left[1 - \frac{\ln\sqrt{1 + (w/l_{\text{cyc}})^2}}{(n + 1/2)^2}\right]^{1/2}. \tag{6.3}$$

Thus, the localization length in the center of Landau bands is found to increase linearly with Landau band index n. This is exactly the behaviour observed above in the numerical results, Fig. 6.2.

While it is reasonable to conclude that the edge states do mix with the bulk states at the energy where the bulk localization length is equal to the wire width, and the electrons diffuse freely from edge to edge but are localized along the wire, the question arises, how exactly this transition from extended edge states to localized states does occur. One can gain some further insight by connecting the two ends of the wire together to form an annulus. Piercing magnetic flux through the annulus affects only states whose localization length is larger than the circumference of the annulus. Guiding centers of those states which extend around the annulus do shift in position and energy [32] with a change in magnetic flux. As shown above, in the middle of the Landau band, the electrons can diffuse freely from edge to edge, but are localized along the annulus with $\xi > w$. When adiabatically changing the magnetic flux, the energy of an edge state changes continously. However, it cannot enter the band of localized states, so that at the energy E_m, with $\xi(E_m) = w$, the edge state must be transfered to the opposite edge. There it moves up in energy when the magnetic flux is increased further [32].

In the following, we study the states at this transition in detail in order to find out, whether the edge states become localized mainly by mixing completely with the bulk states, or rather the transition from extended chiral edge states to localized states occurs due to the nonlocal coherent superposition of edge states with opposite chirality, located at opposite edges.

6.3 Exact diagonalization

In this section, we study the localization properties of electrons in quasi one-dimensional wires in the presence of disorder and a strong magnetic field by means of exact diagonalization.

6.3.1 The model

The Hamiltonian of the quasi-1D-wire in the presence of a disorder potential V_{dis} and a confinement potential V_{conf}, is given by

$$H = \frac{1}{2m^*} \left(\mathbf{p} + e\mathbf{A} \right)^2 + V_{\mathrm{dis}}(\mathbf{r}) + V_{\mathrm{conf}}(\mathbf{r}) \, , \tag{6.4}$$

where $e > 0$ is the elementary charge and m^* the effective electron mass.

The disorder potential is modelled as

$$V_{\mathrm{dis}}(\mathbf{r}) = \sum_{i=1}^{N_{\mathrm{imp}}} V_i \delta(\mathbf{r} - \mathbf{r}_i), \tag{6.5}$$

E

PSfrag replacements

L_{bulk}

L
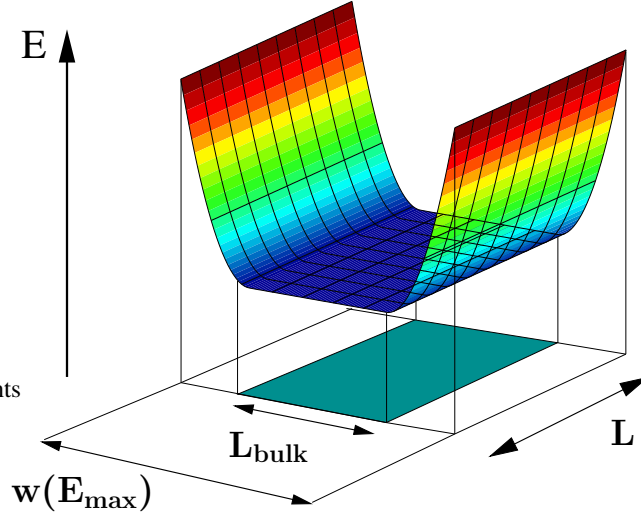
$w(E_{\text{max}})$

Figure 6.3: Model of a quantum wire with length L, parabolic confinement and finite bulk region of width L_{bulk}. The physical width $w(E_{\text{max}})$ is indicated, where E_{max} is the largest energy considered.

where N_{imp} is the number of impurities with uniformly distributed amplitude $V_i \in [-V_0, V_0]$. $\mathbf{r}_i$ is the random position of the impurity.

As we seek to investigate the interplay and localization of edge states and bulk states in a quantum wire, we assume periodic boundary conditions in the x-direction along the wire and choose

$$V_{\text{conf}}(y) = \begin{cases} \frac{1}{2}m\omega_p^2(y - L_{\text{bulk}}/2)^2 & y \geq L_{\text{bulk}}/2 \\ 0 & -\frac{1}{2}L_{\text{bulk}} < y < \frac{1}{2}L_{\text{bulk}} \\ \frac{1}{2}m\omega_p^2(y + L_{\text{bulk}}/2)^2 & y \leq -L_{\text{bulk}}/2 \end{cases} \quad (6.6)$$

as confinement potential in the transversal direction (see Fig. 6.3). This model allows us to tune the confinement strength with the parameter ω_p. The wire width is now defined by the bulk width L_{bulk}. In the limit $L_{\text{bulk}} = L$, we get the usual 2D model for the Quantum Hall effect [39], while for $L_{\text{bulk}} = 0$ we have the parabolic wire model [50]. In the limit of large confinement frequency $\omega_p > \omega_c$, one approaches hard-wall boundary conditions. This type of confinement provides a smooth transition between the edge potential and the potential-free bulk region and renders the situation in real wires better than assuming hard wall boundaries.

The physical width w of parabolic wires w is a function of the Fermi energy E,

$$w(E, L_{\text{bulk}}) = 2 \sqrt{\frac{2E - \hbar\Omega}{\hbar\omega_B}} \, \frac{\omega_B}{\omega_p} \, l_B + L_{\text{bulk}}, \tag{6.7}$$

with $\Omega = \sqrt{\omega_p^2 + \omega_B^2}$. It is obtained by finding the energy eigenvalue of the clean wire which is equal to E and has its guiding center at $\pm w/2$. We fix the basis width L_{basis} to be larger than the physical width $w(E_{\text{max}})$ at the highest considered energy E_{max}. The total number of magnetic flux quanta in the model system is then fixed to $N_\phi = L_{\text{basis}} L/(2\pi l_B^2)$.

6.3.2 Wavefunction analysis

The Hamiltonian, Eq. (6.4) is diagonalized in the Landau representation with basis functions

$$\langle \mathbf{r} | \, nX \rangle = \frac{1}{(l_B L \sqrt{\pi} 2^n n!)^{1/2}} \mathrm{e}^{-\frac{(y-X)^2}{2l_B^2}} H_n\left(\frac{y-X}{l_B}\right) \mathrm{e}^{-\frac{iXx}{l_B^2}} \tag{6.8}$$

Here we have assumed the Landau gauge for the vector potential. The matrix elements of the confinement potential in the Landau representation are given in Appendix A.

The exact diagonalization of the Hamiltonian (6.4) yields eigenenergies E_α with corresponding wavefunctions

$$\psi_\alpha(\mathbf{r}) = \sum_{nX} \langle \mathbf{r} | \, nX \rangle \langle nX \, | \alpha \rangle \tag{6.9}$$

The spatial extention of these wavefunctions is characterized by their participation ratio

$$P_\alpha = \left(L_{\text{bulk}} L \int d^2r |\psi_\alpha(\mathbf{r})|^4 \right)^{-1}, \tag{6.10}$$

which is small for localized states and large for extended states. Note that in this definition, P_α relates to the fixed bulk area $L_{\text{bulk}} L$ while the wave functions can cover a larger area due to the smooth confinement, so that $P_\alpha > 1$ is possible for all states.

In clean 2D systems all states in a Landau level are degenerate. In a disordered wire this degeneracy is lifted by the disorder, and at the edges by the confinement potential. Therefore, localized states in the tail of the Landau bands in the bulk region near the center of the wire coexist with states at the edges at the same energy, and, in principle, mixing of states from the bulk with edge states is possible.

These features are clearly seen in the left part of Fig. 6.4. For a wire of length $L = 40.1 l_B$ in a perpendicular magnetic field of $B = 8\text{T}$, corresponding for $m^* = 0.067$ in units of the bare electron mass to $\hbar\omega_c = 13.82\,\text{meV}$, for three different bulk widths L_{bulk}
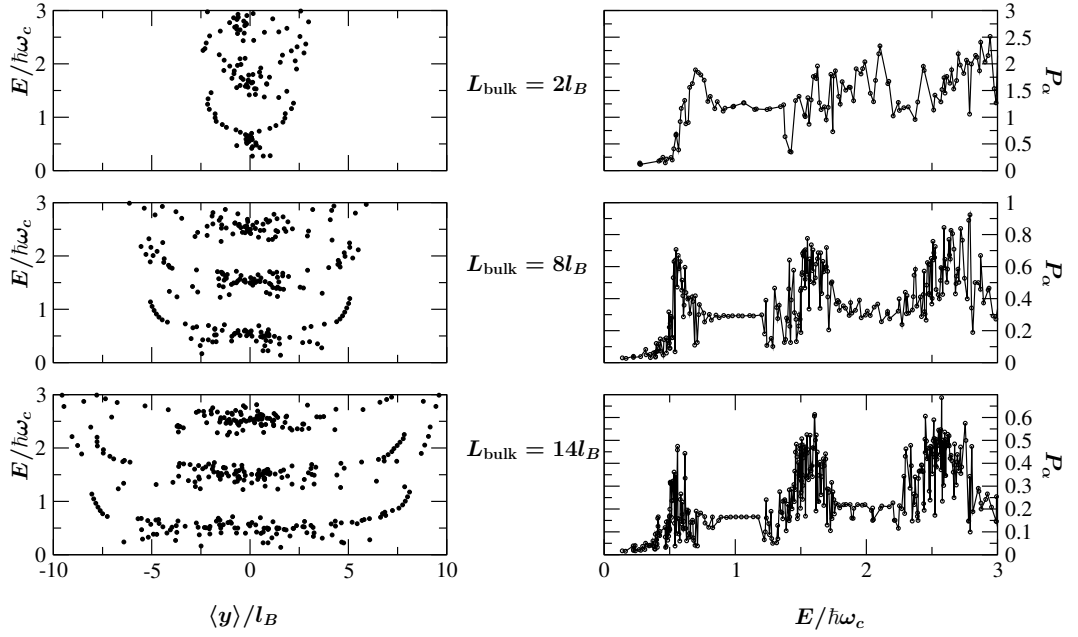
Figure 6.4: Left: The energy eigenvalues E_α of all states in a wire of length $L = 40.1 l_B$ in a perpendicular magnetic field of 8 T for three different bulk widths are plotted versus the expectation value of the transversal position, $\langle \alpha \mid y \mid \alpha \rangle$. The disorder amplitude is fixed to $V_0 = 0.73 \hbar \omega_c$ with $N_i = 150$ impurities and the confinement energy is chosen to have the same magnitude with $\hbar \omega_p = 0.73 \hbar \omega_c$. The basis width is chosen as $L_{\text{basis}} = 1.5 \, w(E_{\text{max}})$, Eq. (6.7), with $E_{\text{max}} = 2 \hbar \omega_c$. Right: Corresponding participation ratio P_α versus E_α.

the eigenenergies are plotted versus the expectation value of their transversal position, $\langle \alpha \mid y \mid \alpha \rangle$. Although we have chosen a smooth confinement potential, these results are in good agreement with earlier results with short ranged disorder in Ref. [94–96]. Obviously, the edge states between the Landau bands are hardly affected by the disorder potential. There is a coupling of edge states of the same chirality in the second and higher Landau bands which leads to the formation of minibands in between the Landau band[94–96] , as seen most clearly in Fig. 6.5. There, we show the same quantities for a longer system with $L = 100 l_B$ and $L_{\text{bulk}} = 8 l_B$ at $B = 8$ T. The disorder is realized by 400 scatterers with $V_0 = 0.73 \, \hbar \omega_c$, with the same value as the confinement energy $\hbar \omega_p = 0.73 \, \hbar \omega_c$. However, there is an abrupt shift of the center of the eigenstates towards the middle of the wire, when their energy is approaching the middle of the Landau band. Still, one can not conclude, if this fact is mainly due to the backscattering
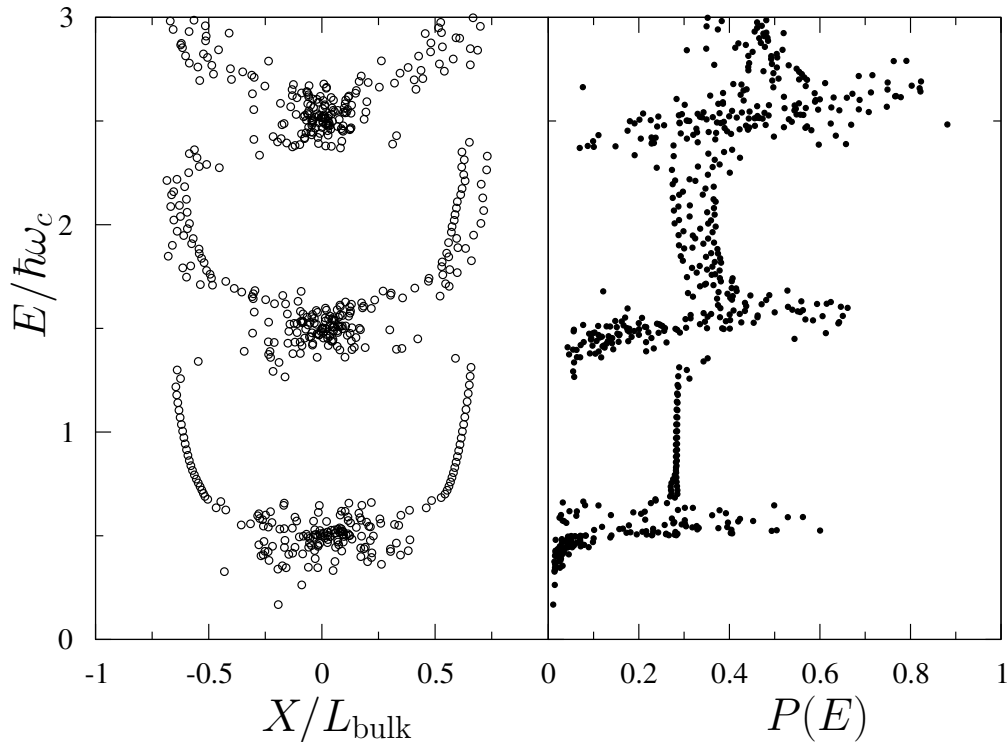
Figure 6.5: Energy dispersion $E(X)$ and corresponding participation ratio $P(E)$ for a longer system with $L = 100 l_B$ and $L_{\text{bulk}} = 8 l_B$ at $B = 8$ T. The disorder is realized by 400 scatterers with uniformly distributed amplitude with maximal value, $V_0 = 0.73 \ \hbar\omega_c$, which equals the confinement energy $\hbar\omega_p = 0.73 \ \hbar\omega_c$.

between edge states from opposite edges, having opposite chirality, or if it is mainly due to a mixing with the bulk localized states.

In order to learn more about the nature of these states, we have calculated the Fermi energy dependence of the participation ratio for different bulk widths with fixed disorder potential and constant magnetic field as shown in the right part of Figs. 6.4, 6.5. It is observed for all three widths that the participation ratio and the eigenenergies, fluctuate as a result of disorder especially in the center of the wire. The participation ratio increases with energy in the tails of the Landau bands and reaches a maximum close to the corresponding center energy (between $0.5 \ \hbar\omega_c$ for $L_{\text{bulk}} \to \infty$ and $0.5 \ \hbar(\omega_c^2 + \omega_p^2)^{1/2}$ for $L_{\text{bulk}} \to 0$). The participation ratio saturates to a constant value between the Landau bands, where only edges states exist, as confirmed by comparison with the left side of Fig. 6.4.

In the following, we scrutinize the localization behaviour in the different energy regions identified above by the energy dispersion and the participation ratio. To determine the nature of the states, we plot the basis state contributions and spatially resolved probabilities for a sample with $L = 100 l_B$ and $L_{\mathrm{bulk}} = 8 l_B$ at typical energies, with disorder amplitude and confinement energy comparable to the cyclotron energy. We concentrate on the lowest Landau level and investigate wavefunctions at energies in characteristic regions of the participation ratio. The result is displayed in figure 6.6.

We find states at $E = 0.3 \hbar \omega_c$ (Fig. 6.6a) which are 2D localized, as confirmed by the fact that they have contributions from basis states with guiding centers in the bulk region, only. In the band center around $E = 0.5 \hbar \omega_c$ the participation ratio fluctuates strongly. In this region we find 2D localized states as well as 1D localized states with a localization length larger than the bulk width, but much smaller than the wire length (Fig 6.6b). In the latter case, basis states from bulk and edge region mix with comparable contributions. Furthermore, we can identify states which cover the whole sample, as shown in Fig 6.6c. These states couple to all regions as well, although the contributions from the left and right edges seem to prevail slightly. The trend indicated by the maxima close to the edges intensifies in the transition region (Fig. 6.6d). At a specific energy, the contribution of the bulk states is small compared to the sharp maxima at the edges, while the electron is found with the same probability on the right *or* the left edge of the wire (Fig. 6.6e). We believe that this nonchiral edge state is unique at least in the thermodynamic limit, of $w \to \infty$ and governs the new type of metal-insulator transition, the CMIT, in quasi-1D quantum Hall wires. This state exhibits notable localization features: being an edge state concerning the participation ratio, it has to be considered localized concerning the conductance, since current flows with equal probability, but reversed sign on both edges. This behaviour is consistent with the sudden breakdown of the conductance observed in Fig. 6.1.

At higher energies, below the next Landau band, edge states are formed as seen in Fig. 6.6. These states are found to be insensitive to disorder.

This sequence of transitions from 2D bulk states, quasi-1-D localized states, states with peaks on both edges of the wire, and decoupled edge states is visible in Fig. 6.7a, where we show the basis state contributions for every fifth state in the lowest Landau level. All features discussed above are seen clearly, with a remarkably narrow transition region from 1D localized states to edge states, as one moves from state 125 to state 145.

In order to visualize this transition in detail, we plot in this interval all states in Fig. 6.7b. The higher energy states are clearly edge states, which are decoupled from the bulk, and are alternatingly located either on the left or on the right side of the wire. The lower the energy, the smaller becomes that peak in intensity at the edge. Still, each state stays located in the edge region, with only a small coupling to the nearest part of the bulk. Then, suddenly, at state ($\alpha = 143$ in Fig. 6.7), there appear two peaks of comparable amplitude on both edges, while the contribution of the bulk is still
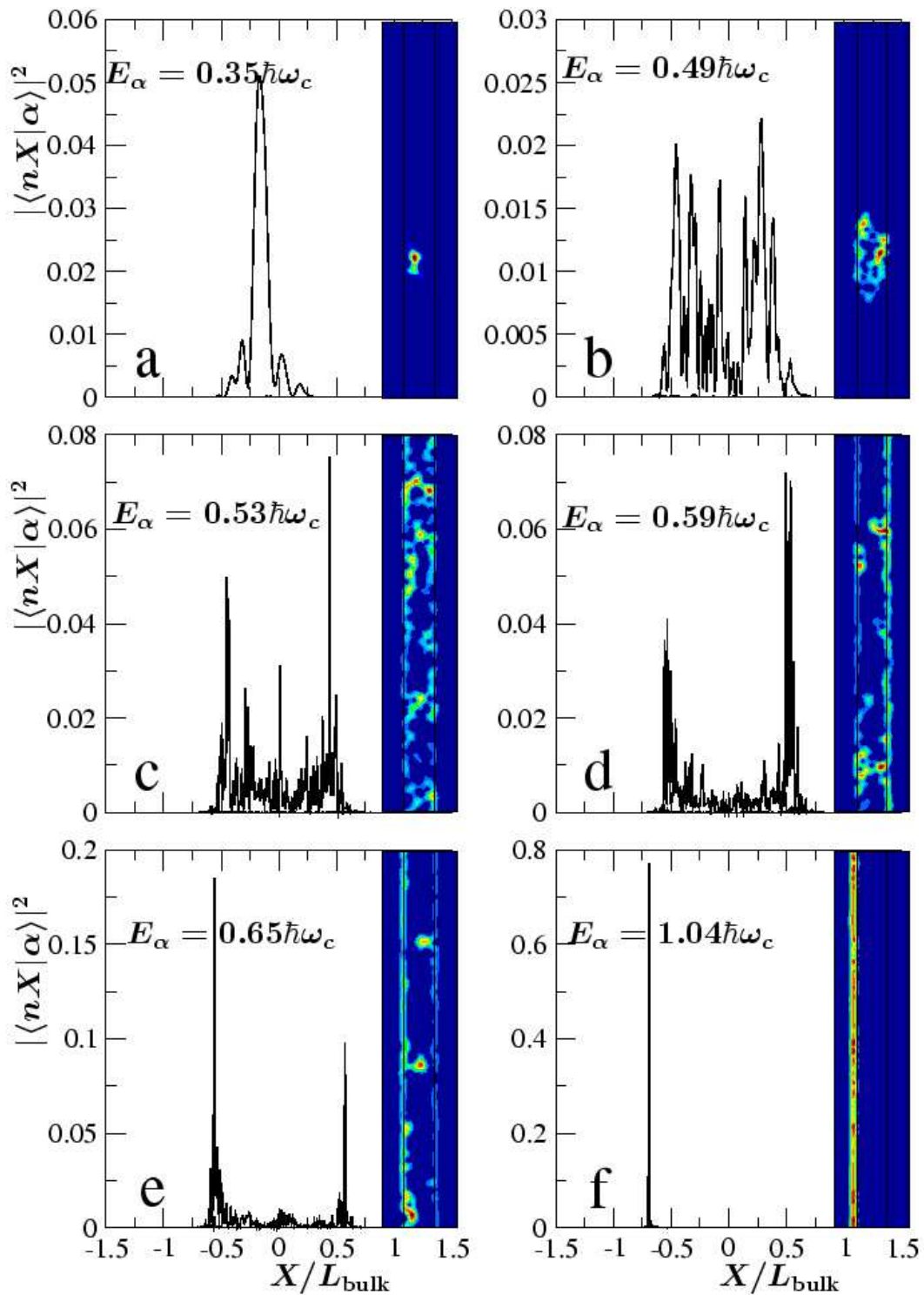
Figure 6.6: Basis state contributions to eigenstates at selected energies. The right insets show the correponding probability densities (blue for low, red for high values), solid lines mark the bulk region. System parameters are the same as in Fig. 6.5.
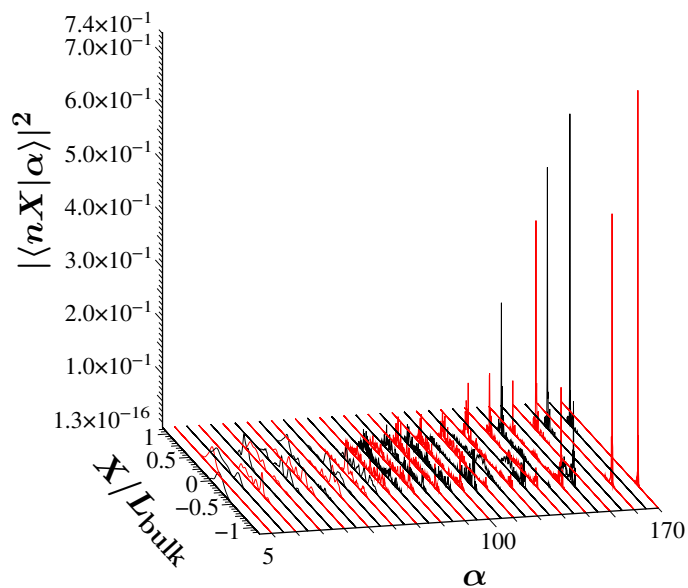
(a)
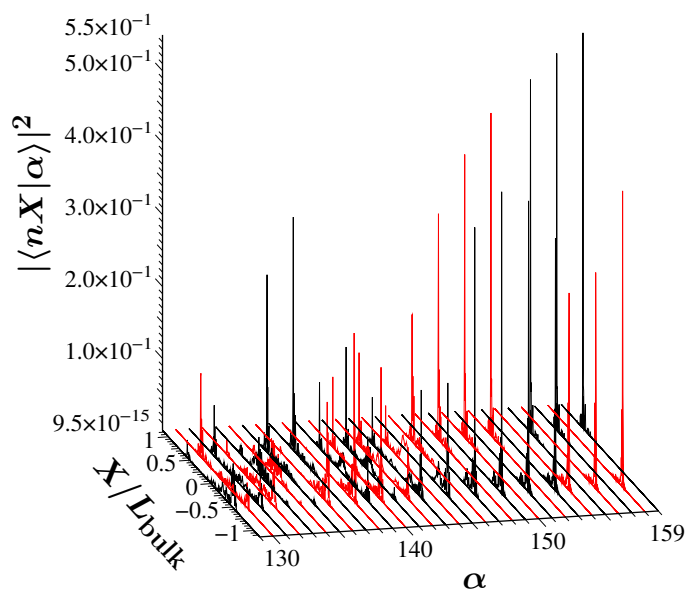
(b)

Figure 6.7: Basis state contributions $|\langle nX|\alpha\rangle|^2$ to eigenstates α at different energies (a) for every fifth state in the lowest Landau level, (b) for every state with energy between $0.6\ \hbar\omega_c$ and $0.8\ \hbar\omega_c$. System parameters are the same as in Fig. 6.5. Different colors are used for adjacent curves in order to distinguish them clearly.
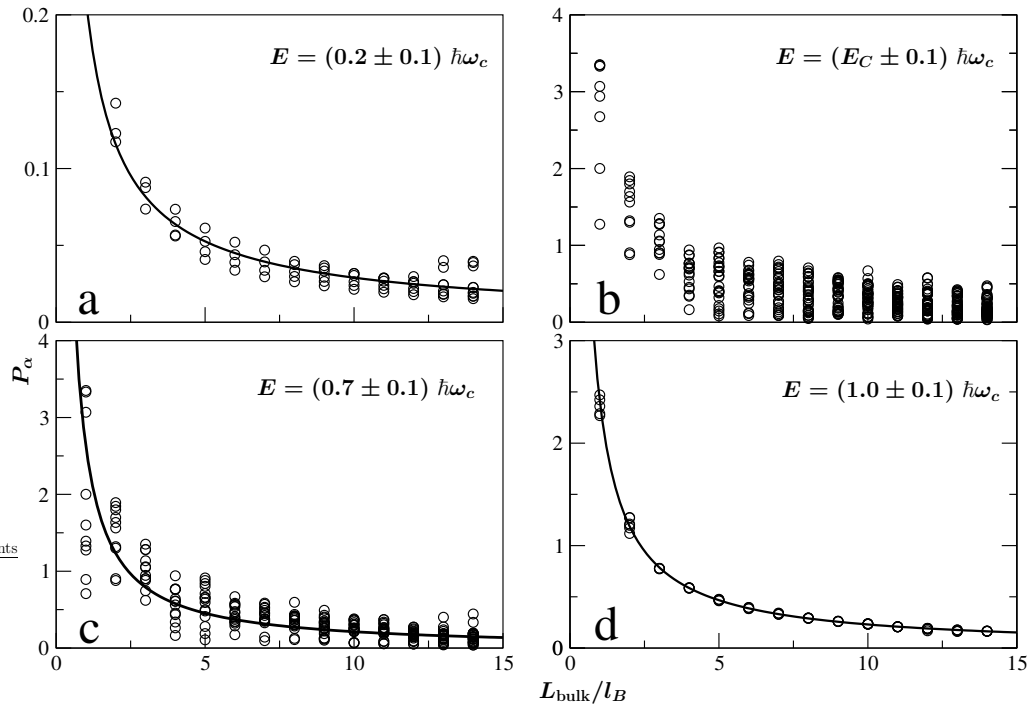
Figure 6.8: Participation ratio in dependence of bulk width for different energies. E_C is determined for each bulk width as the energy, at which the system reaches the maximal participation ratio in the lowest Landau band. System parameters are the same as in Fig. 6.4. Solid lines are fitting functions: (a) $P_\alpha = 0.21\,(L_{\text{bulk}}/l_B)^{-0.86}$, (c) $P_\alpha = 2.62\,(L_{\text{bulk}}/l_B)^{-1.09}$, (d) $P_\alpha = 2.41\,(L_{\text{bulk}}/l_B)^{-1.02}$.

small. All states $\alpha = 139 - 143$ share the two pronounced peak at the edges, while the bulk contribution increaes only slowly with lowering the energy. Before the transition to quasi-1D-states with more or less uniform distribution across the bulk, there is a reappearance of edge like states $\alpha = 135 - 138$, which we attribute to mesoscopic fluctuations due to the random distribution of disorder in this rather mesoscopic sample. The transition which we observed here happens thus rather smooth as compared to the sharp transitions in the transfer matrix results shown in Fig. 6.1. This can be attributed to the fact that the finite system with $L = 100 l_B$ which we have diagonalized here is much smaller than the system which was handled by the transfer matrix method. As expected far away from the thermodynamic limit, $L, w \to \infty, L/w = \text{const.}$, the transition occurs in a finite energy interval rather than at a single point. Finite size effects can be revealed further by studying the dependence of the states on the bulk width.

To this end we next study the system size dependence of the participation ratio. Fig. 6.8 shows the participation ratio of all states in a given energy interval for systems with different bulk widths L_{bulk}. Disorder configuration, wire length and confinement energy $\hbar\omega_p$ are kept fixed for all the systems. As a characteristic example for the behaviour in the low energy region, we investigate states in an interval around energy $E = 0.2\hbar\omega_c$ (Fig. 6.8a). In this region, the participation ratio scales with the wire width approximately as $P \propto L_{\text{bulk}}^{-1}$. This is in agreement with the expected scaling of 2D localized states which give a contribution $\psi_\alpha^2 \propto 1/\xi_{2D}^2$, only within a localization area ξ_{2D}^2 where ξ_{2D} is the 2D localization length of the wavefunction, which is independent of the wire length L and width L_{bulk}. It follows that,

$$P_{2D} \propto \xi_{2D}^2 L^{-1} L_{\text{bulk}}^{-1} \ll 1, \tag{6.11}$$

in good agreement with Fig. 6.8a.

The behaviour changes in the center of the Landau band (Fig. 6.8b). There, the density of states is higher, and the disorder results in a wide range of participation ratios. For large bulk widths, $L_{\text{bulk}} > 5l_B$, the range of participation ratios becomes constant and saturates to a finite value. Note that quasi-1-D localized states cover approximately an area $L_{\text{bulk}}\xi_{1D} \sim gL_{\text{bulk}}^2$, and contribute in this area with probability density $\psi_\alpha^2 \sim 1/(\xi_{1D}L_{\text{bulk}})$. As a result, one expects for quasi-1-D localized states, according to Eq. (6.2),

$$P_{1D} \propto \frac{\xi_{1D}}{L} \sim g\frac{L_{\text{bulk}}}{L}, \tag{6.12}$$

increasing linearly with L_{bulk}. When the wire is comparable or shorter than the quasi-1D localization length, however, the participation ratio shows rather the behavior of 2D extended states which cover the whole wire area Lw with probability density $1/(Lw)$, yielding the typical participation rato of extended states

$$P_{ext} \sim w/L_{\text{bulk}} = \text{const} > 1, \tag{6.13}$$

being independent of the width L_{bulk}. Note that for extended states one would expect $P_\alpha = w/L_{\text{bulk}}$, which according to equation (6.7) converges to unity for $L_{\text{bulk}} \to \infty$. Whereas P_α in Fig. 6.8b is indeed seen to saturate to a constant mean value, this value is found not to exceed 1. This is consistent with the fact that the wavefunction is multi-fractal [47, 121, 122].

The scaling of the participation ratios in the high energy tail of the lowest Landau band (Fig. 6.8c,d) is again a power law $P \propto L_{\text{bulk}}^{-1}$, but with an absolute value much larger than in Fig. 6.8a. This resembles the expected feature for edge states, which cover an area $l_B L$ with probability density $1/(l_B L)$, yielding,

$$P_{\text{edge}} \propto l_B/L_{\text{bulk}}, \tag{6.14}$$

which is both in magnitude and in the functional dependence on L_{bulk} in good agreement with Fig. 6.8d. Note that in the transition region, Fig. 6.8c, the large mesoscopic fluctuations do not allow to distinguish characteristic features of the nonchiral edge states at the transition, but the functional dependence on L_{bulk} is that expected for edge states and localized bulk states alike, which both coexist in this energy region, as we had seen above in Fig. 6.7.

In summary, our model allows to study the mutual influence between the states in the bulk region, where the influence of the disorder potential is strong, and states in the edge region, where the confinement potential prevails. We have found that in the narrow energy region of the CMIT the disorder-induced coupling between the edges creates nonchiral edge states which have comparable weights on both edges, but only a negligible mixing with the bulk.

6.4 Conclusions

We conclude, that in quantum Hall bars of finite width $w \ll \xi_n$ at low temperatures quantum phase transitions occur between extended chiral edge states and a quasi-1D insulator. These are driven by the crossover from 2D to 1D localization of bulk states. These metal-insulator transitions *resemble* first-order phase transitions in the sense that the localization length abruptly jumps between exponentially large and finite values, which we have confirmed by calculating the edge state localization length, explicitly. In the thermodynamic limit, *fixing the aspect ratio $c = L/w$, when sending $L \to \infty$, then $c \to \infty$, the two–terminal conductance jumps between exactly integer values and zero*. The transitions occur at energies where the localization length of bulk states is equal to the geometrical wire width. Then, m edge states mix and electrons are free to diffuse between the wire boundaries but become Anderson localized along the wire. Close to that transition we found with exact diagonalization studies that particular states exist, which are superpositions of edge states with opposite chirality, with an order of magnitude smaller bulk contribution. Although this state is located at the edges, it is a nonlocal state, having comparable weights on opposite sides of the sample. Thus, it can have a mesoscopic extension across the width of the Hall bar, if it is more narrow than the phase coherence length. The Chiral Metal–Insulator Transition is of mesoscopic nature since, at finite temperature, the phenomenon of the CMIT can only be observed, when the phase coherence length exceeds the quasi-1D localization length in centers of Landau bands, $L_{\varphi} > \xi_n$. One then should observe transitions of the two-terminal resistance from integer quantized plateaus, $R_n = h/ne^2$ to a Mott variable-range hopping regime of exponentially diverging resistance. Such experiments would yield information about the coupling between edge and bulk states in quantum Hall bars. At higher temperature, when $L_{\varphi} < \xi_n$, the conventional form of the integer quantum Hall effect is recovered [1].

We have studied the modification of the CMIT by correlations in the disorder potential and due to interactions. These results will be presented in a subsequent publication.

Interaction induced g-factor enhancement in parabolic quantum wires

7.1 Introduction

At high magnetic field the energy spectrum of noninteracting electrons in electron inversion layers in semiconductor heterostructures consists of Zeeman split, disorder broadened Landau bands. In AlGaAs/GaAs the corresponding Landé g-factor can be much larger than the bulk value ($g = -0.44$) and it decreases with increasing electron concentration [67, 97, 123]. This is assigned to electron exchange interaction. When the electron density is varied such that the Fermi energy traverses a Landau band, the Zeeman splitting acquires a maximum when only the energetically lower band (with spin $s = \uparrow$) is occupied. Then, the exchange energy of the electrons will dominate, and the occupied band will be shifted to lower energy.

The 2D electron system (2DES) confined in lateral direction forms a quasi-1D electron system. The degeneracy of the Landau levels is lifted due to the confinement. Still, the enhancement of the Zeeman splitting is present although the Landau subbands corresponding to the two directions of the spin overlap at high energies. For high electron density ρ, such that the partial densities $\rho_\uparrow \approx \rho_\downarrow$, and there is no spin polarization, the Zeeman splitting is close to the bulk value. However, for densities below some crossover value $\rho < \rho_c$, only the lowest spin polarized subband will be occupied at temperatures close to zero. Due to the alignment of the spins, the exchange interaction will decrease the energy and enhance the Zeeman splitting. Eventually, all of the electrons will only occupy the polarized state. It has been suggested that this is similar to a first-order phase transition [36]. Such effect has been observed in magnetotransport measurements done

on GaAs/AlGaAs quantum wires [124, 125] and on narrow silicon inversion channels [126, 127].

In previous works on the 2DES [97, 123] and quantum wires [36, 128] the Hartree contribution to the selfenergy has been neglected. However, for quantum wires, it has been shown that the Hartree term is very important for quantitavely estimating the energy dispersion and the self-consistent potential [129, 130]. Then, one can expect that this must influence ρ_c and change the g-factor. It is indeed not clear whether the g-factor enhancement in a quantum wire is similar to a first-order phase transition or must be considered as a simple crossover, even at zero temperature.

7.2   Mechanism of g-factor enhancement

We address this question by using the selfconsistent Hartree-Fock method. We find that Hartree and Fock selfenergies are of the same order. They partially cancel each other, such that the Hartree-Fock selfenergy is much smaller than the kinetic energy. As a consequence, the interaction does not change the energy dispersion of the occupied spin subband significantly. This implies that it is the spin independent Hartree term that forces the system into the totally polarized state and supports the polarizing effect of the exchange interaction.

We compare the results with magnetocapacitance experiments [35] in which ρ_c and the Zeeman splitting have been estimated. Within experimental errors, the Hartree-Fock results can be fitted reasonably well to the experimental data if the interaction is assumed to be exponentially screened. In contrast to the earlier suggestions [36, 128] we find a smooth crossover from the polarized to the unpolarized state. Our results indicate that correlation effects beyond mean field are likely to be important for understanding the g-factor in nanostructures.

The interacting 2DES in a perpendicular magnetic field, parabolically confined to 1D, is described by the Hamiltonian $H = H_0 + H_i$ where

$$H_0^s = \frac{1}{2m} \sum_{i=1}^{N} \left[(\mathbf{p}_i + e\mathbf{A})^2 + \frac{m}{2}\omega_0^2 x_i^2 + \frac{s}{2}g\mu_0 B \right] \tag{7.1}$$

with the vector potential $\mathbf{A} = (0, Bx, 0)$, the effective mass m, the confinement frequency ω_0, and $s = \pm 1$ the spin directions. The interaction $H_i = \sum_{i<j} V(\mathbf{r}_i - \mathbf{r}_j)$ contains a Yukawa potential $V(\mathbf{r}) = V_0 \exp(-\kappa r)/r$ with $V_0 = e^2/4\pi\epsilon\epsilon_0 > 0$ and a screening parameter κ.

The eigenvalues of the non-interacting part H_0

$$\varepsilon_{nk}^s = \hbar\Omega\left(n + \frac{1}{2}\right) + \frac{\hbar^2 k^2}{2m(B)} + \frac{s}{2}g\mu B. \tag{7.2}$$

consist of the discretization energy due to the confinement and the magnetic field, the kinetic energy in the non-confined y-direction, and the Zeeman contribution. Periodic boundary conditions in y-direction imply wavenumbers $k_j = 2\pi j/L_y$ (integer j, wire length L_y). The effective mass $m(B) = m\Omega^2/\omega_0^2$ contains the renormalized frequency $\Omega = \sqrt{\omega_0^2 + \omega_c^2}$ ($\omega_c = eB/m$ cyclotron frequency). It diverges in the quantum Hall limit, $B \to \infty$. The corresponding wave functions $\langle x, y|nk\rangle = L_y^{-1/2} \exp{(iky)} \chi_n(x - X_k)$ contain the states χ_n of the 1D harmonic oscillator at position $X_k = -k\ell^2 A$ with the characteristic length $\ell = \sqrt{\hbar/m\Omega}$ and $A = \omega_c/\Omega$.

7.3   Hartree-Fock equations and exchange effects for the Q1DEG

The Hartree-Fock equations in Landau representation

$$\sum_{n'k'} \langle nk|(H_0^s + F^s)|n'k'\rangle c_\alpha^s(n'k') = E_\alpha^s c_\alpha^s(nk) \tag{7.3}$$

determine the expansion coefficients $\langle nk|\alpha s\rangle = c_\alpha^s(nk)$ of the electron states and the eigenenergies E_a^s. The size of the basis in a Landau level is determined by the degeneracy $N_\phi = L_x L_y/2\pi\ell^2$. We use indices i, j, a, b for labeling the basis states. The Fock matrix is

$$F_{ij}^s = \sum_{ab} \rho_{ab} M_{ijab} + \sum_{ab} \rho_{ab}^s M_{ibaj}, \tag{7.4}$$

with interaction matrix elements

$$M_{ijab} = \int d\mathbf{q} V(q) \langle i|e^{i\mathbf{q}\cdot\mathbf{r}}|j\rangle \langle a|e^{-i\mathbf{q}\cdot\mathbf{r}}|b\rangle \tag{7.5}$$

and density matrices

$$\rho_{ab}^s = \sum_{E_\alpha^s \leq \varepsilon_F} c_\alpha^{s*}(a) c_\alpha^s(b). \tag{7.6}$$

Furthermore, $\langle i|e^{i\mathbf{q}\mathbf{r}}|j\rangle = \langle nk|e^{iqx}|n', k'\rangle \delta_{q_y, k-k'}$,

$$\langle nk|e^{iqx}|n'k'\rangle = e^{-\left[|q_A|^2 + iq(k+k')A\right]\ell^2/2}$$

$$\times \sqrt{\frac{m}{n}} \left(\frac{q_A \ell}{\sqrt{2}}\right)^{m-n} L_n^{m-n}\left(\frac{|q_A|^2 \ell^2}{2}\right), \tag{7.7}$$

with $q_A = iq - \text{sign}(n - n')(k - k')A$, $n = \text{Min}(n, n')$, $m = \text{Max}(n, n')$, and L_n^{m-n} the associated Laguerre polynomials.

The single particle energies $E_\alpha^s = \epsilon_\alpha^s + \Sigma_\alpha^s$ obtained by solving (7.3) self-consistency contain the selfenergy

$$\Sigma_{\alpha s} = \sum_{ij} F_{ij}^s c_\alpha^{s*}(i) c_\alpha^s(j) \equiv \Sigma_\alpha^{\mathrm{H}} + \Sigma_{\alpha s}^{\mathrm{F}} \tag{7.8}$$

with Hartree and Fock terms, $\Sigma_\alpha^{\mathrm{H}}$ and $\Sigma_{\alpha s}^{\mathrm{F}}$, respectively.

In the self-consistent Hartree-Fock method the charge distribution in the system is determined by searching for the electronic configuration for which the ground state energy $E(\{\alpha, s\}) = \sum_{\alpha s}^{(\mathrm{occ})} E_{\alpha s}$ is minimized,

$$E_{\mathrm{g}} = \mathrm{Min}_{\{\alpha s\}} E(\{\alpha, s\}) . \tag{7.9}$$

This implicitly determines the spin polarization

$$\gamma = \frac{\rho_\uparrow - \rho_\downarrow}{\rho_\uparrow + \rho_\downarrow} = \frac{\delta\rho}{\rho} \tag{7.10}$$

with

$$\rho_s = \sum_{\alpha(\mathrm{g})} \sum_{nk} |c_\alpha^s(nk)|^2 . \tag{7.11}$$

The effective g-factor is defined by

$$g^* = g + \frac{2}{N\mu_0 B} \sum_{\alpha(\mathrm{g})} (\Sigma_{\alpha\uparrow} - \Sigma_{\alpha\downarrow}) . \tag{7.12}$$

The self-consistent numerical solution of the Hartree-Fock equations requires a truncation of the complete othonormal set $|nk\rangle$. This is done by defining a cutoff wave number k_{max} via $X_{k,\mathrm{max}} = k_{\mathrm{max}}\ell^2 = L_x$. The integral over q_x in M_{ijab} (7.5) is approximated by a sum over discrete wave numbers $q_x = 2\pi n_x/w$ with $w \gg L_x$ and n_x integer. We have achieved convergence for the integrals, spectra and the wavefunctions for $w > 50 L_x$ and $-w/\ell < n_x < w/\ell$. For obtaining the results described in the following we have used $w = 100 L_x$.

For electron numbers such that the Fermi energy is located in the second Landau level, there are states with low wave numbers at approximately the same energies as states with high wave numbers of the lower Landau levels (Fig. 7.1). In order to treat these correctly, inter-Landau level interaction matrix elements have to be taken into account. The maximum system size L_x depends then on the number of Landau levels included, and the confinement strength. We have estimated $X_{k,\mathrm{max}}$ by using the spectrum of noninteracting electrons. We have done calculations for increasing $L_x > X_{k,\mathrm{max}}$ until the eigenenergies became insensitive to the value of L_x. The system length L_y, has been used to adjust the size of the basis, independently of L_x, but always $L_y > L_x$.

We have assumed that convergence of the self-consistent Hartree-Fock procedure is achieved when $\Delta\rho/\rho < 10^{-7}$ with $\Delta\rho$ the difference between the densities $\rho = \rho^\uparrow + \rho^\downarrow$ corresponding to successive iterations. In all of the results shown below, the electronic energies have converged within a relative error of 10^{-3}. Due to the translational invariance in the y-direction k is a good quantum number for the Hartree-Fock states.

7.4 Results

Figure 7.1 shows the energy dispersions of the four lowest subbands for different electron numbers. If the electron density is small such that only energy levels in the lowest subband (spin $\uparrow$) are occupied, the Zeeman splitting is large. With increasing density the second subband (spin $\downarrow$) becomes occupied. Then, the Zeeman splitting decreases until it reaches the bulk value. This is periodically repeated when higher spin subbands are occupied.

In order to identify the roles of the Hartree and the Fock parts of the self energy, we consider the lowest subband $(n = 0, \uparrow)$. In a strong magnetic field, both, Fock and Hartree terms depend on the wave number. The Hartree energy is of the same order as the Fock energy, but of opposite sign. The total interaction energy Σ is then much smaller than the absolute values of Σ^H and Σ^F. The latter are comparable to the kinetic energy ϵ_k (Fig. 7.2). This suggests that for determining the crossover density one can replace the selfconsistent Hartree-Fock approximation by lowest-order perturbation theory [36]. The result for the lowest subband is

$$\Sigma_k^H = \frac{2V_0}{\sqrt{2}l} \sum_s \int_{Q_-}^{Q_+} \mathrm{d}k' \int \mathrm{d}q \, \frac{e^{-[q^2 - iAqk']}}{\sqrt{q^2 + q_\kappa^2}} \,, \tag{7.13}$$

$$\Sigma_{ks}^F = -\frac{4V_0}{\sqrt{2}l} \int\limits_{Q_-}^{Q_+} \mathrm{d}k' e^{-[(2A^2-1)k'^2 + q_\kappa^2]/2} K_0\big[(k^2 + q_\kappa^2)/2\big] \tag{7.14}$$

where $Q_\pm = \sqrt{2}l(k \pm k_{Fs})$, $q_\kappa = \kappa l/\sqrt{2}$ and $K_0(z)$ is a modified Bessel function.

In 2DES the Hartree term is often neglected. It is argued that it yields only a constant shift of the energy scale [97, 123]. Intuitively, one would neglect it also for the quasi-1DES [36, 128, 131]. However, for a quantum wire in a strong magnetic field the wave number is associated with a transversal position $X = -kl^2$. At zero temperature, in the totally polarized state, $\rho_\uparrow = \rho$ and $\rho_\downarrow = 0$, when only the lowest subbands is occupied with electrons, additional electrons will occupy states with wave numbers near the Fermi wave number $k_{F\uparrow} = \pi\rho_\uparrow$. These have to be added near the edge of the wire, $|x_{F\uparrow}| = k_{F\uparrow}l^2$ (Fig. 7.1) thus minimizing the electrostatic repulsion. However, if the spin-$\downarrow$ subband starts to become occupied, additional electrons would be added
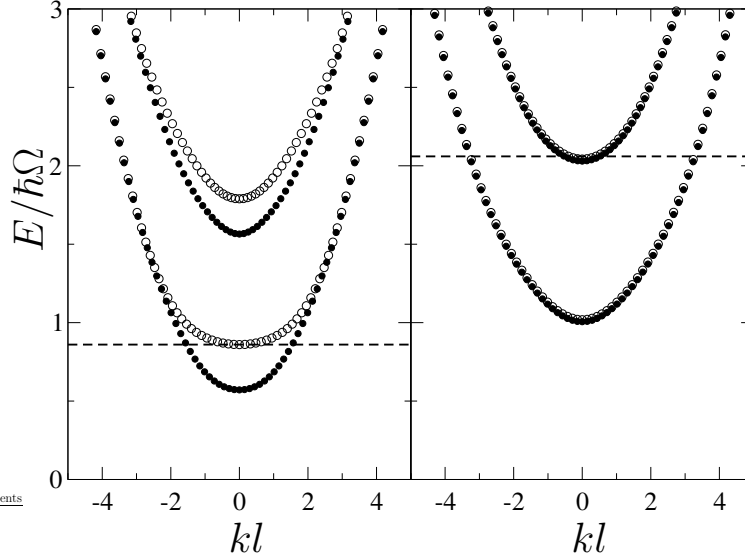
Figure 7.1: Hartree-Fock energies of a quantum wire in a magnetic field for the four lowest
subbands at densities where the 2nd (spin $\downarrow$, left) and 3rd (spin $\uparrow$, right) subbands
start to be occupied (bullets: $s = \uparrow$, circles: $s = \downarrow$, dashed: Fermi level).

at smaller wave numbers in the center of the wire, near the minimum of $E_\downarrow(k)$ where
the electron density is large. This would lead to a strongly repulsive energy contribu-
tion. Thus, it is energetically favorable to continue with the occupation of the states
near the edges in the lowest subband before occupying the states in the second subband.
The crossover density ρ_c is increased and it is due to the avoided Hartree- and *not* the
Fock-energy that the system remains in the totally polarized state.

Figure 7.2 shows results for the Zeeman splitting averaged over the wave number as
a function of the mean electron density ρ. In a given Landau level, g^* increases with
increasing density until the upper spin subband starts to become occupied. Then, at
crossover density ρ_c, $g^*(\rho)$ starts to decrease. The oscillating behavior of g^* is accom-
panied by oscillations in the spin polarization γ. For $\gamma \approx 0$, $g^* \approx g$. Taking into account
the Hartree term, the crossover to the bulk value is smooth, in contrast to the case when
only the Fock term is considered [36]. In the lowest subband, the crossover density ρ_c,
at which the g-factor starts to decrease, agrees within 10% with the result obtained in
lowest order perturbation theory.

The influence of the screening length on ρ_c is shown in Fig. 7.3. The crossover den-
sity decreases with increasing κ. As expected, the self-energy decreases with decreasing
interaction range. For comparison with experiment we assume $\kappa = 2/ell$. This turns
out to reproduce the experimental findings reasonably well.
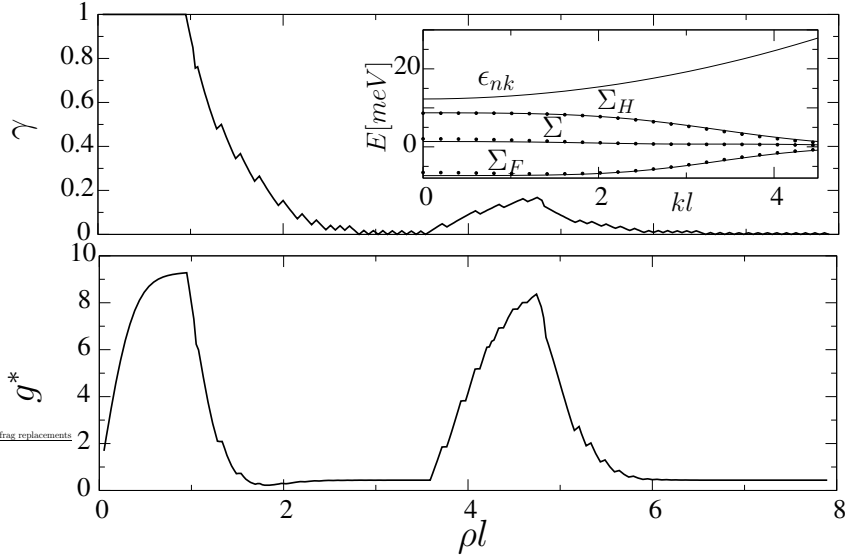
Figure 7.2: Spin polarization γ (top) and effective g-factor g^* (bottom) as functions of the density ρ obtained from the self-consistent Hartree-Fock method taking into account the three lowest Landau bands (Parameters: $B = 14$ T, $\hbar\omega_0 = 6$ meV, $\rho_c = 1.1/\ell$ in the lowest subband, screening parameter $\kappa = 2/\ell$). Inset: Energy $\epsilon(k)$ (dashed) in the noninteracting limit; selfenergies Σ, Σ^F (Fock), and Σ^H (Hartree) at ρ_c, respectively, as functions of the wave number kl; solid: perturbational, bullets: self-consistent results.

The crossover density in the lowest subband as a function of the confinement energy has been determined from measurements of the capacitance of a quantum wire in a strong magnetic field [35]. It has been found that the crossover density increases with increasing magnetic field (Fig. 7.4) and with decreasing the voltage applied to a side gate, V_{side}. For estimating the confinement energy ω_{exp} a parabolic confinement has been assumed. By varying the side-gate voltage from -1.5 V to -3.5 V $\hbar\omega_{\text{exp}}$ increases from 4.8 ± 0.5 meV to 6.6 ± 0.7 meV.

The potential, which corresponds to the experimentally determined confinement energy $\hbar\omega_{\text{exp}}$, is composed of the parabolic external confinement potential $\hbar\omega_0$ tuned by V_{side} and of the screening potential due to the charge density of the electrons in the wire. The confinement energy $\hbar\omega_0$ in general will be larger than the experimentally determined $\hbar\omega_{\text{exp}}$. We assume that the external confining potential dominates such that $\hbar\omega_0 \approx \hbar\omega_{\text{exp}}$. With the screening length $1/\kappa = l/2$ the calculated crossover density ρ_c fits the decrease of experimental data with increasing confinement energy qualitatively (Fig. 7.4). Neglecting the Hartree term [36], the dependence of ρ_c on the confinement
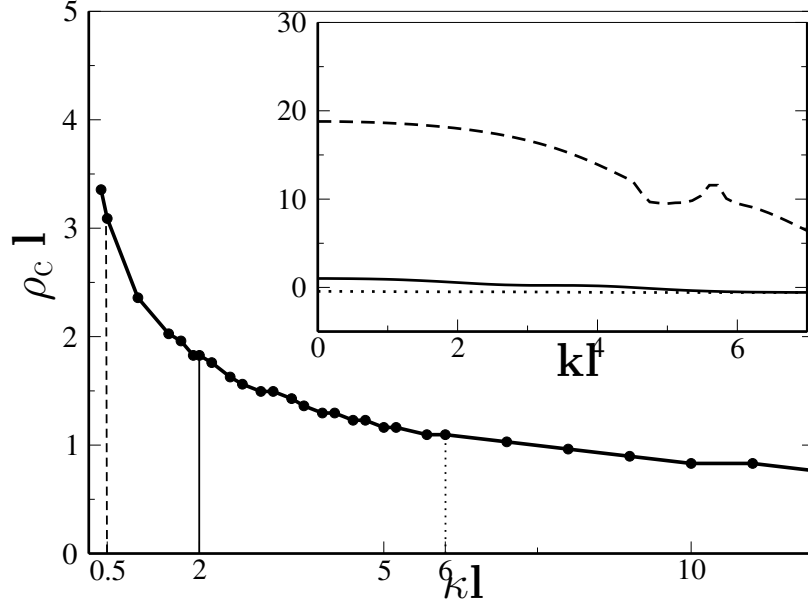
Figure 7.3: Crossover density as a function of the screening length κ^{-1}. Data points: selfconsistent Hartree-Fock approximation with $B = 14\,\mathrm{T}$, $\hbar\omega_0 = 6\,\mathrm{meV}$ in the lowest subband; wire width $16\,\ell$ wire length $50\,\ell$. Inset: selfenergy with $\kappa = 0.5/\ell$ (dashed), $\kappa = 2.0/\ell$ (full) and $\kappa = 6.0/\ell$ (dotted).

is considerably weaker even if the screening length is assumed to be ∞ and thus the exchange-enhanced critical density is maximized (Fig. 7.4 inset).

However, our model does not reproduce the experimental data at very small side gate voltages, $|V_{\mathrm{side}}| \leq 1\,\mathrm{V}$. We believe that in this regime the external potential of the wire is modified by impurities and thus cannot be described by a parabolic potential. Also there are quantitative discrepancies between experimental data and the self-consistent theory at smaller magnetic field strength ($B = 9\mathrm{T}$). Given the relatively large experimental errors, we did not try to get a better fit. In summary, we confirm the experimentally observed trends, namely that by increasing the confinement energy, i.e. decreasing the effective wire width, and decreasing the magnetic field strength, the crossover density for the enhancement of the Zeemann splitting is depleted considerably.

7.5 Conclusions

In summary, we have calculated the Zeeman splitting of the subbands in a quasi-1D quantum wire in a strong magnetic field by using the self-consistent Hartree-Fock approximation to electrons interacting via a screened Coulomb interaction. We have found
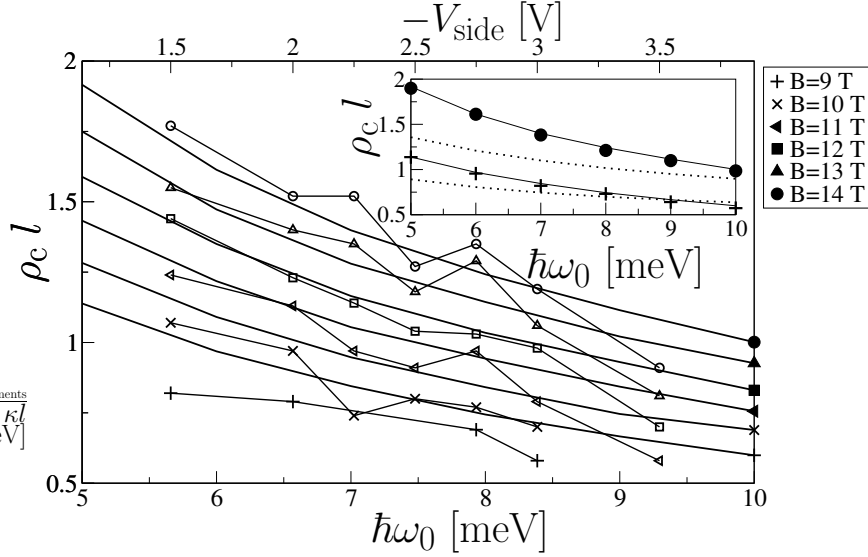
Figure 7.4: Crossover density $\rho_{\rm c}$ at magnetic fields as indicated as a function of the confine-
ment energy $\hbar\omega_0$. Full lines: Hartree-Fock results with screening length $\ell/2$; open
symbols: experimental data of Ref. [9] corresponding to side gate voltages $V_{\rm side}$
from -1.5 to -4 V. Inset: results for B =9 T and B =14 T obtained selfconsis-
tently (dots), and perturbationally (full lines) compared with the results obtained by
neglecting the Hartree term (dashed).

that Hartree and Fock parts of the selfenergy are of the same order but of opposite sign
such that the total selfenergy becomes small. We have quantitatively determined the ef-
fective g-factor and the spin polarization. When γ vanishes g^* is close to the bulk value
while it is strongly enhanced if the spin polarization is close to one. Our results imply
that the Hartree term cannot be neglected for the enhancement of the g-factor in quan-
tum wires. Especially, it appears that it plays a crucial role in determining the crossover
density quantitatively. By comparing calculated crossover densities with experimental
data we have found the the dependence on the confinement energy can be reproduced
within experimental uncertainties for not too small side gate voltages if the screening
length is assumed to be about half of the magnetic length. Since the screening can be
viewed as being due to correlations, our results imply that these cannot be neglected for
understanding the g-factor enhancement in quantum wires.

Conclusions

We have investigated the interplay of Coulomb interaction, spatial confinement and disorder on transport and localization properties of two-dimensional electrons in a strong perpendicular magnetic field under various aspects. Most of our results were based on the wavefunctions and eigenvalues of a suitable single-particle Hamiltonian, which was extended by a self-consistent Hartree-Fock field modelling electron-electron interaction when necessary. In the following, we summarize the most important results.

Coulomb interactions

In the first part, we have investigated the transition from localized states in the tails of the lowest Landau band to extended states in the band center. As a model for disorder, we have used Gaussian scatterers with a finite range of the order of the magnetic length. In lieu of calculating the localization length directly, we extracted the static critical exponent $\tilde{\nu}$ from the participation ratio of the wavefunction, which has a similar power law dependence as the localization length. However, corrections due to the multifractality of the wavefunctions in the critical region have to be taken into account. Our data confirmed the usual value $\tilde{\nu} = 2.3$ within the accuracy limited by the rather small system sizes implied by the used method. This value remains unchanged also in the presence of electron-electron interaction, which was treated in unrestricted Hartree-Fock approximation. Results for the participation ratio of the quasiparticle wavefuntion obtained at fixed magnetic field and fixed filling factor showed spin-split bands with the same value for $\tilde{\nu}$ and the same fractal dimension of the wavefunctions. The results strongly support the universality of the static critical exponent in the lowest Landau level.

Another issue is the analysis of dynamical scaling in the above sort of systems. Measurements have shown that the width of the frequency-dependent magnetoconductivity peak $\sigma_{xx}(\omega)$ scales $\propto \omega^\kappa$, with an exponent $\kappa = 1/(z\tilde{\nu})$. Experimentally, $\kappa = 0.21$ and $\kappa = 0.41$ have been found in systems with supposively interactionless electrons or, respectively, relevant electron interactions. Assuming $\tilde{\nu} = 2.3$, the dynamical exponent z seems to be reduced by a factor of 2 in the presence of interaction.

We calculated the frequency-dependent conductivity tensor directly from the wavefunctions by means of the Kubo formula. We found for systems with uncorrelated disorder and no interactions included a dynamical critical exponent $z \approx 2$, consistent with earlier theoretical work and experiments. A deviation from this value was found for a Gaussian potential with correlation length $d = l_B$, and also for uncorrelated disorder with Hartree-Fock interaction. We carefully conclude that the type of the disorder potential significantly changes the diffusive behaviour of the electrons. Thus, the dynamical critical exponent is reduced. However, our approach cannot produce result with high numerical precision, because the system sizes considered are quite small. In case of interaction present, our Kubo formula represents the current-current correlation function in the random phase approximation, which is not entirely compatible with the Hartree-Fock self-energy, because it neglects exchange local field corrections. A systematic evaluation of the current response in the conserving time-dependent Hartree-Fock approximation could shed some light on the role of correlations for obtaining the dynamical critical exponent. Yet, we conclude that the sensitivity of the dynamical exponent in comparison with the robustness of the static exponent seems to give a hint on the importance of electron-electron interaction for a proper description of the quantum Hall plateau transition.

Another convincing argument for the influence of Coulomb interaction on the quantum Hall phase diagram is provided by experiments measuring the change of the chemical potential. It has been found that charging lines appear parallel to integer filling factors in the plane spanned by magnetic field and electron density. We demonstrated within a refined Hartree-Fock approach, which allows the self-consistent field to relax with respect to a newly entering particle and thus mimics the screening of the particle, that these lines can be reproduced by an effective single-particle pictures including Coulomb interaction. We showed that states at the actual Fermi level behave like true single-particle states concerning their localization-delocalization transition. This gives a consistent picture for the phase diagram in the insulating phases, which are most important for previous finite-size scaling studies in order to obtain the critical exponent. The evidence of charging can be related to significant changes in the compressibility of the localized electrons due to charge rearrangements as a response to density changes. The transition, on the other hand, is governed by states at the Fermi level following more or less the anticipated metal-insulator transition as a function of filling factor. From this

phenomenological point of view, signatures of Coulomb interaction in the compressibility patterns do not contradict the one-parameter scaling assumption.

Confinement

Coulomb interactions are also expected to play a significant role in the wire geometry. We have demonstrated in a clean parabolic wire that the g-factor of the electron is strongly enhanced by interaction as long as only one spin level is occupied. The g-factor decreases to its bulk value when the other spin level is occupied, thus exhibiting smooth oscillation as a function of the electron density. We found that this effect cannot be described properly by considering only the exchange term and is also support by the direct interaction. It is likely that correlations give an important contribution for the understanding of the g-factor oscillations.

Apart from Coulomb interaction, we have studied the effect of spatial confinement on the chiral metal insulator transition. We have shown for disordered quasi one-dimensional quantum wires with a finite, confinement-free bulk region a variety of states can coexist. Localized states in the bulk or at the edges dominate the insulating phases, even if a coupling of the edges by a 1D-localized state occurs. Conducting phases are determined by chiral edge states or 2D-extended states. A new class of states, the non-chiral edge states, has been found. A non-chiral edge state shows no different behaviour in participation ratio or localization length compared to an ordinary edge state, but is not conducting due to the nonchiral coupling of both edges *without* bulk (2D extended) contribution. These states occur in the vicinity of the plateau transition. A calculation of the two-terminal conductance starting from an independet model indeed reveals an abrupt breakdown of the conductance between the plateaux. This behaviour devises a new metal-insulator transition in quantum wires and should be experimentally detectable.

Part IV

Appendices

Matrix elements

A.1   The Fourier components of the density matrix

In finite systems with periodic boundary conditions, the guiding center $X_j = \frac{2\pi l_B^2}{L_y} j$ of the Landau function (1.4) is discrete and determined by the integer number $j = 1, \ldots, N_\phi$. For the matrix element $\langle nX \mid e^{i\mathbf{q}\mathbf{r}} \mid n'X' \rangle \equiv \langle nj \mid e^{i\mathbf{q}\mathbf{r}} \mid n'j' \rangle$ we get

$$\langle nj | e^{i\mathbf{q}\mathbf{r}} | n'j' \rangle = \exp(-\frac{|\mathbf{q}|^2 l^2}{4}) \exp(\frac{i\pi n_x(j + j')}{N_\phi}) \delta'_{n_y, j'-j} A_{nn'} \qquad \text{(A.1)}$$

with

$$A_{nn'} = \begin{cases} \sqrt{\frac{n'!}{n!}} \left[\frac{(iq_x + q_y)l}{\sqrt{2}} \right]^{n-n'} L_{n'}^{n-n'}(\frac{|q|^2 l^2}{2}) & (n \geq n') \\[4mm] \sqrt{\frac{n!}{n'!}} \left[\frac{(iq_x - q_y)l}{\sqrt{2}} \right]^{n'-n} L_n^{n'-n}(\frac{|q|^2 l^2}{2}) & (n < n') \end{cases} \qquad \text{(A.2)}$$

The Kronecker delta is for the periodic case is defined as

$$\delta'_{mn} = \begin{cases} 1 & n = m \mod N_\phi \\ 0 & \text{else} \end{cases}$$

A detailed calculation and discussion of the matrix element and the adjustment to periodic boundary conditions can be found in [37]. For the case of open boundaries ($\psi(\mathbf{r} \to \pm\infty) = 0$), the periodic Kronecker symbol reduces to ordinary version.

A.2   Coulomb matrix element

In calculations involving Coulomb interaction, the two-particle matrix element in Landau representation

$$M_{n_1 j_1 n_2 j_2 n_3 j_3 n_4 j_4} = \int d^2 r \quad \phi^*_{n_1 X_{j_1}}(\mathbf{r}) \phi^*_{n_2 X_{j_2}}(\mathbf{r'}) V(\mathbf{r} - \mathbf{r'}) \phi_{n_3 X_{j_3}}(\mathbf{r}) \phi_{n_4 X_{j_4}}(\mathbf{r'}), \quad \text{(A.3)}$$

where n is the Landau level index and $X_j = 2\pi l_B^2/L_y \quad j$ is the guiding center of the Landau function. We can write

$$M_{n_1 j_1 n_2 j_2 n_3 j_3 n_4 j_4} = \frac{\gamma l}{L^2} \sum_{q_x, q_y} V(q) \langle n_1 j_1 | e^{i\mathbf{qr}} | n_2 j_2 \rangle \langle n_3 j_3 | e^{-i\mathbf{qr}} | n_4 j_4 \rangle, \quad \text{(A.4)}$$

with $q_x = 2\pi/L_x \, n_x$ and $q_y = 2\pi/L_y \, n_y$ Using the results from section A.1, we find with $\alpha := L_y/L_x$

$$M_{JK}^{n_1 n_2 n_3 n_4} := M_{n_1 j_1 n_2 j_2 n_3 j_3 n_4 j_4} = e^{-\frac{\pi}{N_\phi}\left[n_x^2 + (\frac{J}{\alpha})^2\right]} e^{i\frac{2\pi n_x}{N_\phi}K} A_{n_1 n_3}(J) A_{n_2 n_4}(-J), \quad \text{(A.5)}$$

with $J = j_3 - j_1$ and $K = j_3 - j_2$ and

$$A_{nn'}(J) = \begin{cases} \sqrt{\frac{n!}{n'!}} \left[\frac{\pi}{N_\phi}\sqrt{\alpha}(in_x - J/\alpha)\right]^{n'-n} L_n^{n'-n}\left(\frac{\pi}{N_\phi}(n_x^2 + (J/\alpha)^2)\right) & (n' > n) \\[4mm] \sqrt{\frac{n'!}{n!}} \left[\frac{\pi}{N_\phi}\sqrt{\alpha}(in_x + J/\alpha)\right]^{n-n'} L_{n'}^{n-n'}\left(\frac{\pi}{N_\phi}(n_x^2 + (J/\alpha)^2)\right) & (n' \leq n) \end{cases}$$

$$\text{(A.6)}$$

A.3   Parabolic wire with finite bulk region

A quasi-1D wire with steep confinement potential at the edges and zero potential in the center is modelled by the potential

$$V_{\text{conf}}(\mathbf{r}) = \begin{cases} \frac{1}{2}m\omega_0^2(x-a)^2 & x \geq a \\ 0 & -a < x < a \\ \frac{1}{2}m\omega_0^2(x+a)^2 & x \leq -a \end{cases}$$

The matrix element in Landau representation $\langle nX | V_{\text{conf}} | n'X' \rangle$ is given by

$$\langle nX | V_{\text{conf}} | n'X' \rangle = \delta_{XX'} \frac{1}{\sqrt{\pi}l2^{n+n'}n!n'!} \int_{-\infty}^{\infty} dx \; \chi^*_{nX}(x) V_{\text{conf}}(x) \chi_{n'X'}, \quad \text{(A.7)}$$

where

$$\chi_{nX}(x) = e^{-\frac{(x-X)^2}{2l^2}} H_n\left(\frac{x-X}{l}\right) \tag{A.8}$$

is the not normalized harmonic oscillator function with the Hermite polynomial $H_n(x)$. Using the symmetry of the basis functions, equation (A.7) can be written as

$$\langle nX| V_{\text{conf}} |n'X'\rangle = \delta_{XX'} \frac{1}{\sqrt{\pi}l2^{(n+n')}n!n'!} \left[M_{nn'}(a, X) + (-1)^{(n+n')} M_{nn'}(a, -X) \right] \tag{A.9}$$

and

$$M_{nn'}(a, X) = \int_a^\infty dx \, e^{-\frac{(x-X)^2}{2l^2}} H_n\left(\frac{x-X}{l}\right) H_{n'}\left(\frac{x-X}{l}\right) \left(\frac{x-a}{l}\right)^2 \tag{A.10}$$

$$= l \int_y^\infty d\xi \, e^{-\xi^2} (\xi - y)^2 H_n(\xi) H_{n'}(\xi) \, , \tag{A.11}$$

where $\xi = (x - X)/l$ and $y = (a - X)/l$.

By expanding all polynomials in equation (A.11) into monomials in ξ using the relation

$$H_n(\xi) = n! \sum_{m=0}^{[\frac{n}{2}]} (-1)^m \frac{2^{n-2m}}{m!(n-2m)!} \xi^{n-2m}, \tag{A.12}$$

where $[x]$ denotes the largest integer smaller than x, one gets

$$M_{nn'}(a, X) = l \, n!n'! \sum_{l=0}^{[\frac{n}{2}]} \sum_{k=0}^{[\frac{n'}{2}]} \left[(-1)^{l+k} \frac{2^{n-2l+n'-2k}}{l!k!(n-2l)!(n'-2k)!} \right.$$

$$\times \left. \left(f^{(2+n-2l+n'-2k)}(y) - 2y f^{(1+n-2l+n'-2k)}(y) + y^2 f^{(n-2l+n'-2k)}(y) \right) \right]$$

In the last expression,

$$f^{(M)}(y) = \int_y^\infty d\xi \, \xi^M e^{-\xi^2} = \frac{M-1}{2} f^{(M-2)}(y) + y^{M-1} \frac{1}{2} e^{-y^2} \tag{A.13}$$

This recursive formula can be obtained by repeated partial integration and is valid for even and odd M. An explicit evaluation requires the initial expressions

$$f^{(1)}(y) = \frac{1}{2} e^{-y^2} \tag{A.14}$$

$$f^{(0)}(y) = \frac{1}{2} \sqrt{\pi} \, \text{erfc}(y) \, , \tag{A.15}$$

with the complementary error function

$$\mathrm{erfc}(y) = \int\limits_{y}^{\infty} d\xi \; e^{-\xi^2}. \tag{A.16}$$

A.4 Current density matrix elements

A.4.1 Exact expressions

Expressions like the Kubo formula (4.23) require the evaluation of current density matrix elements. In the presence of a magnetic fields and the formation of Landau levels, it turns out that matrix elements between states pertaining to the same Landau level vanish. This requires some care in the evaluation of current response functions, since the single band approximation fails even for strong magnetic fields.

In the following, we derive an expression for matrix elements of arbitrary states $\psi_\alpha(\mathbf{r})$ written in Landau functions $\phi_{nX}(\mathbf{r})$ as

$$\psi(\mathbf{r}) = \sum_{nX} C_{nX}^\alpha \phi_{nX}(\mathbf{r}). \tag{A.17}$$

For reasons of generality, we choose the Landau functions for the 1D parabolic confinement $\frac{1}{2}m\omega_0^2 x^2$ in Landau gauge $\mathbf{A} = (0 - Bx, 0)$. As usual, we define $\Omega = \sqrt{\omega_c^2 + \omega_0^2}$ and $\ell = \sqrt{\hbar/m\Omega}$ as renormalized versions of the cyclotron energy $\omega_c = eB/m$ and the magnetic length $l_B = \hbar/(m\omega_c)$.

The vector-valued current density matrix can be written as

$$\mathbf{j}_{\alpha\beta} = \frac{e^2}{i2m} \left[\psi_\alpha^* \nabla \psi_\beta - \psi_\beta \nabla \psi_\alpha^* \right] - \frac{e^2}{m} \mathbf{A} \psi_\alpha^* \psi_\beta \tag{A.18}$$

The components are written

$$
\begin{aligned}
j_{\alpha\beta;y} &= \frac{e^2\hbar}{2im} \left[\left(\sum_{nX} C_{nX}^{\alpha*} \phi_{nX} \right) \left(\sum_{n'X'} C_{n'X'}^{\beta} \frac{-iX'}{\ell^2} \phi_{n'X'} \right) \right. \\
&\quad - \left. \left(\sum_{n'X'} C_{n'X'}^{\beta} \phi_{n'X'} \right) \left(\sum_{nX} C_{nX}^{\alpha*} \frac{iX}{\ell^2} \phi_{nX} \right) \right] - \frac{e^2}{m} Bx \psi_\alpha^* \psi_\beta \\
&= \frac{e\hbar}{2m} \left[\sum_{nn'} \sum_{XX'} C_{nX}^{\alpha*} C_{n'X'}^{\beta} \phi_{nX} \phi_{n'X'} \frac{X + X'}{\ell^2} \right] - \frac{e^2}{m} Bx \psi_\alpha^* \psi_\beta \quad \text{(A.19)}
\end{aligned}
$$

and similarly

$$
\begin{aligned}
j_{\alpha\beta;x} &= \frac{e^2\hbar}{2im}\left[\sum_{nn'}\sum_{XX'}C_{nX}^{\alpha*}C_{n'X'}^{\beta}\left(\frac{\sqrt{2n'}}{\ell}\phi_{nX}^*\phi_{n'-1X'}-\frac{\sqrt{2n}}{\ell}\phi_{n-1X}^*\phi_{n'X'}\right)\right.\\
&\quad+\left.\frac{X'-X}{\ell^2}\phi_{nX}^*\phi_{n'X'}\right]
\end{aligned}
\tag{A.20}
$$

using

$$
\nabla\phi_{nX}(\mathbf{r})=\begin{pmatrix}\frac{\sqrt{2n}}{\ell}\phi_{n-1X}-\frac{x-X}{\ell^2}\phi_{nX}\\[2mm]-\frac{iX}{\ell^2}\phi_{nX}\end{pmatrix}
\tag{A.21}
$$

The calculation of the matrix elements can be done by straightforward integration using the orthonormality conditions of the Landau functions and the relation

$$
H_{n+1}(x)=2xH_n(x)-2nH_{n-1}(x)
\tag{A.22}
$$

for Hermite polynomials H_n and leads after some tedious algebraic manipulations to

$$
\langle\alpha\mid j_x\mid\beta\rangle=\int d^2r j_{\alpha\beta;x}=\frac{e}{\sqrt{2}i}\ell\Omega\sum_n\sum_X C_{nX}^{\alpha*}C_{n+1X}^{\beta}\sqrt{n+1}-C_{nX}^{\alpha*}C_{n-1X}^{\beta}\sqrt{n}
\tag{A.23}
$$

and

$$
\langle\alpha\mid j_y\mid\beta\rangle=e\ell(\omega_c-\Omega)\sum_{nX}\frac{X}{\ell}C_{nX}^{\alpha*}C_{nX}^{\beta}+\frac{e\ell\omega_c}{\sqrt{2}}\sum_{nX}C_{nX}^{\alpha*}C_{n+1X}^{\beta}\sqrt{n+1}+C_{nX}^{\alpha*}C_{n-1X}^{\beta}\sqrt{n}
\tag{A.24}
$$

A.4.2 Semiclassical expressions (guiding center velocity approximation)

In this section we give an expression for the classical velocity operator for electrons in strong magnetic field and disorder for comparison with the quantum mechanical expression for the current density.

We see from equations (A.23) and (A.24) that the current density operator for the quantum Hall system couples neighboring Landau bands. Therefore, it is prohibitive to work with currents and conductivities in a single band approximation even for the strong-field limit with vanishing energetic overlap of the bands. In order to circumvent this difficulty, it has been proposed for long-range correlated disorder $V(x,y)$ [39, 132, 133] to replace the current density operator with the semiclassical velocity operator of

the center-of-mass coordinate (X, Y) of the wavefunction. The velocity components can then be written as [39]

$$\dot{X} = \frac{l_B^2}{\hbar} \frac{\partial V}{\partial y} \quad ; \quad \dot{Y} = \frac{l_B^2}{\hbar} \frac{\partial V}{\partial x} \tag{A.25}$$

As devised in the preceding section, we calculate the matrix element $\left\langle \alpha \mid (\dot{X}, \dot{Y}) \mid \beta \right\rangle$. We assume a long-range potential $V(x - x_i, y - y_i)$ with a set of randomly distributed scatterers located at positions $\mathbf{r}_i$.

Using its Fourier transform $V(\mathbf{q}\,;\mathrm{x_i},\mathrm{y_i})$ and $\nabla_{\mathbf{r}} V = -\nabla_{\mathbf{r}_i} V$, we get

$$\begin{aligned}
\left\langle \alpha \mid \dot{X} \mid \beta \right\rangle &= \frac{l_B^2}{\hbar} \sum_{nn'} \sum_{XX'} C_{nX}^{\alpha*} C_{n'X'}^{\beta} \left\langle nX \mid \dot{X} \mid n'X' \right\rangle \\
&= -\frac{l_B^2}{\hbar} \sum_{nn'} \sum_{XX'} C_{nX}^{\alpha*} C_{n'X'}^{\beta} \left\langle nX \mid \frac{\partial V}{\partial y_i} \mid n'X' \right\rangle \\
&= -\frac{2\pi l_B^2}{\hbar L_x L_y} \sum_{nn'} \sum_{XX'} C_{nX}^{\alpha*} C_{n'X'}^{\beta} \sum_{\mathbf{q}} \frac{\partial}{\partial y_i} V(\mathbf{q}\,;\mathrm{x_i},\mathrm{y_i}) \left\langle nX \mid \mathrm{e}^{-i\mathbf{q}\cdot\mathbf{r}} \mid \mathrm{n'X'} \right\rangle \\
&= -i\frac{2\pi l_B^2}{\hbar L_x L_y} \sum_{nn'} \sum_{XX'} C_{nX}^{\alpha*} C_{n'X'}^{\beta} \sum_{\mathbf{q}} q_y \frac{\partial}{\partial y_i} V(\mathbf{q}\,;\mathrm{x_i},\mathrm{y_i}) \left\langle nX \mid \mathrm{e}^{-i\mathbf{q}\cdot\mathbf{r}} \mid \mathrm{n'X'} \right\rangle
\end{aligned} \tag{A.26}$$

$$\left\langle \alpha \mid \dot{Y} \mid \beta \right\rangle = i\frac{2\pi l_B^2}{\hbar L_x L_y} \sum_{nn'} \sum_{XX'} C_{nX}^{\alpha*} C_{n'X'}^{\beta} \sum_{\mathbf{q}} q_x \frac{\partial}{\partial y_i} V(\mathbf{q}\,;\mathrm{x_i},\mathrm{y_i}) \left\langle nX \mid \mathrm{e}^{-i\mathbf{q}\cdot\mathbf{r}} \mid \mathrm{n'X'} \right\rangle \tag{A.27}$$

Material data for GaAs

The presented calculations have been performed with material data for GaAs, because this semiconductor is commonly used in experiments. It follows a collection of material parameters and numerical values for quantities used in the calculations.

Electrons in bulk GaAs have an effective mass of $m^* = 0.067m_0$, an effective g-factor $g = -0.44$ and a dielectric constant $\epsilon = 12.4$. These quantities were used to scale the simulation parameters.

Landau energy:

$$E_N = (N + \frac{1}{2})\hbar\omega_c = \hbar\frac{eB}{m^*} = 1.728\frac{\text{meV}}{\text{T}}B[\text{T}] \tag{B.1}$$

Zeeman energy:

$$E_Z = \sigma g\mu_B B = \pm\frac{1}{2}g \cdot 5.788 \cdot 10^{-2}\frac{\text{meV}}{\text{T}}B[\text{T}] \tag{B.2}$$

Coulomb energy:

$$E_C = \frac{e^2}{4\pi\epsilon_0\epsilon} = 1.44 \cdot 10^{-6}\text{meV m}\frac{1}{\epsilon} \tag{B.3}$$

Magnetic length:

$$l_B = \sqrt{\frac{\hbar}{eB}} = 2.5656 \cdot 10^{-8}\sqrt{\text{T}}\text{m}\frac{1}{\sqrt{B}} \tag{B.4}$$

Current density:

$$\frac{e\hbar}{m^*l_B} = 2.7684 \cdot 10^{-10}\text{pAm}\frac{1}{l_B} \tag{B.5}$$

Part V

Bibliography

Bibliography

[1] K. v. Klitzing, G. Dorda, and M.Pepper, Phys. Rev. Lett. **45**, 494 (1980).

[2] D. C. Tsui, H. L. Störmer, and A. C. Gossard, Phys. Rev. Lett. **48**, 1559 (1982).

[3] P. W. Anderson, Phys. Rev. **109**, 1492 (1958).

[4] B. Kramer and A.MacKinnon, Rep. Prog. Phys. **56**, 1469 (1993).

[5] D. Belitz and T. R. Kirkpatrick, Rev. Mod. Phys **66**, 261 (1994).

[6] P. A. Lee and T. V. Ramakrishnan, Rev. Mod. Phys **57**, 287 (1994).

[7] E. Abrahams, P. W. Anderson, D. C. Licciardello, and V. Ramakrishnan, Phys. Rev. Lett. **42**, 673 (1979).

[8] T. Brandes and S. Kettemann, eds., *Anderson localization and its ramifications* (Springer-Verlag, New York, 2003).

[9] S. Hikami, Prog. Theor. Phys. Suppl. **107**, 213 (1992).

[10] B. Huckestein and B. Kramer, Phys. Rev. Lett. **64**, 1437 (1990).

[11] B. Huckestein, Rev. Mod. Phys. **67**, 357 (1995).

[12] B. Mieck, Z. Physik B **90**, 427 (1993).

[13] D. Z. Liu and S. Das Sarma, Phys. Rev. B **49**, 2677 (1994).

[14] D. Z. Liu and S. Das Sarma, Mod. Phys. Lett. **49**, 2677 (1994).

[15] V.K.S. Shante and S. Kirkpatrick, Advances in Phys. **30**, 325 (1971).

[16] J. T. Chalker and P. D. Coddington, J. Phys. C **21**, 2265 (1988).

[17] D. H. Lee, Z. Wang, and S. Kivelson, Phys. Rev. Lett. **70**, 4130 (1993).

[18] S. A. Trugman, Phys. Rev. B **27**, 7539 (1983).

[19] G. V. Mil'nikov and I. M. Sokolov, JETP Lett. **48**, 536 (1988).

[20] S. L. Sondhi, S. M. Girvin, J. P. Carini, and D. Shahar, Rev. Mod. Phys. **69**, 315 (1997).

[21] H. Wei, D. Tsui, M. Paalanen, and A. Pruisken, Phys. Rev. Lett. **61**, 1294 (1988).

[22] S. Koch, R. Haug, K. von Klitzing, and K. Ploog, Phys. Rev. Lett. **67**, 883 (1991).

[23] F. Hohls, U. Zeitler, R. J. Haug, R. Meisels, K. Dybko, and F. Kuchar, Phys. Rev. Lett. **89**, 276801 (2002).

[24] F. Hohls, U. Zeitler, and R. J. Haug, Phys. Rev. Lett. **88**, 036802 (2002).

[25] L. W. Engel, D. Shahar, C. Kurdak, and D. Tsui, Phys. Rev. Lett. **71**, 2638 (1993).

[26] M. Furlan, Phys. Rev. B **57**, 14818 (1998).

[27] N. Q. Balaban, U. Meirav, and I. Bar–Joseph, Phys. Rev. Lett. **81**, 4967 (1998).

[28] E. P. Wigner, Phys. Rev. **46**, 1002 (1934).

[29] P. K. Lam and S. M. Girvin, Phys. Rev. B **30**, 473 (1984).

[30] R. Price, X. Zhu, S. Das Sarma, and P. M. Platzman , Phys. Rev. B **51**, 2017 (1995).

[31] R. B. Laughlin, Phys. Rev. B **23**, 5632 (1981).

[32] B. I. Halperin, Phys. Rev. B **25**, 2185 (1982).

[33] V. Fock, Z. Phys. **47**, 446 (1928).

[34] S. Ilani, J. Martin, E. Teitelbaum, J. H. Smet, D. Mahalu, V. Umansky, and A. Yacoby, Nature **427**, 328 (2004).

[35] I. Pallecchi, Ch. Heyn, J. Lohse, B. Kramer, and W. Hansen, Phys. Rev. B **65**, 125303 (2002).

[36] J. M. Kinaret and P. A. Lee, Phys. Rev. B **42**, 11768 (1990).

[37] A. Struck, Diploma thesis, Universität Hamburg (2002).

[38] T. Ando, J. Phys. Soc. Jpn. **52**, 1893 (1983).

[39] T. Ando, J. Phys. Soc. Jpn. **53**, 3126 (1984).

[40] F. Wegner, Z. Physik B **36**, l209 (1979).

[41] A.Szabo and N. S. Ostlund, *Modern quantum chemistry: Introduction to Advanced Electronic Structure Theory* (Dover Publications, Dover, 1989).

[42] M. Tsukada, J. Phys. Soc. Jpn. **41**, 1466 (1976).

[43] B. Kramer, T. Ohtsuki, and S. Kettemann, cond-mat/0409625 (2004).

[44] A. MacKinnon and B. Kramer, Phys. Rev. Lett. p. 1546 (1981).

[45] H.Aoki, J. Phys. C: Solid State Phys. **16**, L205 (1983).

[46] H.Aoki, Phys. Rev. B **33**, 7310 (1986).

[47] W. Pook and M. Janssen, Z. Phys. B **82**, 295 (1991).

[48] C. Halsey, M. H. Jensen, L. P. Kadanoff, I. Procaccia, and B. I. Shraiman, Phys. Rev. A **33**, 1141 (1991).

[49] M. Janssen, Int. J. Mod. Physics B **8**, 943 (1994).

[50] M. Janßen, O. Viehweger, U. Fastenrath, and J. Hajdu, *Introduction to the Theory of the Integer Quantum Hall Effect* (VCH-Verlagsgruppe, Weinheim, Germany, 1997).

[51] J. Bauer, T.-M. Chang, and J. L. Skinner, Phys. Rev. B **42**, 8121 (1990).

[52] S.-R. E. Yang, A. H. MacDonald, and B. Huckestein, Phys. Rev. Lett. **74**, 3230 (1995).

[53] F. Kuchar, R. Meisels, K. Dybko, and B. Kramer, Europhys. Lett. **49**, 480 (2000).

[54] A. M. M. Pruisken, Phys. Rev. Lett. **61**, 1297 (1988).

[55] D. J. Thouless, Phys. Rev. Lett. **39**, 1167 (1977).

[56] J. T. Chalker and G. J. Daniell, Phys. Rev. Lett. **61**, 593 (1988).

[57] F. Evers and W. Brenig, Z. Phys. B **94**, 155 (1994).

[58] B. Huckestein and M. Backhaus, Phys. Rev. Lett. **82**, 5100 (1999).

[59] S.-R. E. Yang, Z. Wang, and A. H. MacDonald, Phys. Rev. B **65**, 041302 (2002).

[60] Y. Avishai and J. M. Luck, cond-mat/9609265 (1996).

[61] R. Kubo, J. Phys. Soc. Jpn. **12**, 570 (1957).

[62] L. Schweitzer, *Anderson localization and its ramifications* (Springer-Verlag, New York, 2003), cond-mat/0303198.

[63] G. D. Mahan, *Many particle physics* (Plenum Press, New York and London, 1990).

[64] G. Czycholl, *Theoretische Festkörperphysik* (Springer-Verlag, Heidelberg/Berlin, 2000).

[65] J. Rammer, *Quantum transport theory*, vol. 99 (Frontiers in physics, Reading, Massachusetts, 1994).

[66] E. Gornik, R. Lassnig, G. Strasser, H. L. Störmer, A. C. Gossard, and W. Weigmann, Phys. Rev. Lett. **54**, 1820 (1985).

[67] F. F. Fang and P. J. Stiles, Phys. Rev. **174**, 823 (1968).

[68] J. P. Eisenstein, H. L. Strmer, V. Narayanamurti, A. Y. Cho, A. C. Gossard, and C. W. Tu, Phys. Rev. Lett. **55**, 875 (1985).

[69] J. P. Eisenstein, L. N. Pfeiffer, and K. W. West, Phys. Rev. Lett. **68**, 674 (1992).

[70] S. Ilani, A. Yacoby, D. Mahalu, and Hadas Shtrikman, Phys. Rev. Lett. **84**, 3133 (2000).

[71] D. Yoshioka, Phys. Rev. B **29**, 6833 (1984).

[72] A. L. Efros and B. I. Shklovskii, J. Phys. C **8**, L49 (1975).

[73] L.P. Kouwenhoven, G. Austing, and S. Tarucha, Rep. Prog. Phys. **64**, 701 (2001).

[74] E. Prange and S.M. Girvin, eds., *The Integer Quantum Hall Effect* (Springer, New York, 1990).

[75] Z. Wang and S. Xiong, Phys. Rev. B **65**, 195316 (2002).

[76] H. B. Chan, P. I. Glicofridis, R. C. Ashoori, and M. R. Melloch, Phys. Rev. Lett. **79**, 2867 (1997).

[77] D. H. Cobden, C. H. W. Barnes, and C. J. B. Ford, Phys. Rev. Lett. **82**, 4695 (1999).

[78] G. Onida, L. Reining, and A. Rubio, Rev. Mod. Phys. **74**, 601 (2002).

[79] P. S. Bagus, Phys. Rev. **139**, A619 (1965).

[80] B. Huckestein and L. Schweitzer, Phys. Rev. Lett. **72**, 713 (1994).

[81] T. Ando, J. Phys. Soc. Jpn. **36**, 1521 (1974).

[82] A. H. MacDonald, C. A. Oji, and K. L. Liu, Phys. Rev. B **34**, 2681 (1986).

[83] N. H. March, ed., *Electron correlation in the Solid State* (Imperial College Press, London, 1999).

[84] L. Schweitzer, B. Kramer, and A. MacKinnon, Z. Phys. B **56**, 297 (1984).

[85] A. Struck, T. Ohtsuki, B. Kramer, and S. Kettemann, Phy. Rev. B **72**, 035339.

[86] R. J. Haug and K. von Klitzing, Europhys. Lett. **10**, 489 (1989).

[87] G. Timp, A. M. Chang, P. Mankiewich, R. Behringer, J. E. Cunningham, T. Y. Chang, and R. E. Howard, Phys. Rev. Lett. **59**, 732 (1987).

[88] E. Peled, D. Shahar, Y. Chen, D. L. Sivco, and A. Y. Cho, Phys. Rev. Lett. **90**, 246802 (2003).

[89] T. Ando, Phys. Rev. B **49**, 4679 (1994).

[90] B. J. van Wees, L. P. Kouwenhoven, E. M. M. Willems, C. J. P. M. Harmans, J. E. Mooij, H. van Houten, C. W. J. Beenakker, J. G. Williamson, and C. T. Foxon, Phys. Rev. B **43**, 12431 (1991).

[91] B. I. Shklovskii, Pis'ma Zh. Eksp. Teor. Fiz. **36**, 43 (1982).

[92] A. V. Khaetskii and B. I. Shklovskii, Zh. Eksp. Teor. Fiz. **85**, 721 (1983).

[93] M. E. Raikh and T. V. Shahbazyan, Phys. Rev. B **51**, 9682 (1995).

[94] T. Ohtsuki and Y. Ono, Solid State Commun. **65**, 403 (1988).

[95] T. Y. Ono and B. Kramer, J. Phys. Soc. Jpn. **58**, 1705 (1989).

[96] T. Ohtsuki and Y. Ono, J. Phys. Soc. Jpn. **58**, 956 (1989).

[97] T. Ando and Y. Uemura, J. Phys. Soc. Jpn. **36**, 959 (1974).

[98] T. Ando, J. Phys. Soc. Jpn. **37**, 622 (1974).

[99] R. G. Mani and K. v. Klitzing, Phys. Rev. B **46**, 9877 (1992).

[100] K. R. G. Mani and K. Ploog, Phys. Rev. B **51**, 2584 (1995).

[101] P. G. N. d. Vegvar, A. M. Chang, G. Timp, P. M. Mankiewich, J. E. Cunningham, R. Behringer, and R. E. Howard, Phys. Rev. B **36**, 9366 (1987).

[102] M. L. Roukes, A. Scherer, S. J. Allen, Jr., H. G. Craighead, R. M. Ruthen, E. D. Beebe, and J. P. Harbison, Phys. Rev. Lett. **59**, 3011 (1987).

[103] T. Ando, Phys. Rev. B **42**, 5626 (1990).

[104] S. Kettemann, B. Kramer, and T. Ohtsuki, JETP Lett. **80**, 316 (2004).

[105] A. J. B. Pendry and P. J. Roberts, Proc. R. Soc. London A **67**, 437 (1992).

[106] S. Kettemann, J. Phys. Soc. Jpn. Suppl. A **72**, 197 (2003).

[107] S. Kettemann, Phys. Rev. B **69**, 035339 (2004).

[108] F. Wegner, Nucl. Phys. B **316**, 663 (1989).

[109] S. Hikami, Prog. Theor. Phys. **64**, 1466 (1980).

[110] A. K. B. Efetov and D. E. Khmel'nitskii, Zh. Eksp. Teor. Fiz. **79**, 1120 (1980).

[111] A. MacKinnon and B. Kramer, Z. Phys. B **53**, 1 (1983).

[112] B. Huckestein and B. Kramer, Phys. Rev. Lett. **64**, 1437 (1990).

[113] A. G. Galstyan and M. E. Raikh, Phys. Rev. B **56**, 1422 (1997).

[114] M. D. P. Arovas and B. Shapiro, Phys. Rev. B **56**, 4751 (1997).

[115] B.Huckestein, Phys. Rev. Lett. **84**, 3141 (2000).

[116] K. B. Efetov, *Supersymmetry in Disorder and Chaos* (Cambridge University Press, Cambridge, 1997).

[117] K. B. Efetov and A. I. Larkin, Zh. Eksp Teor. Fiz. **85**, 764 (1983), sovPhys. JETP 58, 444.

[118] O. N. Dorokhov, Pis'ma Zh. Eksp. Teor. Fiz. **36**, 259 (1982), jETP Lett. 36, 318 (1983).

[119] O. N. Dorokhov, Zh. Eksp. Teor. Fiz. **85**, 1040 (1983).

[120] O. N. Dorokhov, Solid State Commun. **51**, 381 (1984).

[121] B. Huckestein and R. Klesse, Phys. Rev. B **55**, R7303 (1997).

[122] B. Huckestein, B. Kramer, and L. Schweitzer, Surf. Sci. **263**, 125 (1993).

[123] J. F. Janak, Phys.Rev. **178**, 1416 (1968).

[124] J. Wrobel, T. Brandes, F. Kuchar, B. Kramer, K. Ismail, K. Y. Lee, H. Hillmer, W. Schlapp, and T. Dietl, Europhys. Lett. **29**, 481 (1995).

[125] J. Wrobel, T. Brandes, F. Kuchar, B. Kramer, K. Ismail, K. Y. Lee, H. Hillmer, W. Schlapp, and T. Dietl, Surf. Sci. **305**, 615 (1994).

[126] M. A. Kastner, S. B. Field, J. C. Licini, and S. L. Park, Phys. Rev. Lett. **60**, 2535 (1988).

[127] R. Mottahedeh, M. Pepper, R. Newbury, J. Perenboom, and K.-F. Berggren, Sol. St. Commun. **72**, 1065 (1989).

[128] O. G. Balev and P. Vasilopoulos, Phys. Rev. B **56**, 6748 (1997).

[129] T. Suzuki and T. Ando, J. Phys. Soc. Jpn. **62**, 2986 (1993).

[130] T. Suzuki and T. Ando, Physica B **201**, 345 (1994).

[131] G. Y. Hu and R. F. O'Connell, Phys. Rev. B **42**, 1290 (1990).

[132] H.Aoki, J. Phys. C: Solid State Phys. **10**, 2583 (1977).

[133] H. Aoki, J. Phys. C: Solid State Phys. **11**, 3823 (1978).

Acknowledgements

List of publications

- Alexander Struck, Bernhard Kramer: *Electron correlation and single-particle physics in the Integer Quantum Hall Effect*, submitted to Phys. Rev. Lett., 2005 (cond-mat/0502095)

- Alexander Struck, Bernhard Kramer, Tomi Ohtsuki, Stefan Kettemann: *Nonchiral Edge States at the Chiral Metal Insulator Transition in Disordered Quantum Hall Wires*, Phys. Rev. B **72**, 035339 (2005) (cond-mat/0501294). This article has been selected for the 1st August 2005 issue of the Virtual Journal of Nanoscale Science &Technology.

- Alexander Struck, Siawoosh Mohammadi, Stefan Kettemann, Bernhard Kramer, Wolfgang Hansen, Ilaria Palecchi: *Confinement induced depletion of the enhanced g-factor in quantum wires*, to be submitted, 2005

- Ronald Meisels, Friedemar Kuchar, Alexander Struck, Bernhard Kramer: *Interaction corrections to dynamical scaling in the IQHE*, in preparation